Spatial Modulation in the Underwater Acoustic Communication Channel

by

Daniel Brian Kilfoyle

Submitted in partial fulfillment of the requirements for the degree of

Doctor of Philosophy

at the

MASSACHUSETTS INSTITUE OF TECHNOLOGY

and the

WOODS HOLE OCEANOGRAPHIC INSTITUTION

June, 2000

Author _____
Department of Electrical Engineering and Computer Science,
Joint Program in Oceanography and Oceanographic Engineering,
Massachusetts Institute of Technology / Woods Hole Oceanographic Institution,
May 11, 2000

Certified by _____
Arthur B. Baggeroer
Ford Professor of Electrical and Ocean Engineering, MIT, Thesis Supervisor

Certified by _____
James. C. Preisig
Assistant Scientist, WHOI, Thesis Supervisor

Accepted by _____
Michael Triantafyllou
Chairman, MIT/WHOI Joint Committee for Applied Ocean Science and Engineering

Accepted by _____
Arthur C. Smith
Chairman, MIT EECS Departmental Committee on Graduate Students

Spatial Modulation in the

Underwater Acoustic Communication Channel

by

Daniel Brian Kilfoyle

Submitted in partial fulfillment of the requirements for the degree of

Doctor of Philosophy
at the
Massachusetts Institute of Technology
and the
Woods Hole Oceanographic Institution
June, 2000

Abstract

A modulation technique for increasing the reliable data rate achievable by an underwater acoustic communication system is presented and demonstrated. The technique, termed spatial modulation, seeks to control the spatial distribution of signal energy such that multiple parallel communication channels are supported by the single, physical ocean channel. Results from several experiments successfully demonstrate higher obtainable data rates and power throughput.

Given a signal energy constraint, a communication architecture with access to parallel channels will have increased capacity and reliability as compared to one with access to a single channel. Assuming the use of multiple element spatial arrays at both the transmitter and receiver, an analytic framework is developed that allows a multiple input, multiple output physical channel to be transformed into a set of virtual parallel channels. The continuous time, vector singular value decomposition is the primary vehicle for this transformation. Given knowledge of the channel impulse responses and assuming additive, white Gaussian noise as the only interference, the advantages of using spatial modulation over a deterministic channel may be exactly computed.

Improving performance over an ensemble of channels using spatial modulation is approached by defining and then optimizing various average performance metrics including average signal to noise ratio, average signal to noise plus interference ratio, and minimum square error.

Several field experiments were conducted. Detailed channel impulse response measurements were made enabling application of the decomposition methodology. The number, strength, and stability of the available parallel channels were analyzed. The parallel channels were readily interpreted in terms of the underlying sound propagation field. Acoustic communication tests were conducted comparing conventional coherent modulation to spatial modulation. In one case, a reliable data rate of 24000 bits per second with a 4 kHz bandwidth signal was achieved with spatial modulation when conventional signaling could not achieve that rate. In another test, the benefits of spatial

modulation for a horizontally distributed communication system, such as an underwater network with autonomous underwater vehicles, were validated.

Thesis Supervisor: Arthur B. Baggeroer
Title: Ford Professor of Electrical and Ocean Engineering, MIT

Thesis Supervisor: James C., Preisig
Title: Assistant Scientist, WHOI

Acknowledgements

Looking back over the last five years, I am mindful of the many people and organizations that helped me succeed in this dissertation. Some aided me in clear, definitive ways while others contributed more subjective, abstract support. Rather than take on the unnecessary and difficult task of saying who helped the most, I choose to reflect on these people chronologically.

Dr. Josko Catipovic sponsored my early years in the Joint Program. I am grateful for his direction as well as flexibility as I cast about for a suitable thesis project. Even though he left the institution half way through my tenure, he remained an active and supportive member of my committee.

Lee Freitag, Matt Grund, and Paul Bouchard willingly lent me their expertise, equipment, and advice. Without the vast acoustic communication support structure they have in place and shared with me, I would not have been able to completely focus on the merits of spatial modulation and accumulate the many experimental results contained in this thesis. I am deeply appreciative of what they offered without recompense.

Dr. Dan Nagle and other members of the ACOMMS Advanced Technical Demonstration program allowed me to incorporate my research goals into their testing program on several occasions. I would like all of them to know that I thank them for the help.

Prof. Jeffrey Shapiro and Prof. David Forney each gave valuable guidance on the theoretical aspects of this work. The opportunity to have the advice and oversight of such renowned and insightful people is a supreme strength of the Joint Program. They have my gratitude and I only hope I was able to offer them value in return.

My co-advisors, Dr. Jim Preisig and Prof. Arthur Baggeroer, devoted innumerable hours to steering, coaching, and fostering my research. The willingness of them to take on a mentoring role in spite of their demanding career obligations proved to me their commitment to the educational program of both institutions. I simply could not have achieved all I did without them.

The financial support of the U.S. Office of Naval Research in the persona of Dr. Tom Curtin is deeply appreciated. Specifically, the funding of grant # N00014-97-1-0796 and its extensions enabled my research into spatial modulation. As an engineer, I never forget that my work must always lead, eventually, towards a practical application. I sincerely hope that what I have developed in this thesis will, somehow, strengthen the U. S. Navy's underwater acoustic communication ability.

Although I claimed I would not rate the contributions of those who helped me in this endeavor, I find that I must make an exception. Without offering a single piece of technical advice or assistance, my family has, nevertheless, been the one, irreplaceable feature of my doctoral pursuit. My experience as a father and husband is the center of my life and sustains me in all other roles.

Biographical Note

Daniel Kilfoyle was born in Hagerstown, MD, in 1964. He graduated from Ben Eielson High School, Eielson Air Force Base, AK, in 1982 and then attended the Massachussetts Institute of Technology with the assistance of a United States Air Force Reserve Officer Training Corps scholarship, ultimately earning the degrees of Bachelor of Science and Master of Science in Aeronautical and Astronautical Engineering in 1986 and 1988, respectively. After a two year tour of duty in the U. S. Air Force supporting the Milstar communication satellite system, he joined Science Applications International Corporation (SAIC) in 1990 at their La Jolla headquarters. Until 1993, his work concentrated on development of electromagnetic signature suppression methods and sensor design. He concurrently earned a Master of Science degree in Electrical Engineering from the University of California, San Diego. He returned to Massachusetts in 1993 and continued to support SAIC. His doctoral pursuit began in 1995 with his acceptance and entry into the Massachussetts Institute of Technology and Woods Hole Oceanographic Institution Joint Program in Oceanography. That journey culminated in this thesis and the award of a doctoral degree in Electrical and Ocean Engineering from both institutions.

Contents

List of Figures

List of Tables

Chapter 1 Introduction

Underwater acoustic communication channels are severely restricted in temporal bandwidth compared to their electromagnetic counterparts. Faced with a need for increased data rates at the same reliability, two approaches may be initially considered: a higher symbol rate or a larger symbol constellation. Both of these approaches are limited in their ability to provide greater data rates in the underwater acoustic channel. The thesis of this work is that appropriate array processing of the transmitted signal *spatial* spectrum offers a third, and quite viable, approach to increasing data rates, and communication performance in general, for the underwater acoustic channel. Unlike the electromagnetic wireless channel, most underwater acoustic channels consistently and predictably have multipath, or multiple propagation paths, connecting the source and receiver, thus supporting a rich, spatial spectrum which spatial modulation seeks to exploit.

1.1 The Underwater Acoustic Communication Channel

The underwater acoustic communication channels (UACC) may, roughly speaking, be described by any of three basic channel types based on the ratio of range between source and receiver and the ocean depth (R/D). Close range telemetry applications in deep water (R/D << 1) operate as line-of-sight communication channels with a single, dominant propagation path (or eigenray) connecting source and receiver. A typical application is communication from a surface vessel to an instrument submerged vertically below the ship. The important process governing signal design is ambient noise and, as such, these channels are generally well characterized by their signal to noise ratio (SNR). For channels with R/D ~ 1, multiple eigenrays are found with significant

gain factors. The impulse response has a discrete structure with a total span ranging from several to hundreds of milliseconds. The delay spread in arrival of energy is a direct result of the difference in paths traversed by the eigenrays. The range of directions spanned by the eigenrays, characterized by a horizontal wavenumber spread, is often resolvable by modest transmitter and receiver arrays. As such, this channel is well suited to spatial modulation applications. The most important process governing signal design in this case is the reverberation of energy. Incoherent systems seek to mitigate the reverberation by hopping the signal's power in time and frequency in order to leave "guard bands" that allow the later eigenray arrivals to terminate before that frequency is used again. Coherent systems simply let the reverberation "smear" the transmitted symbols together leading to intersymbol interference (ISI). Such systems employ adaptive algorithms to filter the received signal and remove much of the ISI induced distortion. Many telemetry architectures involving ships and submerged vehicles experience channels such as this. The final channel type is found in surf-zone or littoral regions where $R/D >> 1$. The impulse response may be spread over hundreds of milliseconds and has a more continuous nature. Furthermore, the horizontal wavenumber spread is not readily resolved with arrays. Conventional acoustic communication under these conditions is challenging and remains a focus of research.

Several processes affect acoustic telemetry signals. Vertical gradients in the sound velocity diffract the signals much as an optical lens diffracts light. Minima in the sound velocity profile can lead to trapped eigenrays that propagate without reflection from the surface or bottom of the ocean. This structure drives the long-term, deterministic features of the impulse response. Rough boundaries introduce scattering

losses that can severely diminish the signal's energy with each interaction. If either the surface or the signal source is moving, the reflected signal will have an amplitude and phase that varies in time. Even non-reflecting eigenrays will have a time varying gain factor due to the Doppler effect. Coherent telemetry systems must be able to estimate this variability. Individual eigenrays may split into many, closely located eigenrays, micro-multipath, due to small scale roughness or spatial inhomogeneities. The coherent combination of these micro-multipaths leads to amplitude and phase fluctuations at the receiver (fading) that must be dealt with.

The preceeding discussion seeks to offer a quite general overview of the UACC. Further details may be found in texts [1] [2] as well as review articles [3, 4] [5]. For the reader familiar with other communication channels, it may prove useful to highlight the unique aspects of the UACC. The relatively slow speed of sound (~1500 m/sec) can lead to high latency in that the time it takes for the signal to propagate from source to receiver is appreciable compared to the length of a message. For instance, a 10 km range implies over a 12 second latency in a round trip signal transmission. Another consequence of the slow sound speed is that the delay spread of the impulse response is measured in milliseconds. Most electromagnetic wireless channels have delay spreads measured in microseconds. As such delay spreads are compared to the inverse of the signal bandwidths, the reverberation cannot be ignored. Finally, the Doppler effect, proportional to the ratio of platform speed to propagation speed, becomes apparent even with speeds as low as 1 – 2 knots. Furthermore, many acoustic telemetry signals have a high ratio of bandwidth to carrier frequency which makes the Doppler effect more than a

simple frequency shift. All of these features make the UACC a complex and challenging medium through which to communicate.

1.2 Classical Approaches to Increasing Data Rates

1.2.1 Higher symbol rates

Higher symbol rates lead to larger signal bandwidths. In an additive, white Gaussian noise (AWGN) channel, the signal to noise ratio (SNR) is halved for each doubling of bandwidth (for a constant transmit power) due to increased noise power in the transmission band. In an underwater channel, not only does noise power increase with bandwidth but received signal power drops due to increasing absorption with frequency. Molecular absorption of narrowband sound pressure waves in the ocean at telemetry frequencies may be approximated by [2],

$$\alpha \approx \kappa f^2 \qquad 1.1$$

where α = intrinsic attenuation (dB/km), $\kappa = 2.2 \times 10^{-3}$ (dB/km/kHz), and f = frequency (kHz). At a carrier frequency of 50 kHz, one may, therefore, expect 5.5 dB/km of attenuation not considering spreading loss. A more detailed model might include the effects of surface scattering loss, ionic resonances, and bottom loss but the theme of substantial signal penalty with increasing frequency remains.

In addition to the impact of absorptive processes, scattering processes also become more burdensome with increasing frequency. Underwater channels have both reflective boundaries and sound speed gradients, predominantly vertical. The result is a spatial dispersion of the signal giving temporally spread impulse responses at the receiver. The multiple arrivals (multipath) give rise to ISI. The multipath arrivals are spread over an *absolute* period of time. As the symbol rate increases, the number of degrees of freedom (DoFs) required to describe the multipath thus grows linearly. This

poses a substantial adaptive equalization processing burden whose computational complexity increases linearly or quadratically with signal bandwidth, depending on the particular equalization algorithm chosen. In addition to this computational issue, the ability of the adaptive process to converge to a stable solution is slowed as the number of DoFs increases. In a time-varying channel, this may be a crucial issue. As the equalizer performance is impaired, the level of uncompensated, or residual, ISI also typically increases adding to the effective noise power. Spreading is also found in the frequency domain as a result of moving platforms and the fluctuating sea surface. The impact of Doppler spread becomes more pronounced and more difficult to deal with at higher frequencies or bandwidths. In short, the achievement of higher data rates in the underwater acoustic channel by simply increasing the symbol rate faces severe obstacles.

1.2.2 Larger Symbol Constellations

The alternative of using larger symbol constellations (with higher power to maintain reliability) is practically constrained by three factors that limit the maximum achievable SNR. First, a number of important underwater acoustic channels are limited by residual ISI as the dominant noise mechanism. The combined effect of a time-varying channel with substantial reverberation leads to a noise level that is proportional to signal power. More power, in this case, does not improve performance. Second, many underwater telemetry applications involve platforms with constrained energy storage capacity such as long-term moorings or autonomous underwater vehicles. The greater energy per bit of information required by larger constellations may simply not be available. Finally, the onset of non-linear effects in the transducer limit the amount of electrical power that may be converted into acoustic power posing an upper bound irrespective of available energy supplies. As the ability to increase SNR saturates, noise

levels become unacceptable as one strives to increase data rate by increasing the size of the symbol constellation. Nevertheless, these two approaches have been the only tools available to the communication engineer. As such, he is forced to consider complex coding and modulation schemes to provide some degree of noise immunity.

1.2.3 Channel Coding in the UACC

The use of complex codes in the hope of realizing large coding gains, however, is severely challenged by the dynamic nature of the underwater channel and, of course, limited by the channel capacity. In a time-varying dispersive channel, adaptive equalization is required to track and mitigate the effects of ISI if bandwidth efficient, coherent modulation techniques are to be used. The adaptive process is commonly implemented in a decision-directed mode where the residual error between the decoded symbol and the equalizer output is used to modify the tap weights [6]. Excessive delays in the feedback process compromise the ability of the equalizer to track the channel [7]. Furthermore, incorrect decisions begin an unstable feedback loop that typically results in divergence of tap weights from their optimal values. In convolution-coded systems, however, there is an approximate proportionality between code constraint length and coding gain. Decoding delays on the order of several code constraint lengths are practically required before the promised coding gain is actually achieved with little gain for early decisions. This conflict between the code and equalizer can be resolved but at the expense of additional, potentially unacceptable, signal processing complexity. Alternatively, one could use a linear equalizer structure without decision feedback. The cost of doing so is relatively higher mean square errors for channels with spectral nulls due to noise enhancement [8]. Coding may thus be applied to underwater channels, but integration with the equalization algorithm is a serious issue.

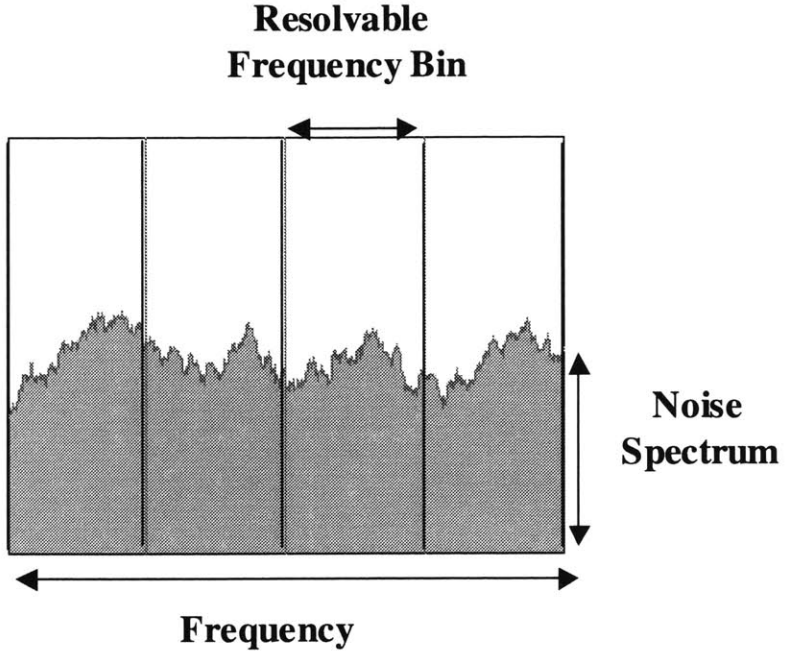

Figure 1.1. The noise spectrum of a model communication channel is shown with the resolvable frequency increments overlayed as four frequency bins. The question of how to best allocate information and energy across this spectrum is a fundamental concern of communication theory. Frequency, in this case, may equally apply to temporal frequency or spatial frequency.

The methods explored in this work offer another approach which exploits the spatial structure of underwater acoustic signals and, as will be shown later, actually increase the capacity of underwater channels by using rather than simply mitigating the effects of the spatial dimension. The achievable performance gains are in addition to rather than instead of those offered by classical approaches based on temporal modulation.

1.3 A Description of Spatial Modulation

Given the frequency spectrum of a channel, it seems clear that the transmitted signal benefits from taking that spectrum into account. Figure 1.1 describes the distribution of noise power as a function of frequency, i.e. the noise spectrum, for a model communication channel. The smallest increments in frequency that can be resolved are driven by factors such as the temporal stability of the channel and the total

signal duration. In the example of figure 1.1, four such frequency bins are resolvable. One may consider three strategies for allocating the given signal energy over that spectrum. First, all the energy may be put in one frequency bin. Second, the energy may be spread among the frequency bins but the same information may be sent in each. Finally, the energy and the information may be spread over the bins. Clear engineering criterion may be used to choose among these strategies and many readers undoubtedly have a sound intuition regarding these criterion. While the use of the term frequency in describing figure 1.1 likely brought to mind temporal frequency, i.e. one component of the transform pair, frequency and time, it may equally apply to spatial frequency, i.e. one component of the transform pair, frequency and spatial location. Just as temporal modulation considers the allocation of energy within the available temporal spectrum, or resolvable frequency bins, spatial modulation is the controlled distribution of multiple communication signals through the available spatial spectrum, or propagation paths, in the channel. Given the rich and complex nature of spatial multipath in the underwater acoustic channel, the need to take the spatial spectrum into account when designing the transmitted signal seems clear. At a fundamental level, the availability of multiple, resolvable propagation paths can be interpreted as increased spatial bandwidth with signal design strategies and subsequent benefits similar to those associated with increased frequency bandwidth. Given the severe bandwidth constraints of the underwater acoustic channel, substantial advantages are foreseen when spatial modulation is used in conjunction with conventional signaling methods.

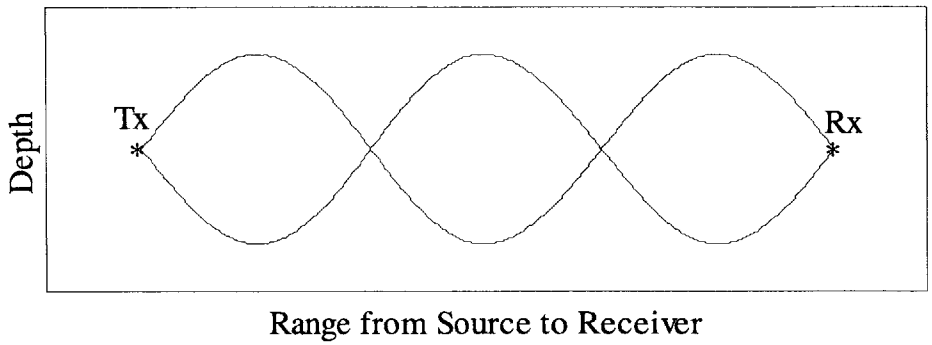

Figure 1.2. A simplified model of convergence zone propagation in the ocean is shown here. The existence of a sound velocity minimum causes energy leaving the transmitter to diffract into the "eye pattern" shown here. At specific locations, the existence of two, spatially distinct propagation paths that connect the source (Tx) and receiver (Rx) is evident.

As a tool for introducing the idea and benefits of spatial modulation, consider a simplified model of long-range acoustic propagation in the ocean. The vertical profile of sound speed in the ocean can lead to periodic convergence of propagation paths (eigenrays) as a function of range. Simple boundary reflections can lead to the same behavior. Using classical ray theory assumptions, the paths traversed through an ocean channel with a stratified sound velocity profile by the energy that reaches the receiver traces an eye pattern (figure 1.2). Existing underwater communication systems would send the same information down both paths with equal energy resulting in an SNR of X at the receiver. One approach to spatial modulation would send independent data streams, each with half the total power, over the separate paths resulting in an SNR of $X/2$ for each data stream at the receiver assuming they are completely separable. Further assume that 4 bits per symbol period were required. Thus, an existing coherent system would use a 16-level complex symbol constellation. The proposed spatially modulated system, however, would only need to employ 4-level complex symbol constellations to achieve the same data rate. Assuming square constellations, AWGN channels, and SNR per bit greater than 10 dB, the spatially modulated system would require 6.9 dB less SNR than

the conventional system to achieve an equivalent error rate. Splitting the data, however, only reduces the SNR by 3 dB leaving a performance advantage equivalent to 3.9 dB. This example was quite simple and specific but it is solely intended to introduce the idea of spatial modulation.

1.4 Previous and Current Work

Spatial modulation, or spatial multiplexing, in communication theory can be traced back to the 1960's. In fact, the roots of spatial modulation spring from the notion of parallel channels in information theory. The classical definition of parallel channels is a communication system or model with multiple channels where the distortion introduced in one channel is independent of the signal or distortion in all other channels. This leads naturally to channel models based on eigenfunctions of the overall system. Gallager considered the problem of coding for reliable communication when the parallel channels are known and fixed [9]. If the identical parallel channels are used independently, the combined capacity is the sum of the individual capacities. Ebert extended this work to examine the optimal signal power distribution among known parallel channels with an average power constraint and the resulting probability of error [10]. He also treats the additional degree of freedom allowed by separate coding on each of the channels. These works offer fundamental performance bounds for any system attempting to exploit the spatial bandwidth of a physical channel. Analysis in the context of parallel channels, however, sidesteps the issue of how effectively a given transmitter can excite these channels without cross-channel interference. While this work also follows the parallel channel paradigm, a decomposition methodology is presented that exactly relates the physical channel to an appropriate parallel channel model.

Spatial modulation, as a means to increase channel capacity, was first specifically discussed by Greenspan [11]. Propagation through the time-invariant (turbulence free) electromagnetic radiation channel can be modeled with a linear time-invariant (LTI) filter. For narrowband signals, the temporal and spatial filtering effects separate allowing an analysis that focuses entirely on spatial effects. By employing a normal mode analysis, Greenspan shows that the prolate-spheroidal functions form an orthonormal set of eigenfunctions over both the transmitter and receiver aperture with the channel impulse response only imparting a scaling factor (identical to the eigenvalue). A characteristic of these eigenfunctions is that a finite number, D, of the lowest orders have eigenvalues near unity while the remainder have negligible eigenvalues. Each eigenfunction is then naturally construed as a parallel communication channel with total channel capacity equal to D^*C, where C is the single channel capacity. Neglecting the effects of cross-channel interference and employing a noise model that is white in both temporal and spatial terms, the optimum (maximum likelihood) receiver is developed and a rate-reliability curve is derived. This thesis will provide decomposition tools appropriate for an *arbitrary* impulse response with temporal support exceeding the symbol period, which contradicts the narrowband assumption.

The consequences of turbulence for spatial modulation were examined by Shapiro in the context of the optical atmospheric channel [12]. The premise of the work was to adaptively estimate the particular spatial modulation at the transmitter that will maximize energy transfer to the receive aperture, i.e. the channel eigenfunction with the largest eigenvalue. The reciprocity of the channel was carefully established allowing the use of a conjugate transponder beacon. With this feedback, the transmitter would converge to

the optimal (maximum energy transfer) spatial modulation state. The turbulence was modeled with the "frozen-field" approximation in that it was viewed as stepping through a random sequence of fixed states each of which is fixed long enough for the conjugate feedback technique to track the system. The underwater acoustic channel is quite dynamic over time scales relevant for telemetry applications and may pose unique challenges to channel feedback techniques. Later work refined the reciprocity arguments [13]. Additional research extended the theory of wide-sense stationary uncorrelated-scatter (WSSUS) channels in a temporal sense (time-delays and temporal-frequency shifts) to its spatial analog with equivalent definitions for overspread and underspread channels [14]. While the issue of channel information feedback is not explicitly addressed in this thesis, the framework developed by Shapiro may provide a suitable foundation for future extensions and may be potentially quite valuable for autonomous underwater vehicle (AUV) applications.

There are two additional references in the literature for using spatial modulation as a means to explicitly increase overall bandwidth efficiency for optical channels. Anderson proposed using the spatial modes of a laser beam to carry information [15]. Data is carried by overall beam intensity (independently of spatial mode structure) while additional bits of information are denoted by the particular combination of spatial modes used. Killen also discussed simultaneous temporal and spatial modulation in a digital optical channel leading to an estimated error probability and an optimum receiver design [16].

The capacity of a general deterministic multi-input, multi-output (MIMO) linear time-invariant Gaussian channel, the so-called multi-variate case, was rigorously derived

without the explicit construct of parallel channels [17]. While these authors follow an approach closely related to that taken in this thesis, they restricted their analysis to capacity calculations and provided no guidance on code construction or, equivalently, what the transmitter should do. In this thesis, specific modulation strategies are derived that enable the construction of parallel channels within the physical channel and optimize several average performance measures.

When spatial modulation was first discussed in the late 1960's, it was considered of limited usefulness to terrestrial wireless radio frequency channels. Such large apertures would be required for a receiver to resolve each transmitter that no further work was done for 25 years. That is not to say that the value of multiple spatial elements was ignored. Since the crucial role of diversity in a Rayleigh fading environment was elucidated by Kennedy [18], many schemes for obtaining diversity have been devised including the use of multiple receive elements [19]. More recently, the idea of using multiple transmitter elements to generate diversity even with a single receive element has been investigated [20, 21]. Narula (1999), in particular, summarizes much of the work in this area and places it into a common context. There is a fundamental difference, however, between spatial diversity and spatial modulation. Diversity seeks to both improve the average SNR available for the channel as well as reduce the probability of low SNR during any given channel realization. Channel capacity scales *logarithmically* with diversity order much as it scales logarithmically with SNR. Under conditions to be discussed in Chapter 2, capacity scales *linearly* with the number of parallel channels much as it scales linearly with additional bandwidth [22]. It should be said that moderate to high SNR is an assumption behind these statements.

Within the last four years, there has been considerable interest in applying spatial modulation to the urban wireless environment. These applications blur the distinction between spatial modulation and spatial diversity by considering the capacity of multi-input, multi-output channels when the physical channel is represented by a matrix of independent, identically distributed (iid) complex Gaussian random variables. A research effort is currently underway at Lucent Technologies to realize the capacity advantages of multiple element arrays. The work is known as Bell Labs Layered Space-Time (BLAST) technology [23, 24]. Given the underlying assumption of iid Rayleigh variables in the channel transfer function matrix, the authors point to the seemingly endless growth in capacity as the number of antenna elements are increased [22]. In fact, those authors propose "cramming in as many antennas as space will allow" as a means to increase capacity. There are, at least, two consequences of the overwhelming emphasis on the iid Rayleigh assumption prevalent in the current research into spatial modulation. First, it masks the limitations that implementations in a physical channel face, namely that more spatial bandwidth can only be achieved if additional propagation paths are resolved. The rank of the transfer function matrix will not grow unbounded with increasing antennas but will saturate as the significant propagation paths become resolvable. Secondly, the iid assumption invariably, and obviously, leads to a signaling strategy that is not channel dependent. Any underlying coherence in the spatial structure is not uncovered or exploited.

Some recent work has begun to extend spatial modulation to the case where the channel transfer function matrix has some degree of coherence. A channel model where the arrivals at each delay in the impulse response are parameterized by a stochastic angle

of arrival has been applied to capacity calculations [25]. The impact of coherence, and the corresponding drop in diversity, is thus accounted for when additional elements are added to the system. A methodology for designing space-time trellis codes has been developed that also allows for correlation between the Rayleigh variables [26]. None of the work to date suggests coherent use of the transmit aperture. In fact, the promised performance may only be obtained if coding is used over enough fading intervals to assure, in some sense, an average channel has been observed.

1.5 Outline of Thesis

The following work, discussing the use of spatial modulation in the underwater acoustic channel, is organized into four chapters.

In chapter 2, the benefits of parallel channels will be developed in an information theoretic context. The increased reliability and capacity that is possible will serve as motivation for the remainder of the work. Having shown that parallel channels are desirable, the transformation of a general, linear time-varying channel into a set of parallel channels will be pursued. Necessary constraints on the time-rate of change for the channel will be introduced. The decomposition will be applied to several, realistic ocean channel simulations. Finally, a set of metrics will be defined and related to the decomposition that enable a communication engineer to optimize performance in such terms as average power throughput, average signal to interference plus noise ratio (SINR) and a mean square error. A significant feature of these metrics is that they may be computed from either an ensemble of channel realizations are from the second and fourth order moment characterizations of the channel. The tools are applied to the same simulations introduced earlier.

In chapter 3, the channel decomposition techniques are applied to data collected in two separate field experiments in the ocean. The number and strength of obtainable parallel channels is given. The temporal stability of the required coherent spatial modulation strategies is explored. The success of the various performance metrics is then assessed when used in these two underwater channels. Finally, in an attempt to relate this work to the ongoing research into spatial modulation through Rayleigh fading channels, the performance metrics are applied to Rayleigh transfer function matrices under various coherence assumptions.

In chapter 4, the communication performance of spatially modulated signals is compared to concurrent signals that are not spatially modulated using telemetry data transmitted during three field experiments. Specifically, symbol error rates and mean square estimation error are reported.

In chapter 5, the body of work is summarized, the principal contributions are enumerated and directions for continued research are outlined.

Chapter 2. A Theoretical Basis for Spatial Modulation in the Underwater Acoustic Channel

While the idea of parallel communication channels distinguished only by their spatial expression has been present in engineering literature for more than three decades, practical applications have thus far been limited to optical channels. Underwater acoustic channels, with their accompanying complex spatial character coupled with severe bandwidth constraints, offer a promising new arena for applying the communication design principles of parallel channels. The following discussion will begin with a review of parallel channels in the context of information theory including a parameterization of the benefits in terms of available power and noise spectrum. A methodology will then be presented that decomposes a general multiple input – multiple output linear time-variant channel description into a set of parallel channels allowing linkage to performance metrics such as the reliability function, capacity, and bit error rate. Application to a range of practical ocean channels will be demonstrated via simulation. A discussion of techniques that provide a decomposition for an ensemble of channel realizations will conclude the chapter. Until the final section, the underwater channel will be considered time-varying but still deterministic.

2.1 The Information Theoretic Value of Parallel Channels

Communication over many physical channels inevitably involves distortion of the original information. The goal of the communications engineer is to design suitable signal processing for both before and after transmission that minimizes some measure of that distortion. In recognition of the dominant trend towards digital communication, the analysis will be restricted to discrete information sources and, therefore, the probability

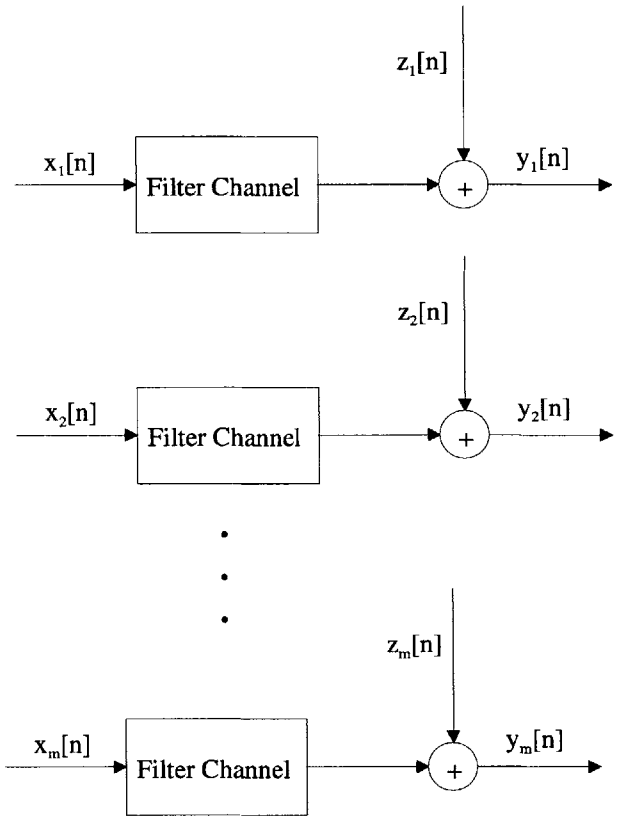

Figure 2.1. Block depiction of a bank of parallel filter channels. As indicated, the output $y_i[n]$ is independent of both the noise $z_j[n]$ and the signal $x_j[n]$ for $i \neq j$.

of error will be the distortion measure of interest. A number of excellent comprehensive texts on information theory have been written [27, 28]. Only relevant results will be summarized, specifically a description of parallel channels and expressions for relating power and noise to the probability of error. Additionally, some familiarity with information theory concepts such as code words and block lengths will be assumed.

A communication channel may be defined as a system whose outputs depend probabilistically on its inputs. Parallel channels are obtained when the distortion posed by one such channel is independent of the signal and distortion on any other available channels. A bank of parallel filter channels with additive noise is shown schematically in figure 2.1. In principle, parallel channels may be formed in several manners. A single

telephone user may have several telephone lines available. A single radio frequency channel may be divided into independent frequency bands. Communication systems employing multi-carrier modulation, in fact, do treat the channel as such. Underwater acoustic channels, as will be shown, support multiple spatial modes accessible by transmit and receive arrays. Irrespective of the underlying physical description, the simple model of figure 2.1 may be used to give useful bounds on the error probability and capacity of parallel channels.

The introduction of parallel channels begins with the assumption that the effect of the physical channel may be reduced to application of a gain factor. This may be justified in two manners. First, each filter channel may be further decomposed into a bank of parallel channels with suitable bandpass filters in front of each. Asymptotically, one may achieve a channel with a uniform frequency response across each signal by making the filters sufficiently narrowband thereby reducing the channel to a complex gain. This claim requires that the channel be underspread, i.e. that its coherence time is much greater than the total delay spread, in order to coherently filter over a long enough period of time to resolve and estimate frequency bins much less than (delay spread)$^{-1}$. This underspread condition will be assumed again later and stands as a primary assumption of this approach. If each of these narrowband channels is to be used as a parallel channel, then the symbol rate on each must be much less than (delay spread)$^{-1}$. The reduction of the physical channel to a set of flat fading channels is not required to implement spatial modulation but serves to demonstrate that the results for AWGN channels are applicable. Another perspective would idealize the channel by moving the filter through the summation and placing the filter inverse in the noise path. Filtering the

received signal cannot diminish the performance of the optimal receiver as any signal not passed by the filter would not pass through the channel. The communication model then becomes one of pure, additive colored Gaussian noise which is also reducible to the complex gain model upon suitable frequency filtering. In any event, these assumptions are only required to simplify the model enough to make reliability calculations tractable. In the next section, the generation of parallel channels in arbitrary underwater channels will be described with the assumptions clearly stated.

Gallager [9] considered the case where the signal power and noise of each channel are fixed and identical block lengths are used for coding. Ebert [10] generalized the analysis allowing the distribution of a fixed amount of signal energy to become an additional degree of freedom. He arrives at a solution for channel capacity that is now commonly known as the "water-filling" theorem describing how a fixed signal power should be allocated among channels of given noise variance. In addition, tight bounds on the exponential behavior of the probability of error P_e are proven. Our description will closely follow that of Greenspan [11] who applied Ebert's results to an electromagnetic radiation channel.

By assuming that a maximum likelihood decoder is used and that the noise statistics are Gaussian, the probability that the receiver will incorrectly decide which of K code words was transmitted is bounded by,

$$P_e \leq Be^{-E[\rho,N_b,S,R]} \tag{2.1}$$

B is a constant related to the free parameter, ρ, the source probabilities, and the code word energy constraint, S, and, as such, will not be further considered. N_b is an energy threshold to be derived. R is the rate at which information is produced by the source. If each code word is equally likely then $R = \log_2 K$ (bits/channel use). The

reliability function, E, is the quantity of interest as it parameterizes the exponential behavior of P_e.

For this analysis, a block length of 1 will be presumed. In general, the reliability function simply scales with the block length. To show this, consider the case where the optimal power distribution for a block length of 1 has been determined. The reliability function for each individual parallel channel may then be computed. Block coding may then be employed on each of the parallel channels thereby scaling the reliability functions by the block length as Gallager shows for the single additive, white Gaussian noise channel [28]. The union bound can then be invoked to state the overall probability of error is upper bounded by the sum of error probabilities for each channel. Finally, each term in the sum can be replaced by the largest term resulting in the desired exponential behavior of error probability with block length. As such, any choice of rate and energy that results in a positive value of E for the parallel combination implies the existence of some block length N_{min} for which any block length greater than N_{min}, P_e could be made smaller than an arbitrary positive value ε. The rate at which the reliability function equals zero is, thus, the channel capacity as reliable transmission is no longer possible for any block length. The reliability function, E, will now be derived in terms of the number and associated noise variances of the available parallel channels. The reader is referred to one of the earlier references for a more complete derivation. Instead, the steps required for a given reliability calculation will be presented.

The first step is to compute the energy threshold, N_b. It is a threshold in the sense that the optimal distribution of signal energy among the parallel channels is defined by,

$$\sigma_i = \max(0, N_b - N_i) \qquad 2.2$$

where N_i is the noise variance and σ_i is the signal variance in the i^{th} parallel channel. There are two regimes to be considered depending on whether or not $dE(\rho)/d\rho$ equals zero for some value of ρ between 0 and 1. For a given value of R (nats/channel use), N_b may be *provisionally* computed with equation 2.3.

$$R = \frac{1}{2} \sum_{N_i \le N_b} \ln \frac{N_b}{N_i} \qquad 2.3$$

This relationship is *only* valid when the total derivative of the reliability function with respect to ρ is zero, i.e. ρ is a stationary point of $E(\rho)$, as it results from setting that condition. The parameter ρ_{opt} is then determined from equation 2.4 with the computed value of N_b and the given value of S.

$$S = \sum_{N_i \le N_b} \frac{(1+\rho)^2 (N_b - N_i)}{1 + \rho - \rho \dfrac{N_i}{N_b}} \qquad 2.4$$

If the calculated value of ρ_{opt} exceeds 1, then ρ_{opt} must be set equal to 1 as the bound which it is based on is not valid for $\rho > 1$. In this case, equation 2.3 is invalid and N_b is, instead, computed directly from equation 2.4 with $\rho = 1$. Equation 2.4 is valid for all admissible ρ given S. Having now determined N_b and ρ_{opt}, the maximum value of the reliability function can then be computed from equation 2.5.

$$E(\rho_{opt}, N_b, S, R) = \frac{\rho_{opt} S}{2(1+\rho_{opt}) N_b} - \frac{1}{2} \sum_{N_i \le N_b} \ln\left(1 + \rho_{opt} - \rho_{opt} \frac{N_i}{N_b}\right) + \frac{\rho_{opt}}{2} \sum_{N_i \le N_b} \ln \frac{N_b}{N_i} - \rho_{opt} R \qquad 2.5$$

If $\rho_{opt} <= 1$ and equation 2.3 is valid then the last two terms cancel. While this derivation was brief, the following analysis simply exercises these three equations.

There are several critical values that serve to describe the overall behavior of the reliability function and, hence P_e. By inspection, if ρ =0 then the reliability function goes to zero. Thus, $\rho = 0$ occurs at the capacity of the set of parallel channels. Defining M to be the number of parallel channels whose noise variance falls below N_b and are therefore used, then equations 2.3 and 2.4 may be used to define the capacity C (nats/channel use) by setting $\rho_{opt} = 0$.

$$C = \frac{1}{2} \sum_{N_i \le N_b} ln \frac{\left(S + \sum_{N_j \le N_b} N_j \right)}{MN_i} \qquad 2.6$$

In the special case that the M parallel channels have identical noise variances $N_0/2$, this reduces to equation 2.7.

$$C = \frac{M}{2} \ln\left(1 + \frac{2S}{N_0 M} \right) \qquad 2.7$$

Figure 2.2 shows the ratio of M-channel capacity to single channel capacity for values of M as a function of signal to noise ratio (S/N_0). For low values of S/MN_0, the overall capacity is asymptotically unaffected by the number of parallel channels and tends towards S/N_0. For large values of S/MN_0, the capacity is essentially proportional to M in that it tends towards $(M/2)\ln(2S/MN_0)$. For the case of equal noise variance per channel, it is always better to spread your energy over as many channels as possible. For large values of S/N_0, the benefit is large. For small values of S/N_0, the benefit is small and asymptotically vanishes as S/N_0 vanishes. Spatial modulation, therefore, is mostly beneficial in bandwidth limited scenarios rather than power limited scenarios.

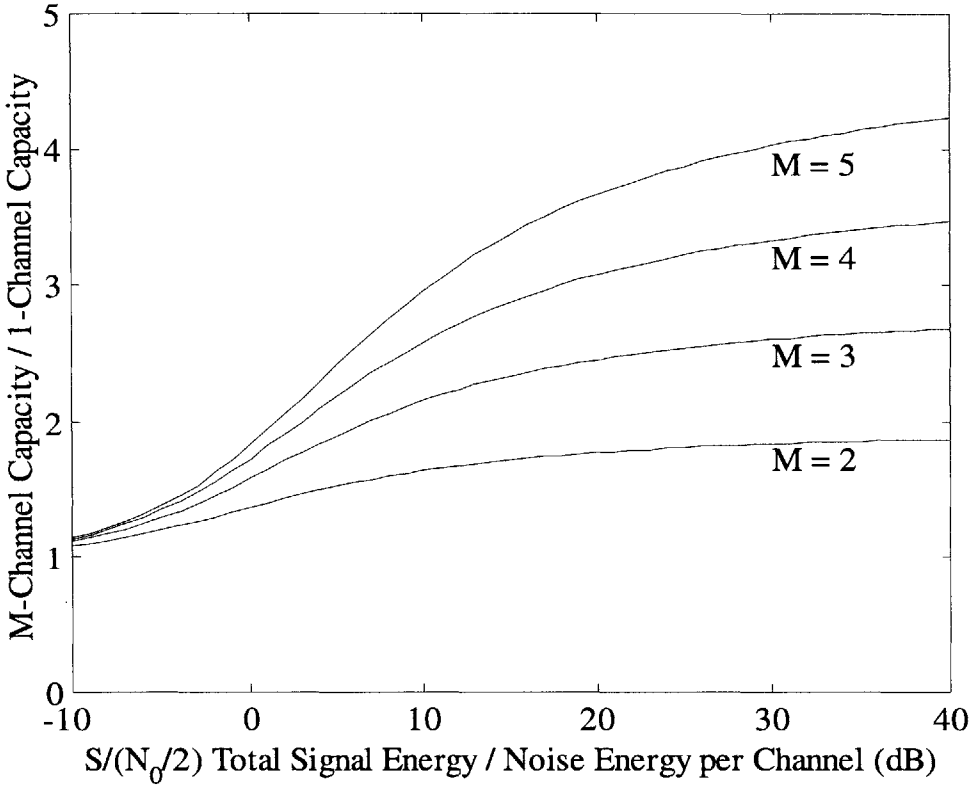

Figure. 2.2. Assuming M channels of identical noise energy, $N_0/2$, the ratio of the M-parallel channel capacity to the 1-channel capacity is shown as a function of the ratio between total signal energy, S, and $N_0/2$ (SNR). For low SNR per channel, the capacity ratio is essentially 1 implying no benefit to distributing energy over more than 1 channel. For modest to high values of SNR, the capacity roughly scales with M.

Another important limiting case is when the signal energy, S, is fixed and M is allowed to grow large. In this case, the M-channel capacity asymptotically approaches S/N_0 while the 1-channel capacity is fixed at ½ ln(1+ S/N_0). For large values of S/N_0, the capacity initially grows almost linearly with M but begins to saturate as $M > S/N_0$.

In most practical scenarios, the noise variances of the available channels are not equal. As such, it is useful to consider the capacity improvement for a two parallel channel system as a function of the difference in noise variance between the two channels. In that case,

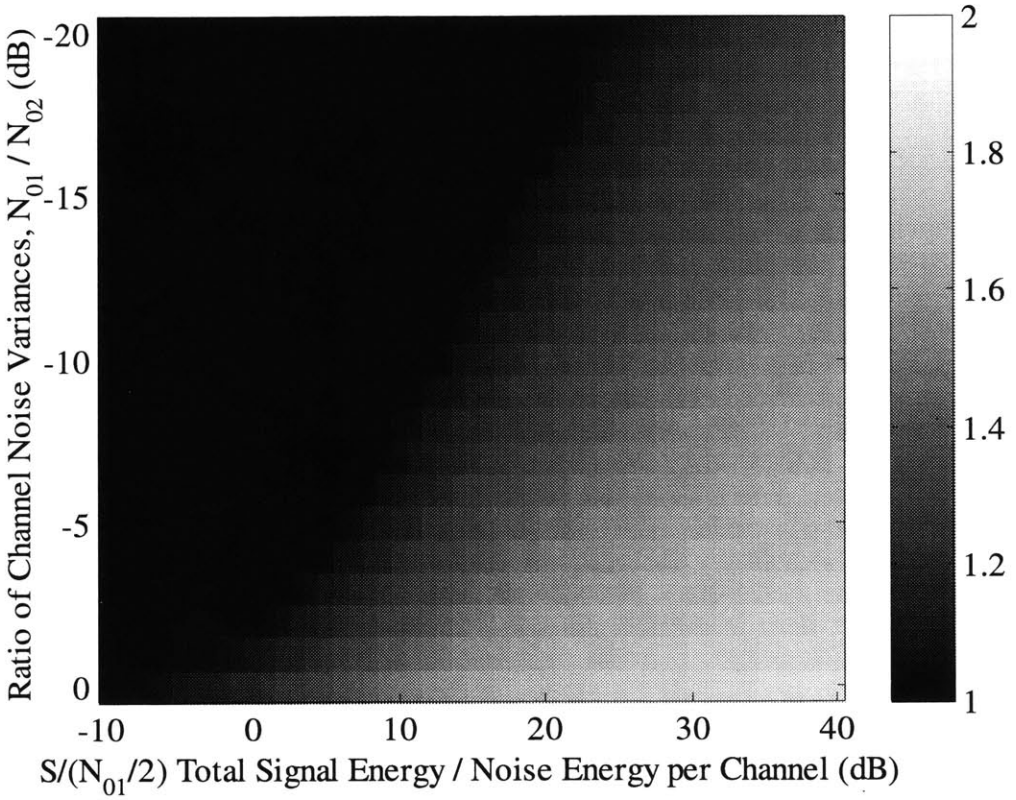

Figure 2.3. Assuming two parallel channels where the first channel has noise variance, $N_{01}/2$, and the second channel has noise variance, $N_{02}/2$, the ratio of the two channel capacity to the capacity of only the first channel is shown. S is the code word energy constraint. For SNR values between 10 and 20 dB, significant capacity benefits remain even with 3 to 8 dB greater noise variance on the second channel.

$$C = \begin{cases} \frac{1}{2}\left\{ ln\left(\frac{S}{N_0} + \frac{1}{2} + \frac{1}{2\alpha} \right) + ln\left(\alpha\frac{S}{N_0} + \frac{1}{2} + \frac{\alpha}{2} \right) \right\} & if\ \alpha\left(1 + \frac{S}{N_0} \right) \le 1 \\ \frac{1}{2} ln\left(1 + \frac{2S}{N_0} \right) & otherwise \end{cases} \qquad 2.8$$

where $N_0/2$ is the noise variance of the first channel and α is the ratio between the noise variance of the first channel and the second channel. The ratio of the 2-channel capacity to that of only using the first channel is shown as a function of α and $S/(N_0/2)$ in figure 2.3. For SNR ranging between 10 and 20 dB, significant capacity benefits remain even if the second channel has a 3 to 8 dB greater noise variance.

Existing communication systems in the underwater channel typically fall far short of ideal performance limits. To clarify the value of parallel channels for more practical signals, consider the improvements in symbol error probability afforded by parallel channels to *P*-ary quadrature amplitude modulation (QAM) over a single channel. An exact expression for the probability of symbol error for independent QAM over *M* parallel channels with a symbol constellation patterned on a rectangular grid is given in equation 2.9 [19].

$$P_e = 1 - \prod_{m=1}^{M} \left(1 - 2\left(1 - \frac{1}{\sqrt{P}}\right) erfc\left(\sqrt{\frac{3\varepsilon_m}{(P-1)N_{0m}}} \right) \right)^2 \qquad 2.9$$

The number of symbols in the constellation, P, must be an even power of 2 in this expression while ε_m is the average energy per symbol for the m^{th} channel and N_{0m} is the variance of the additive, white Gaussian noise process for the m^{th} channel. As expected, the complementary error function (erfc) also appears. Symbol error probabilities for sending $\log_2(P)$ bits over 1 channel may be compared to sending $\log_2(P/2)$ bits over each of 2 parallel channels at half the average power per symbol (but equivalent power per bit). As a specific example, the transmission of 4 bits per channel use with 16 level quadrature amplitude modulation over 1 channel to simultaneous transmission of 2 bits per channel use with quadrature phase shift keying modulation over two channels will be analyzed (figure 2.4). Note that bit error rate rather than symbol error probability have been presented. Bit error rates were computed by scaling the symbol error rate by the average number of bits errors per symbol error. The use of spatial modulation, in this case, leads to equivalent bit error rates with an SNR reduction of over 4 dB. This performance advantage is termed diversity gain in this work. Under other

communication system constraints, the improvement is even larger. For instance, if the channels are peak power limited rather than average power limited then the 16 QAM constellation minimum symbol distance contracts resulting in an equivalent 2.55 dB SNR decrease relative to the QPSK case. A more subtle constraint exists when the channel noise results from residual intersymbol interference. In such a case, the noise power on each channel is a fraction of the signal power on the channel. Such a condition would, in principle, impart a 3 dB diversity gain to the spatial modulation cases as the additive noise, N_{0m}, for the m^{th} channel is reduced in proportion to the lower symbol energy, ε_m.

Parallel channels, when available, allow communication performance

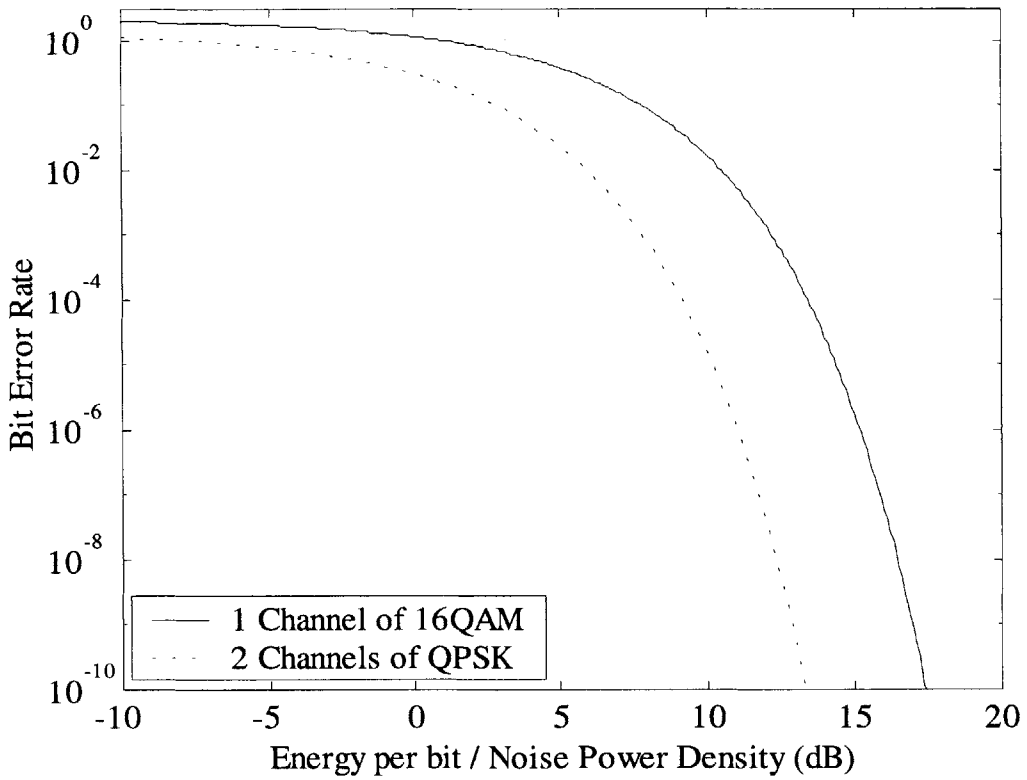

Figure 2.4. Using an expression for the error probability of P-ary quadrature amplitude modulation over parallel additive white Gaussian noise channels, the performance of 16 level quadrature amplitude modulation, 16 QAM, (solid line) over a single channel is compared to the performance of independent 4 level QAM signals over each of 2 parallel channels (dotted line). A constraint is imposed that the average energy per bit is constant and noise power density is the same on all channels. In this example, spatial modulation affords the equivalent of a 4 dB SNR gain.

improvements as quantified by metrics including channel capacity and bit error rate. The effects predominantly accrue to bandwidth limited channels rather than power limited channels. The next task is to show how parallel channels may be obtained from the physical ocean acoustic channel.

2.2 Relating the Physical Channel to Parallel Channels

Evaluation and optimization of a spatially modulated underwater acoustic communication system requires an analytic framework to bridge the gap between the parallel channel formalism and the physical channel. Such an analytic framework begins with the general linear time-variant channel formalism developed by Bello [29]. As noted before, all channel descriptions will be viewed as deterministic. Extensions to stochastic descriptions will be considered in the final section of the chapter. The discussion will begin with the question of how and when continuous-time, vector functions may be decomposed into a set of complete orthonormal (CON) singular functions. These are relevant because the singular functions have the essential property that when one of each function pair (the right singular vector) is applied to the channel input, it generates an output that is orthogonal (in an inner product sense) to the output due to any other right singular vector. Each singular vector pair describes a parallel channel within the overall physical channel. A more detailed discussion of their properties is embedded in the following analysis. This first section will focus on the time-variant impulse response, $h(t,u)$, which represents the signal received at time, t, due to an impulse at time u. Although the technique is valid for general, time-varying channels, the impulse response will be assumed stationary, i.e. only a function of $(t-u)$, over the observation interval and a particular decomposition strategy will be outlined.

The next section will present an alternative derivation of, essentially, the same decomposition strategy. Rather than manipulate the time-variant impulse response, this second approach begins by defining the input delay spread function, $g(t,\delta)$ which represents the response at time t due to an impulse δ seconds in the past. If one considers a communication architecture where there are S transmitters and R receivers, then there exist $S*R$ input delay spread functions or, equivalently, time-variant impulse responses coupling all of the transmitter and receiver pairs. For notational convenience, the set of input delay spread functions is redefined to be the R by S matrix $\mathbf{g}(t,\delta)$ and the set of time-variant impulse responses to be the R by S matrix $\mathbf{h}(t,u)$. Having shown the decomposition steps, a series of examples will then be presented to gain insight into the physical nature of the mathematical decomposition.

While the analysis presented in this section may be amenable to a stochastic interpretation, all channels will be considered deterministic. Techniques for creating truly parallel channels (in the sense defined in section 2.1) will be developed. Crafting spatial modulation strategies that give desirable performance over an ensemble of channels is considered in section 2.3. In that case, interference between the multiple spatially modulated signals inevitably exists and design strategies are sought to minimize that interference.

2.2.1 Decomposition of the Time-Variant Impulse Response

The pressure signal, $\mathbf{y}(t)$, measured at the R receive array elements may be expressed in terms of a superposition of the pressure signal present at the S transmit array elements, $\mathbf{x}(t)$, and $\mathbf{h}(t,\delta)$. The impulse response is a composite one in that all filtering effects including modulation, pulse-shaping, channel dispersion, and receive bandpass

filtering are viewed as a single, aggregate system response. The received pressure signal is then,

$$\mathbf{y}(t) = \int_0^{T_1} \mathbf{h}(t,u)\mathbf{x}(u)\mathrm{d}u \qquad 2.10$$

where the input, $\mathbf{x}(u)$, is defined over an interval $[0,T_1]$ for the time index, u. A set of CON vector functions, $\phi_i(u)$, will be sought such that the channel outputs when excited by two such functions, $\phi_i(u)$, and $\phi_j(u)$, are orthogonal in the sense of equation 2.11.

$$\lambda_i^2\delta_{ij} = \int_{t_0}^{t_0+T_2} \mathbf{y}_i^H(t)\mathbf{y}_j(t)dt \qquad 2.11$$

As before, δ_{ij} represents the Kroenecker delta. The channel output, $\mathbf{y}(t)$, is defined over an interval $[t_0,t_0+T_2]$ for the time index, t. The received energy when the channel is excited with $\phi_i(u)$ is λ_i^2. The above requirement imposes a constraint on which set of CON functions may be used. Expanding 2.11 with the use of 2.10,

$$\lambda_i^2\delta_{ij} = \int_{t_0}^{t_0+T_2} \left[\int_0^{T_1} \phi_i^H(u_1)\mathbf{h}^H(t,u_1)du_1\right]\left[\int_0^{T_1} \mathbf{h}(t,u_2)\phi_j(u_2)du_2\right]dt \qquad 2.12$$

If the order of integration is changed, the constraint may be rewritten in a, perhaps, more familiar form.

$$\lambda_i^2\delta_{ij} = \int_0^{T_1} du_1 \int_0^{T_1} du_2 \phi_i^H(u_1)\mathbf{K}_x(u_1,u_2)\phi_j(u_2) \qquad 2.13$$

The input kernel function, $\mathbf{K}_x(u_1,u_2)$, is defined as,

$$\mathbf{K}_x(u_1,u_2) = \int_{t_0}^{t_0+T_2} \mathbf{h}^H(t,u_1)\mathbf{h}(t,u_2)dt \qquad 2.14$$

Viewing the time-variant impulse response as a deterministic quantity leads one to interpret the input kernel function as a simple average over the output time interval. While this analysis may be amenable to a stochastic treatment of $\mathbf{h}(t,u)$, random behavior of the channel will not be considered until section 2.3. By invoking the orthonormal properties of $\phi_i(u)$, a necessary and sufficient condition for the equality in 2.13 is,

$$\lambda_i^2\phi_i(u_1) = \int_0^{T_1} du_2 \mathbf{K}_x(u_1,u_2)\phi_i(u_2) \qquad 2.15$$

If the input kernel function is non-negative definite, then Mercer's Theorem [30] ensures that $\mathbf{K}_x(u_1,u_2)$ may be expanded in the input singular functions, $\phi_i(u)$.

$$\mathbf{K}_x(u_1,u_2)=\sum_{k=1}^{\infty}\lambda_k^2\phi_k(u_1)\phi_k^H(u_2) \tag{2.16}$$

To prove the non-negativeness of $\mathbf{K}_x(u_1,u_2)$, consider exciting the channel with an arbitrary, finite-energy, waveform $\mathbf{x}(u)$. The channel output is easily found with 2.10. Paralleling 2.11 – 2.13, the energy in the output waveform, ε, is found to be,

$$\varepsilon=\int_0^{T_1}du_1\int_0^{T_1}du_2\mathbf{x}^H(u_1)\mathbf{K}_x(u_1,u_2)\mathbf{x}(u_2) \tag{2.17}$$

Since the channel is known to be a physically realizable, passive medium, the output energy must be finite and non-negative. The fact that 2.17 is non-negative for all finite-energy functions, $\mathbf{x}(u)$, is sufficient to declare $\mathbf{K}_x(u_1,u_2)$ non-negative definite and allow Mercer's Theorem to be applied.

To obtain the output singular functions, $\theta_i(t)$, we begin by *postulating* that they must provide a singular value decomposition of the time-variant impulse response.

$$\mathbf{h}(t,u)=\sum_{k=1}^{\infty}\lambda_k\theta_k(t)\phi_k^H(u) \tag{2.18}$$

By evaluating 2.18 at $t = t_1$, post-multiplying each side by its transpose at another time, t_2, and integrating over the input time interval, the following equality is obtained.

$$\mathbf{K}_y(t_1,t_2)\equiv\int_0^{T_1}\mathbf{h}(t_1,u)\mathbf{h}^H(t_2,u)du=\int_0^{T_1}\sum_{k=1}^{\infty}\sum_{j=1}^{\infty}\lambda_k\lambda_j\theta_j(t_1)\phi_k^H(u)\phi_j(u)\theta_j^H(t_2)du \tag{2.19}$$

By invoking the orthonormal properties of the singular functions, the requirement that 2.18 be true requires the output kernel function, $\mathbf{K}_y(t_1,t_2)$, to be expressible as a sum over the output singular functions, $\theta_k(t)$.

$$\mathbf{K}_y(t_1,t_2)=\sum_{k=1}^{\infty}\lambda_k^2\theta_k(t_1)\theta_k^H(t_2) \tag{2.20}$$

Recognizing this as Mercer's Theorem, $\mathbf{K}_y(t_1,t_2)$, must be shown to be non-negative definite. Specifically, equation 2.17 must be proven for $\mathbf{K}_y$. While reciprocity is not

required of the channel in this development, if such a condition holds then $\mathbf{K}_x$ and $\mathbf{K}_y$ simply interchange roles for propagation from the receive array to the transmit array.

If the definition of K_y (equation 2.19) is substituted into equation 2.17 with $\mathbf{K}_x$ for $\mathbf{K}_y$, a rearrangement of terms results in equation 2.21.

$$\varepsilon = \int_0^{T_1} \left[\int_0^{T_2} \mathbf{z}(t_1)\mathbf{h}(t_1,u)dt_1 \right]^H \left[\int_0^{T_2} \mathbf{z}(t_2)\mathbf{h}(t_2,u)dt_2 \right] du \equiv \int_0^{T_1} \mathbf{q}^H(u)\mathbf{q}(u)du \geq 0 \qquad 2.21$$

While $\mathbf{q}(u)$ does not have a simple interpretation, it clearly must have non-zero energy. Thus, $\mathbf{K}_y$ is shown to be non-negative definite.

Finally, each side of 2.20 is post-multiplied by $\theta_j(t_2)$ and integrated over the output observation interval yielding the expected integral eigenvalue equation for the output kernel function.

$$\lambda_j^2 \theta_j(t_1) = \int_{t_0}^{t_0+T_2} dt_2 \mathbf{K}_y(t_1,t_2)\theta_j(t_2) \qquad 2.22$$

While 2.15 and 2.22 may be solved to yield a singular value decomposition for an arbitrary time-varying impulse response matrix, the task may prove daunting. Solution techniques exist for several classes of kernel functions such as time shift invariant processes with rational or bandlimited spectra or a non-stationaryWiener random process [30]. For the present application, two simplifying assumptions will be made. First, the impulse response matrix is assumed to be stationary, or time-shift invariant, over the observation interval (but still possibly time-variant as with a pure Doppler shift) implying that all impulse response time dependencies are of the form ($\delta = t\text{-}u$). As a practical matter, an accurate representation of the impulse response for an underwater acoustic telemetry channel requires an in-situ measurement. The lengthy propagation delays (channel latency) as well as the averaging inherent in many measurement approaches

limit the estimates to mean values over an interval. This assumption will clearly lead to residual errors but results in a stationary estimate. The second assumption is that the observation interval is substantially longer than the total delay spread of the channel. In particular, $1/T_1$ and $1/T_2$ represent frequency scales that are much smaller than the scale over which the channel frequency response varies. This assumption ensures that the kernel functions are approximately functions of $(u_1 - u_2)$ and $(t_1 - t_2)$. With these assumptions in hand, asymptotic solutions to 2.15 and 2.22 will be sought.

If the observation intervals were infinite and the impulse response was time-invariant, one singular function equation becomes,

$$\lambda_j^2 \theta_j(t_1) = \int_{-\infty}^{+\infty} dt_2 \mathbf{K}_y(t_1 - t_2)\theta_j(t_2) \qquad 2.23$$

In this case, the singular functions are complex exponentials. As an approximation, begin by defining two constants, $f_x = 1/T_1$ and $f_y = 1/T_2$. The following solutions forms will be tried,

$$\theta_n(t) = \frac{1}{\sqrt{T_2}} \hat{\theta}_n e^{j2\pi f_y n t} \quad ; \quad \phi_m(u) = \frac{1}{\sqrt{T_1}} \hat{\phi}_m e^{j2\pi f_x m u} \qquad 2.24$$

The vectors, $\hat{\theta}_n$ and $\hat{\phi}_m$, are unique constants vectors for each singular function. If these trial solutions are used inside the integrals of 2.15 and 2.22, the kernel functions, $\mathbf{K}_x(u_1 - u_2)$ and $\mathbf{K}_y(t_1 - t_2)$, are expressed in terms of their Fourier integrals ($\mathbf{S}_x(f)$ and $\mathbf{S}_y(f)$), and the integrations over u_2 and t_2 are carried out, the singular function equations become,

$$\lambda_m^2 \phi_m(u_1) = \frac{1}{\sqrt{T_1}} \hat{\phi}_m \int_{-\infty}^{+\infty} df e^{j2\pi f u_1} \mathbf{S}_x(f) \left[\frac{\sin(\pi T_1(mf_x - f))}{\pi(mf_x - f)} \right] \qquad 2.25a$$

$$\lambda_n^2 \theta_n(t_1) = \frac{1}{\sqrt{T_2}} \hat{\theta}_n \int_{-\infty}^{+\infty} df e^{j2\pi f t_1} \mathbf{S}_y(f) \left[\frac{\sin(\pi T_2(nf_y - f))}{\pi(nf_y - f)} \right] \qquad 2.25b$$

Recalling the earlier assumption regarding the observation intervals, T_1 and T_2, the sinc functions may be approximated as Dirac delta functions centered at mf_x and nf_y respectively. With that assumption, the trial solution is found to satisfy the singular function equation. Finally, expressions for the time-independent components of the input and output singular functions are obtained.

$$\lambda_m^2 \hat{\phi}_m = \mathbf{S}_x(mf_x)\hat{\phi}_m \text{ and } \lambda_n^2 \hat{\theta}_n = \mathbf{S}_y(nf_y)\hat{\theta}_n \qquad 2.26$$

If there are S transmitters and R receivers, then the Fourier transformed stationary kernel functions, $\mathbf{S}_x$ and $\mathbf{S}_y$, are of dimension S by S and R by R, respectively. To aid in the bookkeeping of singular functions, the subscripts may be modified to indicate both which frequency component as well as which solution of 2.26 they represent. The input (right) singular functions are then denoted by $\hat{\phi}_{sm}$, where $1 \leq s \leq S$ and $0 \leq m \leq \infty$, and the output (left) singular functions are denoted by $\hat{\theta}_{rn}$, where $1 \leq r \leq R$ and $0 \leq n \leq \infty$.

The development embodied in equations 2.23 to 2.26 transform the decomposition from a single, continuous time, vector SVD to a set of independent, conventional SVDs. If T_1 is set equal to T_2, a single frequency step constant, f_0, may be defined. The decomposition for each frequency index, m, is then the SVD of $\mathbf{T}(mf_0)$ where $\mathbf{T}$ is the channel transfer function, the Fourier transform of $\mathbf{h}(\delta)$, and is related to the vector constants, $\hat{\theta}_m$ and $\hat{\phi}_m$, by,

$$\mathbf{T}(mf_0) = \Theta(mf_0)\Lambda(mf_0)\Phi^H(mf_0) \qquad 2.26a$$

The columns of Θ and Φ are the eigenvectors defined in 2.27 and Λ is a diagonal matrix with entries defined by the eigenvalues of 2.27.

The singular value decomposition process for a stationary matrix of channel impulse responses is then as follows. The matrix is Fourier transformed in the single

delay variable (t-u). At each frequency, the singular values and right singular functions of $\mathbf{S}_x(m/T_1)$ are computed. If the channel is then excited with a right singular function, it will respond with the corresponding left singular function with the singular value defining the amount of transferred energy for a unit energy input. In fact, the left singular functions may be computed by exactly that operation. The complete equivalence of spatial degrees of freedom and temporal degrees of freedom is clear in this analysis as no distinction is made between them (subscripts s, r, m, and n). If the channel is band-limited (bandwidth, W), a finite number of these singular functions are expected to have significant, non-zero singular values. In that case, if the singular functions are arranged in order of decreasing singular value, only singular functions with indices in the range $0 < m < 2W\min(T_1,T_2)$ are expected to convey significant energy through the channel. Similarly, the product of the array apertures and the wavenumber spread of the channel relates to the number of useful spatial degrees of freedom. Referring to the band-limited channel again, the maximum number of degrees of freedom is $2W*\min(T_1,T_2)*\min(S,R)$. Therefore, spatial degrees of freedom *multiplicatively increase* the total degrees of freedom. The results of this section may also be reached through an approach emphasizing filtering theory as follows in the next section.

2.2.2 Decomposition of the Input Delay Spread Function

The alternative derivation begins at the same point but considers the input delay spread function rather than the time-variant impulse response. The pressure signal, $y(t)$, measured at the R receive array elements may be expressed in terms of a delay integral involving the pressure signal present at the S transmit array elements, $x(t)$, and a composite channel input delay spread function matrix, $g(t,\tau)$. The delay-spread response

is a composite one in that all filtering effects including modulation, pulse-shaping, channel dispersion, and receive bandpass filtering are viewed as a single, aggregate system response. The received pressure signal is then,

$$\mathbf{y}(t) = \int_{0}^{+\infty} \mathbf{g}(t,\tau)\mathbf{x}(t-\tau)d\tau \qquad 2.27$$

The input signal, $\mathbf{x}(t)$, is the vector sum of the signals for the K parallel channels, $\sum_{k=1}^{K} \mathbf{x}_k(t)$. Anticipating the strategy for separating the overall channel into a set of parallel channels, consider an estimate for the source time series, $s_k(t)$, sent over the k^{th} channel formed through convolution of the received signal with an arbitrary time varying filter, $\mathbf{b}_k$. The transmitted signal vector for the k^{th} channel, $\mathbf{x}_k$, is formed by convolving s_k with an arbitrary time-varying vector filter $\mathbf{a}_k$.

$$\mathbf{x}_k(t) = \int_{-\infty}^{+\infty} \mathbf{a}_k(t,\delta)s_k(t-\delta)d\delta \qquad 2.28$$

The estimate, $\hat{\mathbf{x}}_k(t)$, may then be expressed as,

$$\hat{\mathbf{x}}_k(t) = \int_{-\infty}^{+\infty} \mathbf{b}_k^H(t,\delta)\mathbf{y}(t-\delta)d\delta \qquad 2.29a$$

$$\hat{\mathbf{x}}_k(t) = \int_{-\infty}^{+\infty} \mathbf{b}_k^H(t,\delta)\int_{-\infty}^{+\infty} \mathbf{g}(t-\delta,\tau)\sum_{k=1}^{K} \mathbf{x}_k(t-\delta-\tau)d\tau d\delta \qquad 2.29b$$

$$\hat{\mathbf{x}}_k(t) = \int_{-\infty}^{+\infty}\int_{-\infty}^{+\infty}\int_{-\infty}^{+\infty} \mathbf{b}_k^H(t,\delta)\mathbf{g}(t-\delta,\tau)\sum_{k=1}^{K} \mathbf{a}_k(t-\delta-\tau,\chi)s_k(t-\delta-\tau-\chi)d\chi d\tau d\delta \qquad 2.29c$$

The entire process for the k^{th} channel is shown in figure 2.5. While different parallel channels have unique filters, all are filtered by the same physical channel, $g(t,\delta)$. In addition, the actual input to the physical channel is the vector sum of all x_k and the output of the physical channel is the vector sum of all y_k.

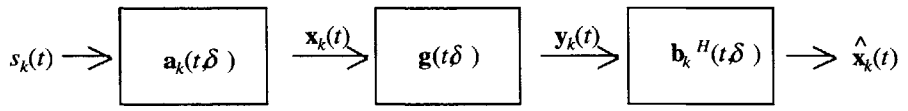

Figure 2.5. A schematic portrayal of all filtering effects between the input for the k^{th} parallel channel and the estimate of what was sent over it is given here. While only a single parallel channel is shown, the actual input and output of $\mathbf{g}(t,\delta)$ is the vector sum of all $\mathbf{x}_k(t)$ and $\mathbf{y}_k(t)$.

Practically, s_k will have finite support only over some range of t while $g(t,\delta)$ will have finite support only over some range of δ. Keeping the integration intervals infinite will nevertheless reinforce the assumption of stationarity and allow the transitions between the time and frequency domains. Considering large intervals to be infinite is consistent with the assumptions made in the previous section. Although a_k and b_k have been allowed to be arbitrary, it is clear that "good" estimates of x_k will require certain filters.

A key assumption must now be invoked. The characteristic time scale over which the filters and impulse response vary is assumed to be large compared to the filter support and delay spread (maximum value of δ with a non-zero response). This is equivalent to a quasi-stationarity assumption. In other words, the delay-bandwidth product of the channel must be much less than unity. Such a channel is known as an underspread channel. In underwater acoustic communication channels, the principal contributor to time-variability is a Doppler shift due to the range rate which, with correct processing, may be removed from consideration. Empirically, it has been observed that many useful channels are underspread [3]. The symbol estimate then becomes,

$$\hat{\mathbf{x}}_k(t) = \int_{-\infty}^{+\infty}\int_{-\infty}^{+\infty}\int_{-\infty}^{+\infty} \mathbf{b}_k^H(t,\delta)\mathbf{g}(t,\tau)\sum_{k=1}^{K}\mathbf{a}_k(t,\chi)s_k(t-\delta-\tau-\chi)\,d\chi\,d\tau\,d\delta \qquad 2.30$$

Equation 2.30 is valid for any pre- and post- filters one might choose. Filters will now be sought that have the properties of yielding estimates that are independent of the

information sent on the other (k-1) channels. In fact, parallel channels are defined as a set of channels where the noise and signals are independent from channel to channel. Stated in a more intuitive manner, the pre-processing filters, $\mathbf{a}_k(t)$, should create spatial signatures on the receive elements that are readily separable using the post-processing filters, $\mathbf{b}_k(t)$.

As an initial step, consider the time variant transfer function matrix, $\mathbf{T}(f,t)$, which is the Fourier transform of the input delay spread function matrix over the delay variable. It may be defined as,

$$\mathbf{T}(f,t) \equiv \int_{-\infty}^{+\infty} \mathbf{g}(t,\delta) e^{-j2\pi f\delta} d\delta \qquad 2.31$$

For each time, t, and frequency, f, a singular value decomposition may be performed.

$$\mathbf{T}(f,t) = \mathbf{U}(f,t)\mathbf{S}(f,t)\mathbf{V}^H(f,t) \qquad 2.32$$

The columns of $\mathbf{V}$ are the right singular vectors and form an orthonormal basis over the source array such that $\mathbf{V}_k^H(f,t)\mathbf{V}_j(f,t) = \delta_{kj}$. Similarly, the columns of $\mathbf{U}$ are the left singular vectors forming an orthonormal basis over the receiver array. Use of the k^{th} right singular vector will result in receiving the k^{th} left singular vector. $\mathbf{S}$ is a diagonal matrix, with the singular values appearing on the diagonal, reflecting the attenuation imposed by the channel with the use of each singular vector pair. As the reader may anticipate, the inverse Fourier transform of the singular vectors will form the pre- and post- filters defined earlier.

An unconstrained degree of freedom enters the problem formulation at this point in that the set of singular vectors obtained at each frequency may be "connected" over frequency in an arbitrary manner prior to implementing the inverse Fourier transform and forming the parallel channel filters, i.e. transforming $\mathbf{V}(f,t)$ to $\mathbf{v}(t,\delta)$. This is actually a

consequence of defining the orthonormal condition at each frequency rather than globally for the filters. A reasonable criterion would be to insist that these functions have derivatives with respect to frequency that are as small as possible. If the transforms are discrete, an approximate criterion would be to "connect" singular vectors that involve the minimum change in the scalar derivative of the singular vector with respect to frequency. If the sampling over frequency is excessively coarse, the proper linkage between singular vectors may be unclear. Although *any* linkage will create parallel channels, it is desirable to form the smoothest functions over frequency as possible to generate the shortest filter lengths over time as possible. One might also seek to maximize total power in one channel. In that case, the singular vectors with the largest singular value at each frequency may be "connected." This approach may, however, result in filters that have longer temporal support. One might imagine other approaches such as linking the filters that are the most stable over time. By appropriate complex scaling of these vectors at each frequency (any such scaling will still preserve parallel channels), one would also be able to generate impulsive responses at the output of the receive filter. While this may be desirable in some circumstances, most underwater acoustic communication systems involve powerful equalization algorithms that seek to accomplish the same effect. Nevertheless, such a criteria may have application in the growing study of phase conjugate mirror techniques in underwater scenarios.

The input delay spread function may then be expressed in terms of the inverse Fourier transforms of the singular vector functions.

$$\mathbf{g}(t,\delta) = \int_{-\infty}^{+\infty}\int_{-\infty}^{+\infty} \mathbf{u}(t,\delta-\chi)\mathbf{s}(t,\tau)\mathbf{v}^{H}(t,\chi-\tau)\,d\tau\,d\chi \qquad 2.33$$

The orthonormal properties of the singular vectors ensure the following relations hold.

$$\mathbf{U}_k^H(f,t)\mathbf{U}(f,t) = [\delta_{1k}, \delta_{2k}, ..., \delta_{Rk}]$$
$$\mathbf{V}_k^H(f,t)\mathbf{V}(f,t) = [\delta_{1k}, \delta_{2k}, ..., \delta_{Sk}] \qquad 2.34$$

where the subscript k denotes the kth column of the matrix and δ_{ik} is the Kroenecker delta. These relationships hold for each frequency. By invoking Parseval's theorem and recalling that the inverse Fourier transform of a constant is the Dirac delta function, the following may be concluded,

$$\int_{-\infty}^{+\infty} \mathbf{u}_k^H(t,\tau-\delta)\mathbf{u}(t,\delta)\mathrm{d}\delta = [\delta_{1k}\delta(\tau), \delta_{2k}\delta(\tau), ..., \delta_{Rk}\delta(\tau)]$$
$$\int_{-\infty}^{+\infty} \mathbf{v}_k^H(t,\tau-\delta)\mathbf{v}(t,\delta)\mathrm{d}\delta = [\delta_{1k}\delta(\tau), \delta_{2k}\delta(\tau), ..., \delta_{Sk}\delta(\tau)] \qquad 2.35$$

where $\delta(\tau)$ is the Dirac delta function. Using the typical notation for the convolution operation, the result of pre-filtering with the inverse Fourier transform of the right singular vector function and post-filtering with the inverse Fourier transform of the left singular vector function may expressed as follows.

$$\mathbf{u}_l^H(t,\delta) * \mathbf{g}(t,\delta) * \mathbf{v}_k(t,\delta) = \mathbf{u}_l^H(t,\delta) * \mathbf{u}(t,\delta) * \mathbf{s}(t,\delta) * \mathbf{v}(t,\delta) * \mathbf{v}_k(t,\delta) \qquad 2.36$$
$$= \begin{Bmatrix} 0 \text{ if } l \neq k \\ s_{kk}(t,\delta) \text{ if } l = k \end{Bmatrix}$$

By selecting the pre- and post-filters to correspond to the right and left singular vector functions, independent communication over parallel channels formed from the original underwater acoustic channel is possible. As will be seen later, linear combinations of these singular vectors will also support spatial modulation with, perhaps, a performance penalty. To reiterate, the formalism of a singular value decomposition is useful for determining optimal performance bounds but does not reflect the only

excitation strategy that will allow a communication system to exploit the concept of parallel channels. The SVD is an analytic tool to explore possible performance over a known, i.e. deterministic, channel. If the channel is uncertain, to some degree, it may be considered stochastic and other strategies may be considered to implement spatial modulation. Such strategies will be discussed in section 2.3.

The question of how many parallel channels are available is a somewhat subtle one. At a given frequency, one may expect, at most, rank$\{\mathbf{T}(f,t)\}$, parallel channels to be available. An estimate based on the singular values will be given in a subsequent section. The underwater channel is often frequency selective, however, which would result in a variable number of parallel channels for each frequency. In this case one might heuristically define a mean by averaging the rank of the time-variant transfer function over frequency. Of course, one may also resort to the expressions for reliability and capacity given in section 2.1 for colored, additive Gaussian noise channels as a definitive characterization of the maximum signaling rate.

One should note that while the inter-*channel* interference is removed, the inter-*symbol* interference (ISI) present on each parallel channel must still be accommodated. The ISI is characterized by $\mathbf{s}(t,\delta)$. The right singular vectors used as pre-transmission filters could be modulated over frequency to ensure $\mathbf{s}(t,\delta)$ be equivalent to the Dirac delta function but this form of pre-coding has typically not been used. Rarely would the channel knowledge be adequate to completely avoid the use of an equalizer at the receiver.

The results of this analysis may be summarized as follows. If the input delay spread functions of the channel vary slowly compared to the temporal delay spread, the

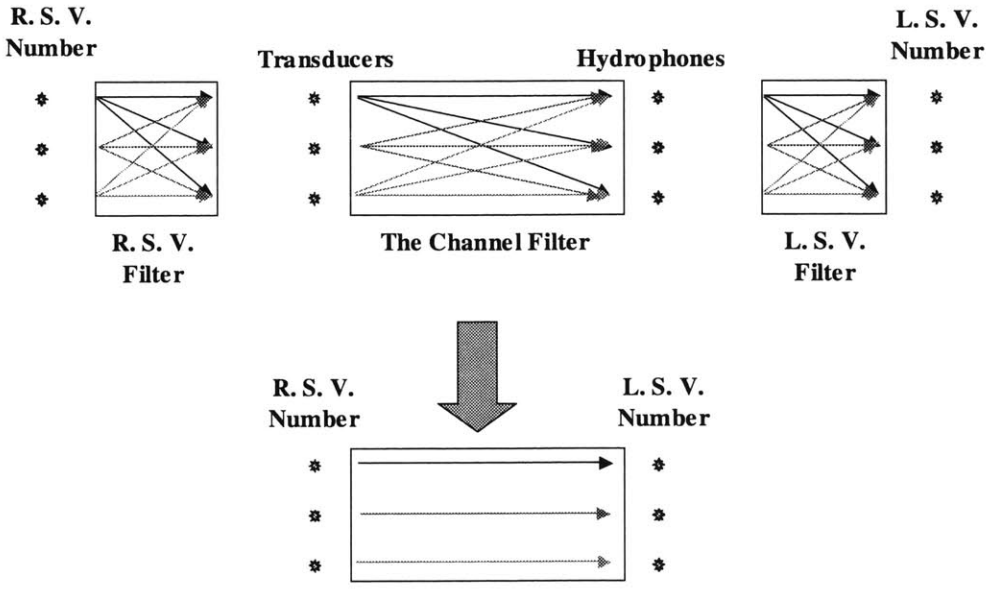

Figure 2.6. If the physical, time-varying channel varies "slowly enough" compared to the total delay spread it induces, the SVD analysis will yield a set of pre- and post- processing filters (the right and left singular vectors, R.S.V.'s and L.S.V.'s) that transform the physical channel into a set of parallel channels, each of which may be frequency selective.

channel may be decomposed into a set of slowly evolving broadband, spatial singular functions which may, in turn, be treated as parallel channels as sketched in figure 2.6.

A possibly fruitful extension may be to consider the output Doppler spread function, $\mathbf{G}(f,\nu)$, of the channel which is simply the input delay spread function Fourier transformed in both its arguments. On a purely speculative note, the constraint on the time-bandwidth product for the channel might be relaxed by considering separate singular value decompositions for each value of ν in $\mathbf{G}(f,\nu)$. Practically, one would accomplish this by passing both the input and output of the channel through a bank of narrowband filters before and after the channel estimation and spatial filtering operations. The process would be similar to computing an ambiguity function from the channel output and performing the decomposition at each frequency sample of the ambiguity function. The complexity of such processing would likely preclude any practical tracking

for instantaneously Doppler spread channels. Such an approach may, however, have application when a few, dominant Doppler rates are present in the system.

A number of simplified, time-invariant channels will now be simulated as an aid to understanding the decomposition process. Four examples will be considered. First, a water column with both a surface duct and deep duct will be idealized with a single transmitter/receiver pair in each channel. Second, a set of transmitter and receiver arrays communicating over a single eigenray will be examined. Third, the same array configuration will be used in a channel composed of two eigenrays. Finally, a parabolic equation based analysis of a shallow ocean waveguide, namely a constant depth water column with a pressure release surface and sandy bottom, will be considered.

2.2.3 Examples of the Decomposition

Example 1: Double Duct

Under some conditions, two ocean sound speed minimums may form over the water column depth with one centered near the surface and the other centered at a much lower depth. If a transducer is placed at each minimum and a receiving hydrophone at some distant range at the same depths (if the system is range invariant), two parallel channels result as depicted in figure 2.7. The lines in that figure represent ray paths, or the path energy emitted by the transducers travels to the hydrophones. The time-variant transfer function, $\mathbf{T}(f,t)$, and its decomposition for this scenario is shown in equation 2.36.

$$\mathbf{T}(f,t) = \begin{bmatrix} 1 & 0 \\ 0 & 1 \end{bmatrix} \begin{bmatrix} T_1(f) & 0 \\ 0 & T_2(f) \end{bmatrix} \begin{bmatrix} 1 & 0 \\ 0 & 1 \end{bmatrix} \qquad 2.37$$

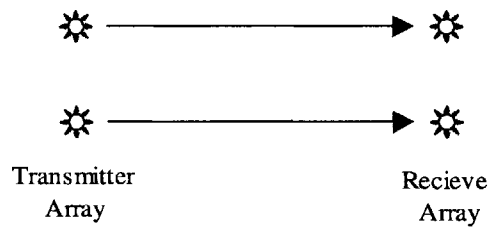

Figure 2.7. The double duct scenario is shown here where each transducers only couples to a unique hydrophone. The lines represent eigenray paths

The function is shown in decomposed form with the transfer functions of the two ducts denoted by T_1 and T_2. In this example, both intuition and analysis concur yielding $\mathbf{u}_1(t) = [\delta(t)\ ,\ 0]$, $\mathbf{u}_2(t) = [0\ ,\ \delta(t)]$, $\mathbf{v}_1(t) = [\delta(t)\ ,\ 0]$, and $\mathbf{v}_2(t) = [0\ ,\ \delta(t)]$, as the pre- and post-filters. Alternatively stated, the top transducer/hydrophone pair form one channel while the bottom pair forms another. The effect of each sub-channel's frequency response must still be equalized but the step is not required for the parallel channel construction. A potentially fruitful avenue of research would consider controlling each parallel channel's frequency response to reduce delay spread (commonly known as pre-coding).

Example 2: Single Eigenray

A more common underwater telemetry scenario includes a modest vertical transducer array used to increase directivity and, hence, signal-to-noise (SNR), for a distant receive array. If the channel was composed of a single eigenray, one would expect the decomposition to yield only one parallel channel with a significant singular value paired with filters that beamform in the appropriate direction. This case is approached with the decomposition formalism developed earlier. $\mathbf{T}_{mn}(f)$, relating transducer n to receiver m, is essentially a pure phase factor,

$$\mathbf{T}_{mn}(f) = e^{j\frac{2\pi f}{c}(d\sin\theta_t)n}\ e^{j\frac{2\pi f}{c}(d\sin\theta_r)m} \qquad 2.38$$

Figure 2.8. The single eigenray example is shown here. A single propagation path connects the M element transducer array to the N element hydrophone array.

where d is the array element spacing (assumed equal for both arrays), c is the sound speed, θ_t is the departure angle of the eigenray and θ_r is the arrival angle (figure 2.8). Without loss of generality, the frequency dependent attenuation factor is neglected as well as the phase factor associated with the distance between array centers.

When a singular value decomposition is performed on this matrix, several items may be noted. First, only one singular value is non-zero at any given frequency corresponding to the idea that only one useful, i.e. capable of conveying energy, spatially distinct communication channel can be culled from the physical channel. The corresponding right singular vector filter, $\mathbf{v}_1(\delta)$, (the transmit array filter) is found to be a steering vector with a constant amplitude that time-delay beamforms precisely to the departure angle of the ray. As it is a linear phase shift in the frequency domain, the time domain response of the filter is a delayed Dirac delta function for each element implying a broadband beamforming operation. The left singular vector, $\mathbf{u}_1(\delta)$, (the receive array filter) is found to also simply broadband beamform in the arrival direction of the channel eigenray. If the channel were frequency selective, only the frequency dependence of the singular values would change. Once again, the analysis and physical intuition align well.

A useful way of graphically depicting the decomposition is to examine the left and right singular vectors in a time-delay versus angle-of-arrival space. Figure 2.9 gives

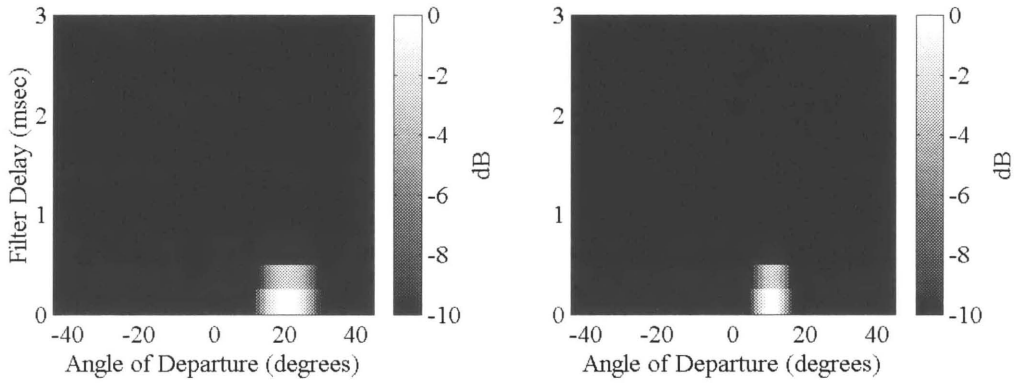

Figure 2.9. The pre-filter (left panel) and post- filter (right panel) corresponding to the largest singular value is shown here in a space described by delay and angle of arrival. The example is based on a signal with 2000 Hz of bandwidth. As such, the filters are impulsive within the signal temporal resolution. The filters focus in beamspace on the modeled departure angle of 20 degrees and arrival angle of 10 degrees. The smaller aperture of the transmit array is reflected in the poorer angle resolution.

such a representation for two singular vectors with non-zero singular values. The parameters selected for this example were a 20 degree departure angle, a 10 degree arrival angle, a 10 element transmit array and a 16 element receive array with a half carrier wavelength spacing, a carrier frequency of 10 kHz, and a signal bandwidth of 2000 Hz in an isovelocity ocean.

Example 3: Two Eigenrays

Adding complexity to the previous example, a channel with two eigenrays corresponding to 10 degree inclination upward- and downward-going rays at the transmitter and 10 degree inclination downward- and upward-going rays at the receiver respectively will now be examined. The array configuration used here is again a 10 element transmitter and a 16 element receiver with half-wavelength separation at the carrier frequency (figure 2.10). The example represents a simplified model of convergence zone propagation in the deep ocean.

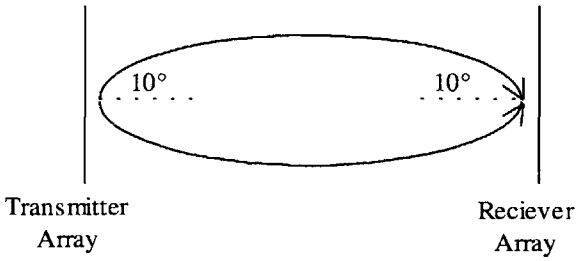

Figure 2.10. The two eigenray example is described here.

Qualitatively, the analysis might be expected to suggest two parallel channels of equal gain with filters that beamform and null in appropriate directions to maintain the orthogonality of the channels. The TVTF, $\mathbf{T}_{mn}(f)$ from transducer n to receiver m is now,

$$\mathbf{T}_{mn}(f) = e^{j\frac{2\pi f}{c}(d\sin\theta_{t1})n} e^{j\frac{2\pi f}{c}(d\sin\theta_{r1})m} + e^{j\frac{2\pi f}{c}(d\sin\theta_{t2})n} e^{j\frac{2\pi f}{c}(d\sin\theta_{r2})m} \qquad 2.39$$

As before, attenuation factors and the phase factor corresponding to mean array separation are neglected. Only two non-zero singular values are found, as expected. Surprisingly, the two parallel channels *do not* correspond to exclusive use of one ray or the other. As seen in figure 2.11, the decomposition results in parallel channels that each use both ray paths. The required orthogonality is produced via the phasing of the signal on each ray. If one examines the phase output of a receiver beamformed on the two ray arrivals, it is apparent that the first parallel channel generates signals 180 degrees out of phase on the two rays while the second parallel channel generates in-phase signals on each ray. Rather than attempting to place nulls, the decomposition places equal energy along both rays with phasing such that the appropriate receive filter constructively combine the rays for the desired parallel channel while destructively combining the rays for the other parallel channel. The creation of sum and difference patterns happens to be unique to this case where the rays are of equal strength. If one ray becomes approximately 5% more attenuated than the other, then the singular vectors simply

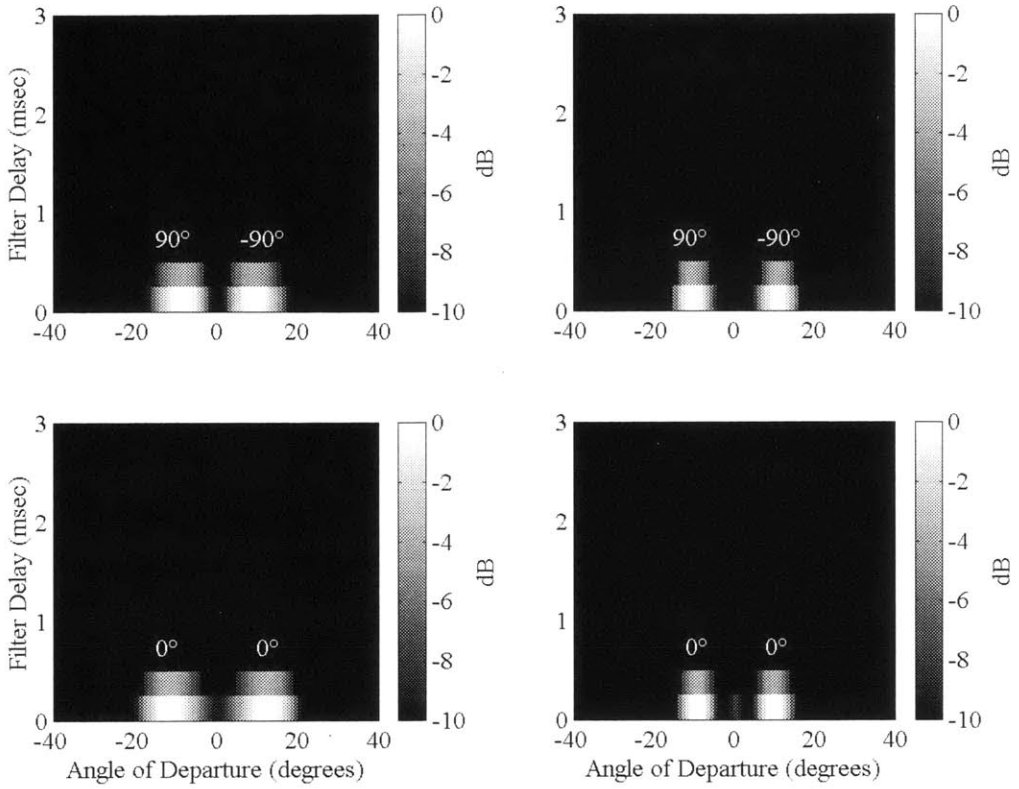

Figure 2.11. The pre-filter (left panels) and post- filter (right panels) corresponding to the largest singular value (top panels) and second largest (bottom panels) is shown here in a space described by delay and angle of arrival. The example is based on a signal with 2000 Hz of bandwidth. As such, the filters are impulsive within the signal temporal resolution. Both filters focus in beamspace on the modeled departure and arrival angles of +/- 10 degrees. The phase of the beamformer response at the peaks is shown in text directly on the plot.

beamform on individual rays. In this case the two singular values are approximately, but not exactly the same.

Although this is a simple example of an underwater acoustic communication channel, it brings to light two interesting aspects of the channel decomposition. First, the mapping from the orthonormal basis provided by the decomposition into the parallel channels to be used for communication is not uniquely determined. In this example, the subspace spanned by the singular vectors has been chosen to define parallel channels. Other appropriate linear combinations of the left and right singular vectors are also valid

filters for the task of generating parallel channels although such combinations will no longer be singular vectors. The second point is that the question of overall spatial and angular resolution is readily approached using the SVD formalism.

In order to see that the singular value decomposition is a more constrained decomposition than is actually required by invoking parallel channels, attention is restricted to a narrowband communication signal such that $\mathbf{T}_{mn}(f)$ is approximately $\mathbf{T}_{mn}(f_{carrier})$ and the analysis may remain in the frequency domain. This constraint implies that $f\text{-}f_{carrier} <$ (delay spread)$^{-1}$. The pre-filters for K parallel channels, $\mathbf{F}_k$, and the post-filters, $\mathbf{G}_k$, ($k = 1,K$) may be expressed as linear combinations of the right and left singular vectors, respectively, since they form a CON basis, where $\mathbf{C}$ and $\mathbf{D}$ are the coefficient matrices.

$$\mathbf{F} = \mathbf{VC} \quad \textbf{and} \quad \mathbf{G} = \mathbf{UD} \tag{2.40}$$

The signal estimate $\mathbf{R}$, for a modulated tone transmitted simultaneously using each pre-filter is then,

$$\mathbf{R} = \mathbf{D}^H \mathbf{U}^H \mathbf{USV}^H \mathbf{VC} \tag{2.41}$$

where $\mathbf{R}_{mn}$ is the estimated signal when the post-filter for the m^{th} parallel channel and the pre-filter for the n^{th} parallel channel is used. The signal estimate matrix easily reduces to,

$$\mathbf{R} = \mathbf{D}^H \mathbf{SC} \tag{2.42}$$

The parallel channel criterion only requires $\mathbf{R}$ to be a diagonal matrix. By selecting $\mathbf{C}$ and $\mathbf{D}$ to be the K^{th} order identity matrix, i.e. use the individual singular vectors as the filters, the criterion is certainly met, recalling that $\mathbf{S}$ is a diagonal matrix. If, instead, only a transmitted power constraint is imposed, thereby insisting that the columns of $\mathbf{F}$ be unit norm (K constraints), a white noise gain constrain is imposed,

thereby insisting that the columns of **G** be unit norm (K constraints), and the columns of **R** are required to be orthogonal (K^2-K constraints) the problem still remains under-constrained. In fact, there are $K^2 + K$ constraints and $2K^2$ unknowns. One approach is to impose sufficient additional constraints to determine **F**, at which point the problem becomes exactly determined except for irrelevant arbitrary phase factors. In other words, one is free to choose **F** in any manner and be assured of finding a post-filter, **G**, that will separate the channels. Of course, different choices will result in different SNR levels at the filter output. Thus, the choice of filters is a design problem. The singular vector formalism thus far simply enables one to determine optimal performance.

Returning to the two-ray example of this section, let us require **C** to be N X 2 with each column of **F** simultaneously forming a beam on one ray and nulling the other. For the sake of brevity, only the results of this calculation will be discussed. $\mathbf{R}_{11}$ and $\mathbf{R}_{22}$ are found to be both equal to 12.26 (in arbitrary units) with $\mathbf{R}_{12}$ and $\mathbf{R}_{21}$ both zero. If the singular vectors had been used as filters, thereby setting **C** and **D** to 2nd order identity matrices, $\mathbf{R}_{11}$ becomes 12.95 and R_{22} becomes 11.98. Opting to use the individual rays as the parallel channels thus results in a 0.1 dB penalty in total energy throughput, if equal energy is transmitted on both channels, compared to using the singular vectors. This choice also reduces the maximum transferred energy on any one channel. In general, the maximum possible received energy can only be equal or lower when using alternative filters. Also, the columns of **F** and **G** may no longer be orthonormal but this feature of singular vectors is not necessary for achieving parallel channels. If additive, white noise is not the performance limiting quantity, however, communication performance improvements may be obtained by using alternative filters. For example, if directional

ambient noise is significant, e.g. shipping noise, using filters orthogonal to the signal subspace occupied by that noise would be helpful. Residual intersymbol interference, such as would result from trying to adaptively equalize the effects of a dynamic multipath environment, may be lessened by selecting a more stable portion of the signal subspace or by confining each parallel channel to a coherent portion of the overall channel.

Expanding on another aspect of this example, the SVD may be used in another manner to provide a generalized measure of end-to-end system resolution that incorporates the dimensions of both arrays as well as channel refraction effects. As an aid to placing that interpretation into context, consider signals with only a temporal character. Twice the product of sampling rate, T, and total available bandwidth in the channel, W, define the number of available, independent degrees of freedom or resolvable temporal channels per channel use. The frequency response of the channel relates transmitted power to received power in each of these temporal channels. For a communication system with a spatial dimension, each singular value of the TVTF matrix describes the power efficiency of an independent, resolvable spatial channel. In both cases, the level of additive noise defines a threshold for determining the number of "useful" channels. For the two ray example described here, one may consider the two non-zero singular values as a function of ray departure and arrival angles and generate a measure of the system's resolving capability. Figure 2.12 shows these singular values as a function of the included angle between the rays. Clearly, an 8 degree ray angle separation is required to extract two useful parallel channels in this case. While a classical computation of array beamwidth would give you the same qualitative picture,

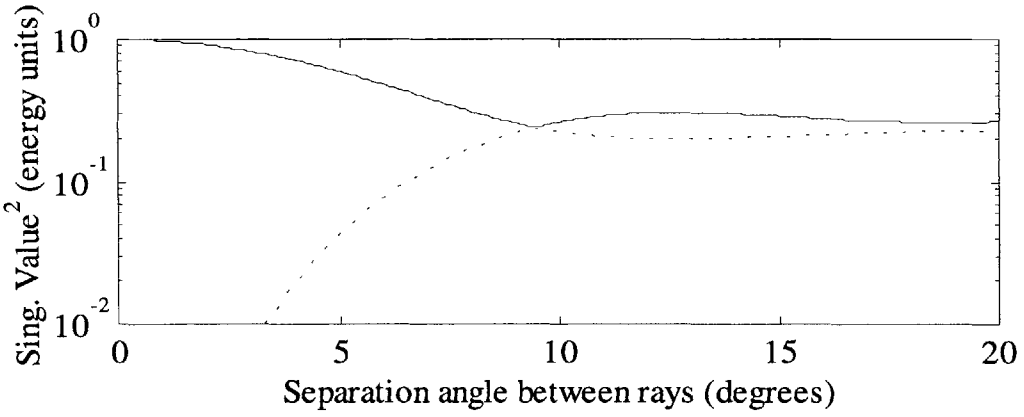

Figure 2.12. The two non-zero singular values for the two-ray example are plotted as a function of included departure angle between the rays. For reference, the null to null beamwidth of the transmitter is 8.85 degrees. As the aperture tends to infinity, the singular values become identical. The angle at which they become nearly equal corresponds to a null to null beamwidth.

the singular values are more direct indicators of system performance, e.g. SNR per channel, incorporating transmitter, channel, and receiver effects.

If the two eigenrays are not of equal strength, the decomposition changes substantially. As an extreme example, suppose one eigenray had a power transfer efficiency 30 dB less than the other. Coherent and simultaneous use of both ray paths would not achieve greater power transfer than exclusive use of the strong path. Thus, as the attenuation factors of each ray begin to differ, the decomposition is expected to transition to exclusive use of one ray or the other. For each of the two singular vector in this example, the apportionment of its power between the ray paths is shown in figure 2.13 as a function of the attenuation factor ratio. For equal attenuation factors, the singular vectors form sum and difference patterns as shown earlier. For attenuation factor ratios less than ½, each singular vector essentially excites an individual ray.

As has been demonstrated thus far, if two ray paths have nearly equivalent strengths, the resulting singular vectors may seek to coherently use them. If the rays are

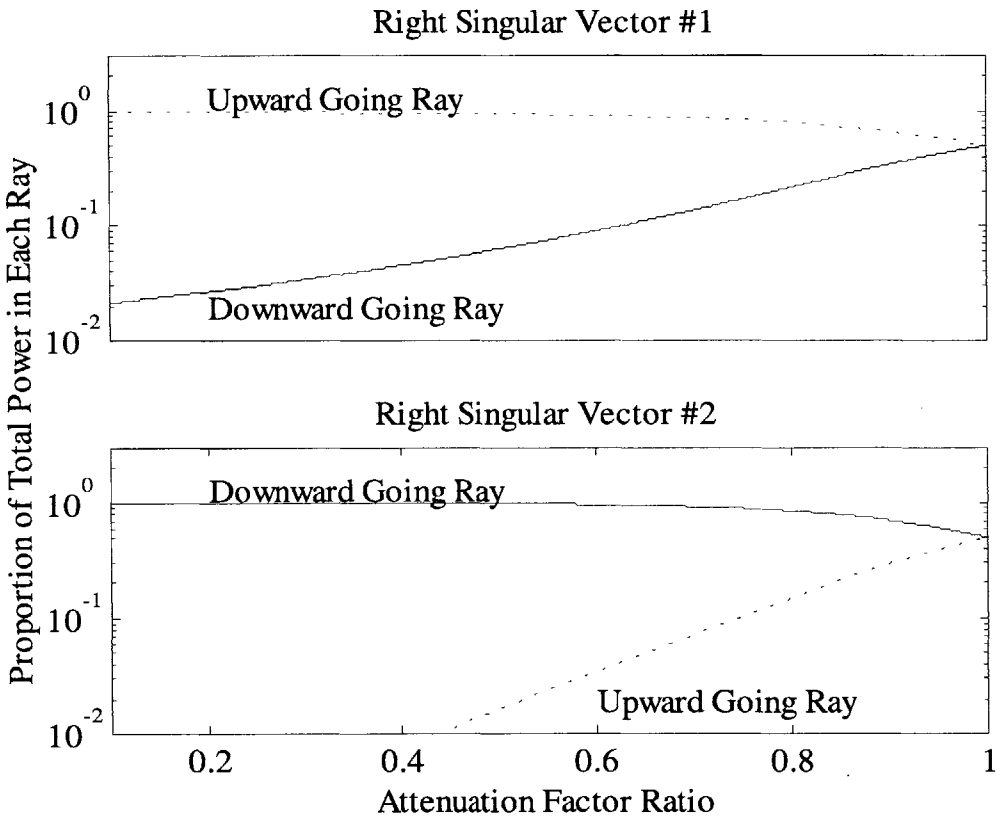

Figure 2.13. The behavior of the singular vectors is examined here as a function of the attenuation factor ratio between the two ray paths. For various ratios, the apportionment of power between the upward and downward going rays by the first right singular vector (upper panel) and the second right singular vector (lower panel) are shown. For equal attenuation factors (ratio = 1), each ray gets half of the power associated with the singular vector. For ratios less than ½, the singular vectors essentially restrict themselves to a single ray.

incoherent, in the sense that they share a random relative phase, the consequences for a communication system may be marginal as will now be shown. For a single frequency and equal ray attenuation factors, the array response due to the first ray path is denoted $\mathbf{R}_1$ while the array response due to the second ray path is denoted $\mathbf{R}_2$. Use of the first singular vector results in an overall receive array response of $\mathbf{R}_1 + \mathbf{R}_2$ while the second singular vector results in an overall response of $\mathbf{R}_1 - \mathbf{R}_2$, which are orthogonal vectors for equal ray attenuation factors. For any given realization, however, the second ray may have an arbitrary phase factor applied resulting in responses of $\mathbf{R}_1+\mathbf{R}_2e^{j\theta}$ and $\mathbf{R}_1-\mathbf{R}_2e^{j\theta}$ due

to use of the same excitation vectors. These responses are not necessarily orthogonal. The magnitude of the cross-correlation coefficient, ρ_c, for the array responses may be used as a measure of their orthogonality.

$$\rho_c \equiv \frac{\left|\left(\mathbf{R}_1^H - e^{-j\theta}\mathbf{R}_2^H\right)\left(\mathbf{R}_1 + e^{j\theta}\mathbf{R}_2\right)\right|}{\left|\mathbf{R}_1 - e^{j\theta}\mathbf{R}_2\right|\left|\mathbf{R}_1 + e^{j\theta}\mathbf{R}_2\right|} = \frac{imag\left(e^{j\theta}\mathbf{R}_1^H\mathbf{R}_2\right)}{\sqrt{\left(\mathbf{R}_1^H\mathbf{R}_1\mathbf{R}_2^H\mathbf{R}_2 - real\left(e^{j\theta}\mathbf{R}_1^H\mathbf{R}_2\right)^2\right)}} \qquad 2.43$$

The second equality makes use of the fact that $\mathbf{R}_1$ and $\mathbf{R}_2$ have equal magnitudes. If the two rays are separated in angle of arrival by a beamwidth or more and the receive array is not prone to grating lobes then this quantity is much less than unity for any value of θ. If the rays are separated by much less than a beamwidth, the second singular value is much less than the first and these rays would probably not be used as two parallel communication channels in any event. Thus, if the rays permit two, useful parallel channels, the variable relative phase does not significantly affect their separability. If the separability is affected, the rays only permit one, useful parallel channel and separability is not required. Recall, however, that the receiver still needs to adaptively track this relative phase in order to isolate the channels.

Example 4: Sandy Bottom, Shallow Ocean Waveguide

As a final illustration of channel decomposition, a range independent, unstratified ocean is considered with a pressure release surface and semi-infinite, penetrable sandy bottom. A typical sandy bottom leads to a critical angle of 56.4° (measured from the depth axis). Thus, all rays with propagation angles less than ±30° with respect to the horizontal are totally reflected at the bottom boundary. Time-variant transfer functions are readily computed for this medium using a parabolic equation technique [31]. A 6 element transmitter array and 16 element receiver array with one wavelength spacing (at 10 kHz) centered in the 14 meter water column will be postulated. The sound power

level due to a single transducer emitting a 10 kHz tone is shown as a function of depth and range in figure 2.14. The local variability seen reflects the coherent interference of eigenrays. The rapid drop in power below 14 meters is due to reflection from and attenuation in the sandy bottom. The spreading loss as a function of range is also evident. To simplify the analysis, only a single frequency will be considered. As shown earlier, the decomposition is done independently at each frequency and, therefore, insight into most aspects of the parallel channel construction is available. The inclusion of receiver range variability should preclude any artifacts due to this simplification. At this point, the primary concern is the availability of parallel channels in the ocean waveguide. To this end, the distribution of singular values as a function of receiver range will be examined. In addition, the singular vectors will be examined in angle of arrival space as was done with previous examples. Finally, the energy transfer efficiency of two fixed pre-filtering schemes will be compared to the ideal limit, namely that achieved when using the right singular vector appropriate for each range.

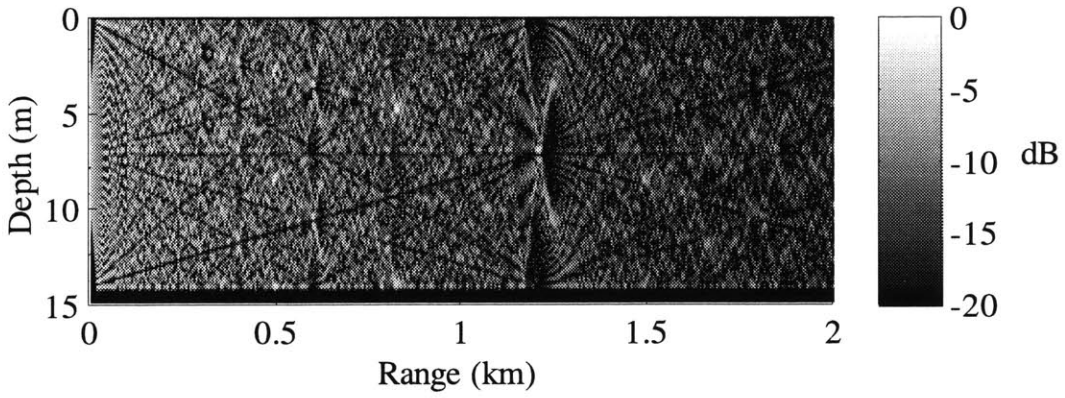

Figure 2.14. The sound power level due to the emission of a 10 kHz tone from a single transducer is shown as a function of depth and range for this constant sound velocity, sandy bottom example. The bottom effect, spreading loss, and coherent interference are all evident.

The distribution of singular values determines the number of spatial degrees of freedom afforded the system. A typical measure of the effective number of degrees of freedom is the normalized sum of singular values, λ, given in equation 2.44 [32].

$$N_{DoFs} = \frac{(\sum \lambda)^2}{\sum \lambda^2} \qquad 2.44.$$

The result, graphically shown in the top panel of figure 2.15, shows a nearly uniform availability of 5 degrees of freedom except for isolated regions. These dips appear to be the result of fading over the receive array as their location is strongly frequency dependent. The transmitter array resolution is roughly 10° implying that it can

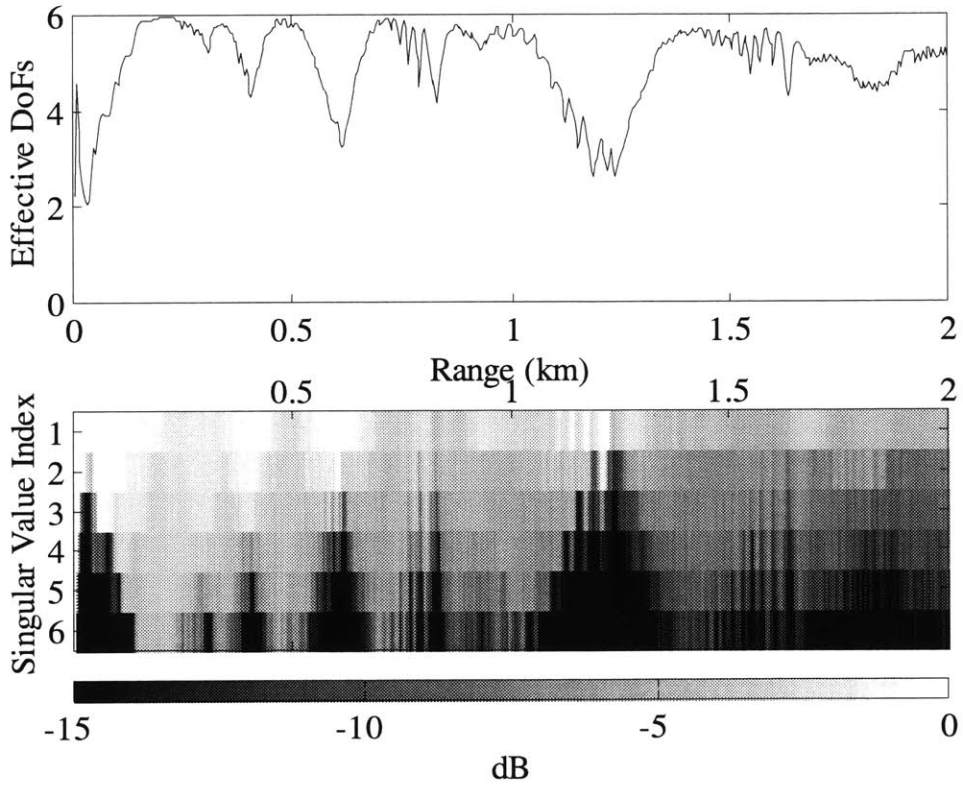

Figure 2.15. The behavior of the singular values computed for a sandy bottom, unstratified shallow ocean with a 6 element, 1 wavelength spaced transducer array and a 16 element, 1 wavelength spaced hydrophone array centered in the water column is shown here. The number of effective spatial degrees of freedom (per equation 2.45) is shown in the top panel as a function of range while the relative energy carried in each parallel channel is shown in the bottom panel.

place six distinct beams in the range of angles undergoing total internal reflection at the bottom. As there is no loss mechanism at the surface, one would expect 5 to 6 degrees of freedom to be consistently available. The relative energy associated with each singular value is also shown as a function of range. The stability of the top two or three singular values is striking and offers encouragement for reliable availability of some parallel channels. If this numerical experiment is repeated with the 16 receiving elements spanning the water column, the variability in range is substantially reduced and the energy associated with the weaker singular values increases on the order of 10 dB. Presumably this is due to the enhanced ability to resolve individual ray arrivals.

Interpretation of the singular vectors in this example is complicated by the presence of many eigenrays for any given receiver location. As the earlier two-ray example demonstrated, the singular vectors may, in fact, excite many of the same rays, relying on appropriate phasing to separate the signals. The first left singular vector at each range has been transformed from element space to angle-of-arrival space in figure 2.16. The lack of any discernible pattern reinforces the point that the decomposition does not isolate rays and, in fact, varies rapidly as a function of range. Comparing angle-space representations of the other left singular vectors shows a great deal of overlap. The lack of clear physical associations for the vectors as well as their apparent variability in range suggests that, at least for this environment, a spatial modulation strategy that requires estimation and tracking of these singular vectors faces a daunting challenge and suggests an approach based on average characteristics may be preferred.

The earlier two-ray example also showed that transformation of the pre-filters from the singular vectors to more physically based ones resulted in only modest

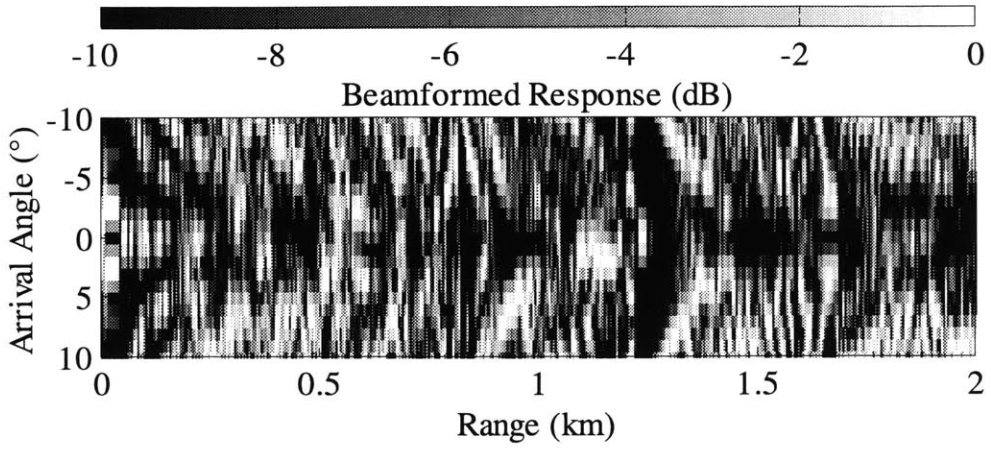

Figure 2.16. The result of applying a beamforming plane wave match filter to the first left singular vector of the decomposition (described in example 4) is shown here as a function of receiver range. The angular spread suggests that multiple rays are energized.

performance penalties. Motivated by this, the change in energy transfer of the parallel channels will be examined if the two particular fixed modulation strategies are used over the entire range. The first set will form sub-arrays from the top and bottom halves of the transducer array. The second filter set will beamform up and down by 5 degrees at the transducer array. Equation 2.42 will be used to estimate the power at the output of each parallel channel's post-filter. Thus, each filter set seeks to generate two parallel channels in this shallow water ocean. The difference in performance of these strategies versus that of using the first two right singular vectors for each range will be measured by computing the total energy transferred by the parallel channel combination. As seen in Figure 2.17, the average reduction in total energy transfer is approximately 3 dB with a modest variance. Although it is not shown in the figure, the same calculation for a water column spanning receive array yields a similar result with a substantially smaller variance. In conclusion, the large variability of the subspace occupied by singular vectors as a function of range, in this example, does not preclude the use of spatial modulation. In

fact, the channel is quite robust in terms of acceptable pre-filters. In the next section, a technique to deduce fixed and useful excitation vectors from a sequence of channel impulse response matrix realizations will be introduced.

One might also compare these fixed strategies to the performance of a phase aligned transmit array. Contemporary transmit arrays in underwater acoustic telemetry applications (typically vertical line arrays) often simply steer beams towards the receiver seeking directivity gains. If the energy transfer of a uniformly phased transmit array is computed with equation 2.42, an average reduction of 3 dB from the optimal 1 channel transfer is again found. Thus, for this example, the two fixed modulation strategies yield two parallel channels of comparable efficiency to a single conventional channel.

An analytic framework has been developed for evaluating the potential for creating parallel communication channels in the underwater acoustic channel. These tools have, in turn, been applied to four examples of increasing fidelity demonstrating the ability to synthesize parallel channels with appropriate arrays. These results, taken with the performance improvements promised by the information theoretic analysis, lay a foundation for the use of spatial modulation in underwater acoustic telemetry systems.

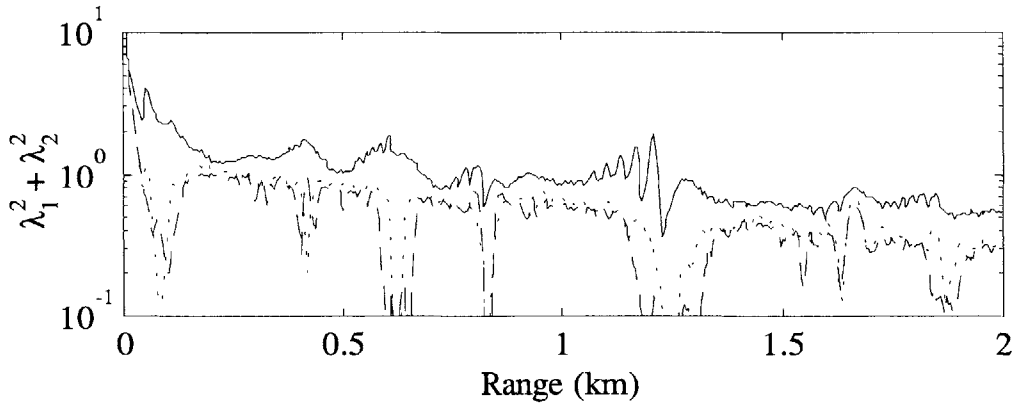

Figure 2.17. The total energy transferred by a two parallel channel combination is compared for three filtering strategies. The first (solid line) simply uses the right singular vectors derived from an SVD at each range and, thus, represents a maximal value. The second (dotted line) divides the transmitter into two subarrays (top three elements and bottom three elements). The third (dashed line) beamforms up and down by 5 degrees to achieve parallel channels. The average energy transfer reduction suffered by the fixed filtering approaches is approximately 3 dB with a modest variance about this value.

The final section of this chapter will discuss strategies for designing appropriate pre- and post- filters based on several criteria that are more appropriate for acceptable performance over an ensemble of channels.

2.3 Decomposition of an Ensemble of Channels

The discussion thus far has focused on the decomposition of a single, given communications channel. Instantaneous knowledge of the channel impulse response matrix by the transmitter, however, is not practical. As the shallow ocean example in the last section demonstrated, a complete decomposition for one channel realization may change substantially as a result of only modest position or propagation variability. While feedback techniques may provide delayed estimates that could be used to continuously update the channel excitation vectors, the ability to generate a single set of fixed channel excitation vectors that provide "good" performance over an ensemble of channels would be a valuable tool. For instance, the acoustic telemetry channel between a source and receiver in the ocean is generally time-varying due to many phenomena including

platform motion, surface waves, and fine-scale turbulence [33]. While the specific propagation paths between two points (eigenrays) persist over time durations much longer than typical telemetry signal durations, the coherence of a given path and that between paths may vary significantly on time scales of milliseconds. If the range of variability could be characterized statistically, one might design transmitter array excitation vectors that give adequate average performance. Even for time-invariant *mediums*, robustness to source and receiver motion could be accommodated by transmission vectors designed for the range of channels such motion would generate. In this section a variety of techniques for designing such average parallel channels will be proposed.

2.3.1 Average Performance Metrics

Before proceeding, a description of the channel model and some fundamental quantities must be given. This analysis will assume that the total signal duration, T, and channel coherence time are much greater than the delay spread, δ. The overall channel may then be decomposed in frequency into narrowband, non-frequency selective sub-channels. Each sub-channel may then be described (in frequency space) as,

$$\mathbf{Y}^q = \mathbf{T}^q\mathbf{X}\mathbf{S} + \mathbf{N}^q \qquad 2.45$$

The vector channel output is $\mathbf{Y}$, the channel transfer function matrix is $\mathbf{T}^q$ (fixed for a given realization), the columns of the matrix, $\mathbf{X}$, are the transmit steering vectors for each parallel channel, the vector $\mathbf{S}$ contains the signal sent on each channel, and $\mathbf{N}$ is a received noise vector. Given S sources, R receivers, and M parallel channels, the dimensions of these may be deduced. The superscript, q, will denote which of the Q channel realizations in the ensemble are used. Note that $\mathbf{X}$ is fixed over the ensemble.

With these definitions, some average performance measures may be defined. The average received power from the k^{th} transmit steering vector, $\mathbf{X}_k$, is,

$$P_k = \frac{1}{Q}\sum_{q=1}^{Q}\mathbf{Y}_k^{qH}\mathbf{Y}_k^{q} = \mathbf{X}_k^H\left\{\frac{1}{Q}\sum_{q=1}^{Q}\mathbf{T}^{qH}\mathbf{T}^{q}\right\}\mathbf{X}_k \equiv \mathbf{X}_k^H\mathbf{A}\mathbf{X}_k \qquad 2.46$$

The average matrix in brackets, denoted **A**, may be interpreted as a sample covariance matrix of **T**. If the Q channel realizations are independent and drawn from an ensemble of channels characterized by stationary statistics, **A** may be expected to converge to the true covariance matrix as Q grows large. If the elements of **T** are Gaussian random variables, then the elements of **A** are governed by Wishart distributions. The examples and experimental applications of these average metrics, however, will be based on finite ensembles of channels rather than statistical models. The matrix multiplication averages the source correlations over the receive array while the explicit sum averages the correlations over the ensemble.

The average crosstalk power from the j^{th} signal imposed on the k^{th} signal subspace is,

$$P_{kj}^{CT} = \frac{1}{Q}\sum_{q=1}^{Q}\left|\mathbf{Y}_k^{qH}\mathbf{Y}_j^{q}\right|^2 \Big/ P_k = \mathbf{X}_k^H\left\{\frac{1}{Q}\sum_{q=1}^{Q}\mathbf{T}^{qH}\mathbf{T}^{q}\mathbf{X}_j\mathbf{X}_j^H\mathbf{T}^{qH}\mathbf{T}^{q}\right\}\mathbf{X}_k \Big/ P_k \equiv \frac{\mathbf{X}_k^H\mathbf{H}^j\mathbf{X}_k}{\mathbf{X}_k^H\mathbf{A}\mathbf{X}_k} \qquad 2.47$$

The quantity in brackets may be interpreted in at least two manners. Each term of the sum projects $\mathbf{X}_j$ onto the rows of $\mathbf{T}^{qH}\mathbf{T}^{q}$ and computes the covariance of this vector which is, of course, rank 1. If the channel ensemble is time-invariant, the average remains rank 1. If the channels do evolve, the rank grows according to how much of the transmit space the projection grows to occupy. If $\mathbf{X}_k$ is contained in a null space of this average matrix, it can create a parallel communication channel over all channel realizations, i.e. the

average crosstalk power is zero. The second interpretation is aided by expressing the bracketed quantity in indical notation.

$$\mathbf{H}_{kl}^{j} = \frac{1}{Q}\sum_{q=1}^{Q}\sum_{m=1}^{S}\sum_{n=1}^{S}\left(\mathbf{T}^{qH}\mathbf{T}^{q}\right)_{km}\mathbf{X}_{jm}\mathbf{X}_{jn}^{H}\left(\mathbf{T}^{qH}\mathbf{T}^{q}\right)_{nl} = \sum_{m=1}^{S}\sum_{n=1}^{S}\left\{\frac{1}{Q}\sum_{q=1}^{Q}\left(\mathbf{T}^{qH}\mathbf{T}^{q}\right)_{km}\left(\mathbf{T}^{qH}\mathbf{T}^{q}\right)_{nl}\right\}\mathbf{X}_{jm}\mathbf{X}_{jn}^{H} \qquad 2.48$$

The indices k and l denote which element of the bracketed matrix in 2.47, denoted $\mathbf{H}^j$ here, is being defined. The index j denotes which transmit steering vector is being considered. The index q denotes which realization of $\mathbf{T}^{qH}\mathbf{T}^{q}$ is intended while k, l, m, and n denote elements of $\mathbf{T}^{qH}\mathbf{T}^{q}$ or $\mathbf{X}_j$ as appropriate. Viewed in this manner, it becomes clear that $\mathbf{H}$ is derived from operations on the fourth moment of the channel impulse response matrix. The average noise power projected onto the received signal space due to transmit vector $\mathbf{X}_k$, may be computed by replacing $\mathbf{Y}_j$ with $\mathbf{N}$ in the expression for P_{kj}^{CT}. If the noise at the receiver was spatially correlated, for instance as with shipping noise or self-platform noise, the noise projection may be a relevant design metric.

A careful examination of equation 2.47 reveals a subtle but important point. P_{kj}^{CT} is, in fact, a weighted average of the crosstalk power. In particular, if P_k^q is the power transferred by $\mathbf{X}_k$ with the q^{th} channel realization, then,

$$P_{kj}^{CT} = \frac{1}{Q}\sum_{q=1}^{Q}\frac{P_k^q}{P_k}P_{kj}^{qCT} \qquad 2.49$$

If the signal power and crosstalk power are assumed to be linearly independent random variables, and each channel realization is independent, then the expected value of P_{kj}^{CT} is *exactly* the average crosstalk power since the independence assumptions assures us that,

$$E\left[\frac{P_k^q}{P_k}P_{kj}^{qCT}\right] = \frac{E\left[P_k^q\right]}{P_k}E\left[P_{kj}^{qCT}\right] = E\left[P_{kj}^{qCT}\right] \qquad 2.50$$

The discussion now turns to how transmit steering vectors may be derived to yield optimal average performance, by various measures. The measures will be:

1. Maximum average power over a single parallel channel.
2. Strictly parallel channels in an average sense.
3. Minimum weighted average crosstalk power over all realizations of the channel.
4. Maximum average signal to weighted average interference plus noise ratios over the channel ensemble.
5. A minimum mean square estimation error criterion.

Performance Measure 1: Maximum Average Power

Referring to equation 2.46 let $\mathbf{X}_l = \mathbf{V}_l$, $l = 1$ to S, be the set of eigenvectors, including those of zero eigenvalue, derived from a decomposition of the transfer function matrix second moment such that,

$$\lambda_l \mathbf{V}_l = \left\{ \frac{1}{Q} \sum_{q=1}^{Q} \mathbf{T}^{qH} \mathbf{T}^{q} \right\} \mathbf{V}_l \qquad 2.51$$

To reiterate a previous point, if one allows the number of channel realizations to become large, the bracketed matrix (a sample covariance matrix) may converge to an ensemble average (true covariance matrix) if the realizations are stochastically independent and the channel is wide-sense stationary. Given a unit norm constraint on $\mathbf{X}_k$, the maximum average power over the channel ensemble is achieved by selecting $\mathbf{X}_k$ to be the eigenvector, $\mathbf{V}_l$, corresponding to the largest eigenvalue. In fact, λ_l, *is* the maximum achievable average received power given the unit norm constraint.

Performance Measure 2: Parallel Channels with Zero Mean Crosstalk

In this case, $\mathbf{X}_k$ and $\mathbf{X}_j$ are derived such that the channel outputs are, *on average*, orthogonal. More quantitatively,

$$E \equiv \frac{1}{Q}\sum_{q=1}^{Q} \mathbf{Y}_k^{qH}\mathbf{Y}_j^{q} = \mathbf{X}_k^{H}\left\{\frac{1}{Q}\sum_{q=1}^{Q}\mathbf{T}^{qH}\mathbf{T}^{q}\right\}\mathbf{X}_j = \mathbf{X}_k^{H}\mathbf{A}\mathbf{X}_j = 0 \qquad 2.52$$

Once again, if the transmit excitation vectors are chosen to be the eigenvectors of the transfer function second moment matrix, this condition is met. As was extensively discussed for a single channel realization, q, choosing $\mathbf{X}_k$ to correspond to the right singular vectors of $\mathbf{T}$ or, equivalently, the eigenvectors of $\mathbf{T}^{qH}\mathbf{T}^{q}$, resulted in a set of parallel channels with power transfer ability given by the singular values. In this case, using the eigenvectors of $\mathbf{A}$ results in parallel channels *on average*. Unfortunately, it is possible to meet this average criterion while never achieving strictly parallel channels over any given realization. By strictly parallel, the condition that the signal and noise on any one channel is independent of the signal and noise on any other channel is intended. To move towards that goal, the third performance measure will now be introduced.

Performance Measure 3: Minimum Weighted Average Interference

Attempting to derive a set of transmit steering vectors that create strictly parallel channels over *all* channel realizations proceeds in a serial fashion. The derivation begins with the *ad hoc* assumption that the first channel should achieve maximum average power transfer. As noted before, this is accomplished by setting $\mathbf{X}_1$ to be the eigenvector with the largest eigenvalue of $\mathbf{A}$. $\mathbf{H}^1$, is then computed by forming the appropriate projections of $\mathbf{X}_1$ onto the fourth order moment of the channel impulse response matrix realizations (as defined in equation 2.48). If $\mathbf{H}^1$ is not full rank, then $\mathbf{X}_2$ is chosen to lie in the null space of $\mathbf{H}^1$ which then assures the average crosstalk power between $\mathbf{Y}_1$ and $\mathbf{Y}_2$ to be zero as long as $\mathbf{X}_2$ has non-zero average received power. To reiterate, if $\mathbf{H}^1$ is not full rank, then an $\mathbf{X}_2$ exists which will enable two parallel channels over all realizations of the channel ensemble with non-zero probability of occurrence. It is important to note that different directions in the null space may result in different average powers through the

channel they create. In fact, the null space of $\mathbf{H}^j$ may lie entirely in the null space of $\mathbf{A}$ thereby precluding $\mathbf{X}_2$ from actually delivering energy to the receiver.

The preceding discussion may be formalized. Let us define a cost function P_{kj}^{CT} to be minimized. The projection of interference into the subspace occupied by $\mathbf{X}_k$ is not a function of the norm of $\mathbf{X}_k$. Therefore, no constraint on its norm is required. The grad condition is then,

$$\nabla P_{kj}^{CT} = \frac{\mathbf{X}_k^H \mathbf{H}^j \mathbf{X}_k}{\mathbf{X}_k^H \mathbf{A} \mathbf{X}_k} = 0 \qquad 2.53$$

which is solved by the solutions to the following generalized eigenvalue problem,

$$\mathbf{H}^j \mathbf{X}_k = \lambda_k \mathbf{A} \mathbf{X}_k \qquad 2.54$$

where the superscript j has been appended to $\mathbf{H}$ to emphasize that it is a function of the given excitation, $\mathbf{X}_j$. The left eigenvectors of $\mathbf{H}^j\mathbf{A}^{-1}$ give the critical points of the cost function and the associated eigenvalues correspond to the value of P_{kj}^{CT} at the critical point. Eigenvectors of zero eigenvalue lie in the null space of $\mathbf{H}_j$ and yield zero weighted average crosstalk power. Vectors that lie in the null space of $\mathbf{A}$ cannot satisfy 2.54 unless they also lie in the null space of $\mathbf{H}_j$. If $\mathbf{X}_k$ lies in the null space of $\mathbf{A}$, it does not transmit power through the channel for any realization. Even if there is no null space, one may still chose a vector that gives a *minimal* amount of average crosstalk power. By applying filtering techniques at the receiver, channels with modest crosstalk may still be separated and estimated although a penalty may be paid in noise enhancement.

One drawback to this metric is its insensitivity to the power actually delivered to the receiver by $\mathbf{X}_k$. The principal advantage is that it is readily computed using second and fourth order moments of the channel realizations.

A possibly fruitful area of future research would determine solely from the fourth order moment channel matrix what parallel channel combinations are possible. The method presented here presumes the first channel is selected through a power criterion. With this design question in mind, the remaining performance measures which lend themselves to design of all the parallel channels simultaneously will be considered.

Performance Measure 4: Maximum Average Signal to Weighted Average Interference plus Noise Ratio ($SINR_{avg}$)

SINR is a common metric in communication systems. An exact expression for an average SINR of a channel created by the excitation vector, $\mathbf{X}_k$, over the ensemble of channel realizations will be formulated. This metric is a weighted average rather than a strict average. For the case where all $\mathbf{X}_j$ ($j \neq k$) are given, an analytic solution for the $\mathbf{X}_k$ that maximizes $SINR_{\text{avg}}$ will be derived. For more general cost functions involving $SINR_{\text{avg}}$ where more than one transmit vector is unconstrained, one must resort to iterative optimization techniques.

$SINR_{\text{avg}}$ may be defined as,

$$SINR_{avg} = \frac{\left(\mathbf{X}_k^H \left\{ \frac{1}{Q} \sum_{q=1}^{Q} \mathbf{T}^{qH} \mathbf{T}^q \right\} \mathbf{X}_k \right)^2}{\mathbf{X}_k^H \left\{ \frac{1}{Q} \sum_{q=1}^{Q} \mathbf{T}^{qH} \left(\mathbf{T}^q \sum_{\substack{j=1 \\ j \neq k}}^{S} \mathbf{X}_j \mathbf{X}_j^H \mathbf{T}^{qH} + \mathbf{N}^{qH} \mathbf{N} \right) \mathbf{T}^q \right\} \mathbf{X}_k} \equiv \frac{\left(\mathbf{X}_k^H \mathbf{A} \mathbf{X}_k \right)^2}{\mathbf{X}_k^H \mathbf{H}^0 \mathbf{X}_k} \quad 2.55$$

The interference matrix, $\mathbf{H}^j$, has been generalized to $\mathbf{H}^0$ to include the interference power from all other channels as well as the received noise field.

The explicit relationship between $SINR_{\text{avg}}$ and the true average SINR is given as,

$$SINR_{avg} = \frac{1}{Q} \sum_{q=1}^{Q} \left(\frac{P_k}{P_k^q} \right)^2 SINR^q \quad 2.56$$

As before, this metric is chosen because it may be expressed directly in terms of second and fourth order moments of the channel. If all $\mathbf{X}_j$ ($j \neq k$) are specified, then the matrices $\mathbf{A}$ and $\mathbf{H}^0$ are constants. For excitation vectors with zero power, $SINR_{avg}$ will clearly be minimized. For excitation vectors with infinite power, $SINR_{avg}$ will clearly be maximized. These solutions are not interesting. The method of Lagrange multipliers will be used to find the critical points of $SINR_{avg}$ with a unit norm constraint on $\mathbf{X}_k$. The equation to solve is then,

$$\nabla\left(SINR_{avg} + \alpha \mathbf{X}_k^H \mathbf{X}_k\right) = \frac{4\left(\mathbf{X}_k^H \mathbf{A}\mathbf{X}_k\right)\mathbf{A}\mathbf{X}_k}{\left(\mathbf{X}_k^H \mathbf{H}^0 \mathbf{X}_k\right)} - \frac{2\left(\mathbf{X}_k^H \mathbf{A}\mathbf{X}_k\right)^2 \mathbf{H}^0 \mathbf{X}_j}{\left(\mathbf{X}_k^H \mathbf{H}^0 \mathbf{X}_k\right)^2} + 2\alpha \mathbf{X}_k = \mathbf{0} \qquad 2.57$$

If equation 2.57 is left multiplied with $\mathbf{X}_k^H$ and invoke the unit norm constraint, the value of α that solves the equation is found.

$$\alpha = -\frac{\left(\mathbf{X}_k^H \mathbf{A}\mathbf{X}_k\right)^2}{\mathbf{X}_k^H \mathbf{H}^0 \mathbf{X}_k} \equiv -SINR_{crit} \qquad 2.58$$

If either the projection of $\mathbf{N}$ is non-zero or the crosstalk power is non-zero, the denominator may be cleared and the terms of 2.57 may be rearranged to arrive at the following equation for $\mathbf{X}_k$.

$$\mathbf{A}\mathbf{X}_k = \left(\frac{1}{2}\frac{\mathbf{X}_k^H \mathbf{A}\mathbf{X}_k}{\mathbf{X}_k^H \mathbf{H}^0 \mathbf{X}_k}\right)\left(\mathbf{H}^0 + \mathbf{X}_k^H \mathbf{H}^0 \mathbf{X}_k \mathbf{I}\right)\mathbf{X}_k \equiv \lambda \tilde{\mathbf{H}} \mathbf{X}_k \qquad 2.59$$

This is similar to a generalized eigenvalue problem. To solve this, one must find a consistent solution. One could hypothesize a value of $\mathbf{X}_k^H \mathbf{H}^0 \mathbf{X}_k$, compute $\tilde{\mathbf{H}}$, solve the generalized eigenvalue problem and see if any eigenvalues are, in fact, equal to what equation 2.59 states it must be. Equation 2.59 has the satisfying interpretation of diagonal loading of $\mathbf{H}^0$. Alternatively, the diagonal loading could be transferred to $\mathbf{A}$.

$$\left(\mathbf{A} - \tfrac{1}{2}\mathbf{X}_k^H \mathbf{A}\mathbf{X}_k \mathbf{I}\right)\mathbf{X}_k \equiv \tilde{\mathbf{A}}\mathbf{X}_k = \left(\tfrac{1}{2}\frac{\mathbf{X}_k^H \mathbf{A}\mathbf{X}_k}{\mathbf{X}_k^H \mathbf{H}^0 \mathbf{X}_k}\right)\mathbf{H}^0\mathbf{X}_k = \lambda \mathbf{H}^0 \mathbf{X}_k \qquad 2.60$$

The loading term is exactly ½ P_k. The solution technique begins with the observation that clear bounds may be placed on the diagonal loading term. Since **A** and $\mathbf{H}^0$ are non-negative definite, the loading terms must be greater than zero. The largest singular value of **A** defines an upper limit. To solve, one may search over the one-dimensional scalar space of the loading term. For each value, one solves the generalized eigenvalue problem and compares the resulting eigenvalues to what equations 2.59 and 2.60 insist they be. Any values of the loading term that lead to consistent eigenvalues yield an extremum of $SINR_{avg}$ subject to the given constraints.

A more general performance criteria such as the actual average *SINR* may be analytically written but the optimization must be done with iterative methods and is not readily expressed in terms of moments of the channel statistics. Furthermore, describing the interference as the projection of $\mathbf{Y}_j$ on the subspace of $\mathbf{Y}_k$ implies a simple match filter receiver algorithm. Adaptive processing techniques enable far superior interference suppression. Rather than pursue an optimal true average *SINR*, the discussion will turn to the final metric which is more indicative of performance for an adaptive receiver.

Performance Measure 5: Minimum Mean Square Estimation Error

The original channel model (equation 2.45) indicated that a parameter vector, **S**, was to be transmitted over these channels. As such, one may define an overall minimum square error (*MSE*) criterion. A particular advantage of this approach is the incorporation of the receiver's ability to coherently remove inter-channel interference with a set of optimal linear weights. The task of relating a set of $\mathbf{X}_k$ to *MSE* begins by defining the parameter estimate as well as the error. The estimate will be formed through a linear

combination of the received signal using a weight optimized against a *MSE* criterion for that specific channel realization. This assumes that the receiver employs adaptive processing such that the optimal weight is continually tracked. The estimate is then,

$$\hat{S}_k = \mathbf{W}_k^{qH}\mathbf{Y}^q \tag{2.61}$$

where $\mathbf{W}_k^{qH}$ is the optimal weight vector for recovering parameter S_k. The overall *MSE* is defined as,

$$MSE = \frac{1}{Q}\sum_{q=1}^{Q}\sum_{k=1}^{K}\left(S_k^H - \hat{S}_k^H\right)\left(S_k - \hat{S}_k\right) \tag{2.62}$$

If one takes **S** and **N** to be random, uncorrelated variables with zero mean and co-variance matrices of $\mathbf{R}_{ss}$ and $\mathbf{R}_{nn}$ respectively, the MSE may expressed as,

$$\begin{aligned}
MSE &= \frac{1}{Q}\sum_{q=1}^{Q}\sum_{k=1}^{K}\left\{\sigma_k^2 - \mathbf{R}_{yk}^{qH}\mathbf{W}_k^q\right\} \\
\mathbf{R}_{yk}^q &= E\left[\mathbf{Y}^q S_k^H\right] = \mathbf{T}^q\mathbf{X}E\left[S_k^H\mathbf{S}\right] \\
\mathbf{R}_{yy}^q &= E\left[\mathbf{Y}^q\mathbf{Y}^{qH}\right] = \mathbf{T}^q\mathbf{X}\mathbf{R}_{ss}\mathbf{X}^H\mathbf{T}^{qH} + \mathbf{R}_{nn} \\
\mathbf{W}_k^q &= \left[\mathbf{R}_{yy}^q\right]^{-1}\mathbf{R}_{yk}^q \\
\sigma_k^2 &= E\left[S_k^H S_k\right]
\end{aligned} \tag{2.63}$$

Note that **X** is the matrix whose columns are $\mathbf{X}_k$. An analytic solution to this optimization problem is not obvious although it lends itself to an iterative numerical solution. Specifically, the maximum of,

$$F = \frac{1}{Q}\sum_{q=1}^{Q}\sum_{k=1}^{K}\left\{\mathbf{R}_{yk}^{qH}\left[\mathbf{R}_{yy}^q\right]^{-1}\mathbf{R}_{yk}^q\right\} \tag{2.64}$$

is sought subject to a power constraint, $\sum_{k=1}^{K}\mathbf{X}_k^H\mathbf{X}_k = 1$. This is a non-linear, constrained optimization problem that may be treated with existing techniques.

These metrics will now be illustrated using the examples of the previous section with some form of variability imposed to generate an ensemble of realizations.

2.3.2 Examples of Average Performance Optimization

Example 5: Two Stochastic Eigenrays

Returning to this simplified model of convergence zone propagation, three sources of variability will be considered; a random time of arrival, Rayleigh fading, and variable wavenumber. For each ensemble of channels generated, transmit steering vectors will be generated using each of three performance measures, namely measure 2 (parallel channels on average), measure 3 (minimum average interference power), and measure 4 (maximum average signal to average interference ratio).

The first ensemble is generated by assigning a uniform, independent probability distribution to the arrival times of each eigenray. The distributions have support from $\pm 8/f_{carrier}$ with zero mean. If the acoustic field over the transmit array is beamformed with a plane wave match filter, one may infer what the transmit steering vectors are trying to accomplish. As figure 2.18 shows, each of the three performance metrics still seek sum and difference patterns as with the unperturbed decomposition. Thus, the decomposition is insensitive to the relative phasing of the eigenrays.

A more realistic variability may be described by an independent Rayleigh fading model with the quadrature channels of the complex amplitude drawn from independent, zero-mean Gaussian distributions. The results of an ensemble decomposition derived from 200 channel realizations are given here. The ensemble was normalized to ensure the mean square magnitude of each attenuation coefficient was equivalent to that of the unperturbed ray. As figure 2.19 indicates, the ensemble decomposition results in nearly exclusive use of one ray for each parallel channel.

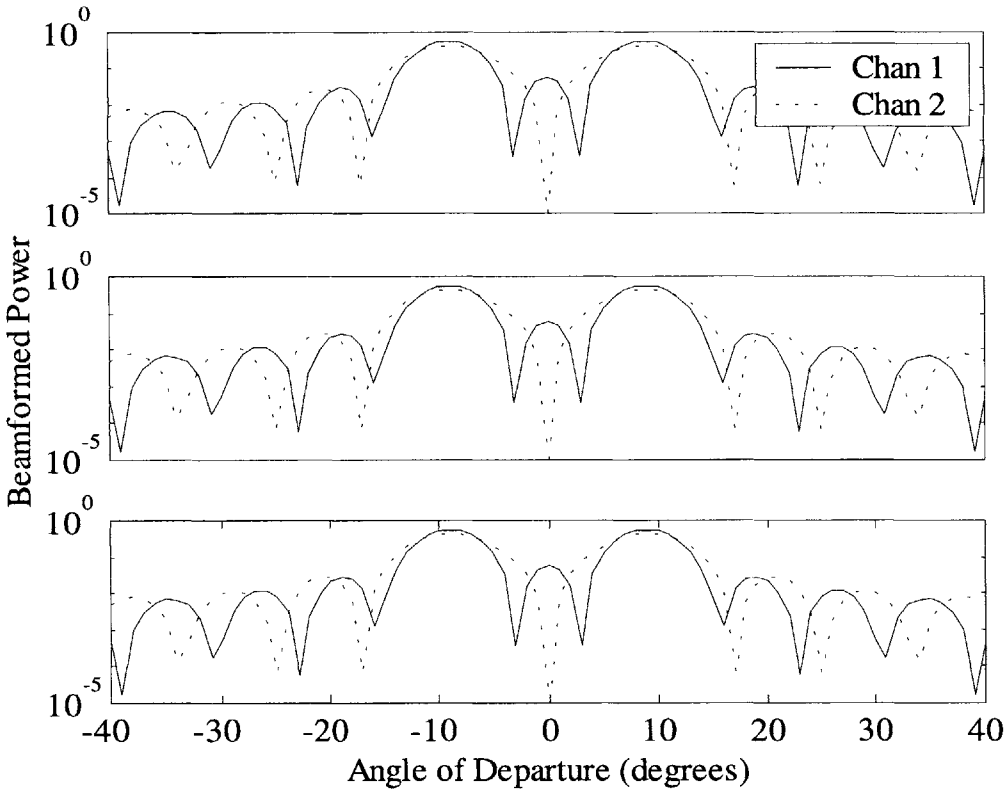

Figure 2.18. The steering vectors that result from an ensemble decomposition of the two eigenray example with random time-of-arrival are shown here transformed into angle space using a plane wave match filter, i.e. a beampattern. The top panel uses measure 2, the middle panel uses measure 3, and the bottom panel uses measure 4 (see text for definition of measures). The ensemble decomposition is not sensitive to relative phase of the eigenrays.

The final source of variability to examine is a wander in the wavenumber of each ray. Specifically, the departure angle of the eigenrays from the transmit array will be drawn from a uniform probability distributions with +/- 10 degree means and a +/- 5 degree support. Since the wavenumber was fixed for the previous two ensembles, it was still possible to achieve strictly parallel channels for all realizations. With a spread in wavenumber, it is no longer possible to achieve this for all realizations in the ensemble with a single, fixed set of transmit steering vectors.

An analogy may be made at this point between Doppler spread channels and wavenumber spread channels. A key issue is whether the communication system's

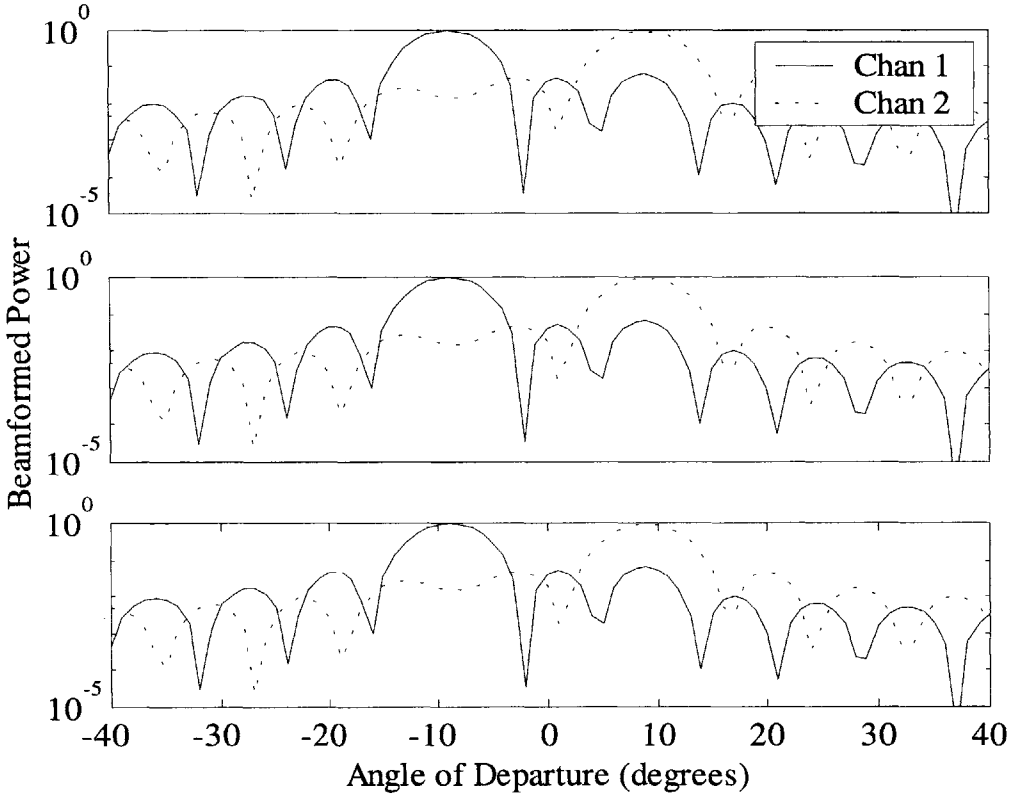

Figure 2.19. The steering vectors that result from an ensemble decomposition of the two eigenray example with Rayleigh fading statistics are shown here transformed into angle space using a plane wave match filter. The top panel uses measure 2, the middle panel uses measure 3, and the bottom panel uses measure 4 (see text for definition of measures). The ensemble decomposition results in the use of one ray per channel.

adaptation rate exceeds the highest frequency component of the random process power spectrum. If it does, the wavenumber spread may be treated as a slow wander instead of an instantaneous spread. Viewed as a slow wander, algorithms akin to phase locked loops may be considered. Such algorithm extensions, however, are beyond the scope of this work. An important distinguishing feature of the performance metrics is illustrated by this example. By examining figure 2.20, it is apparent that measure 3 (minimum weighted average interference power) does not put appreciable power through the second parallel channel. In this case, the critical points of the second measure's cost function do not yield a solution that gets power through the parallel channel.

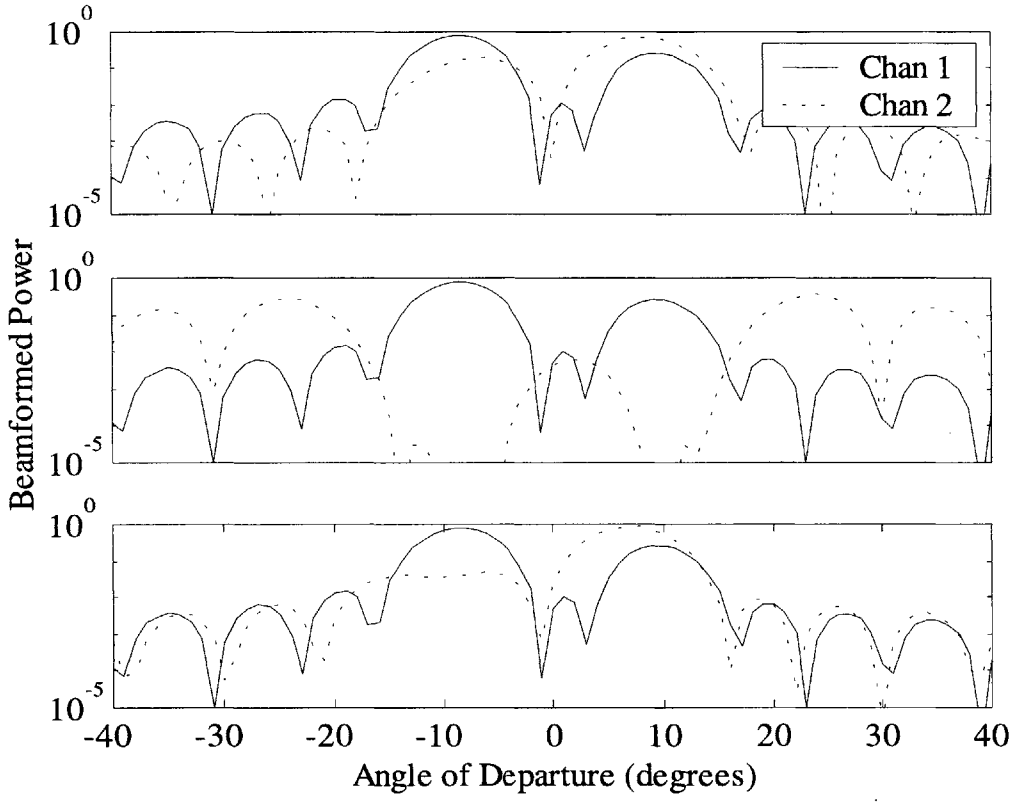

Figure 2.20. The steering vectors that result from an ensemble decomposition of the two eigenray example with wavenumber spread are shown here transformed into angle space using a plane wave match filter. The top panel uses measure 2, the middle panel uses measure 3, and the bottom panel uses measure 4 (see text for definition of measures).

Example 6: Range Robustness in a Shallow Ocean Waveguide

In example 4, the channel decompositions for a range of source – receiver separations was considered. In this example, the same channel is examined but the ensemble decomposition techniques are applied to a collection of time-invariant channels with differing source – receiver separation. One might do this to attain a degree of robustness to uncertainty in array position. A nominal receiver array placement at 1 km range with a uniformly distributed range uncertainty of $\pm 50 m$ defining the ensemble of channels will be assumed.

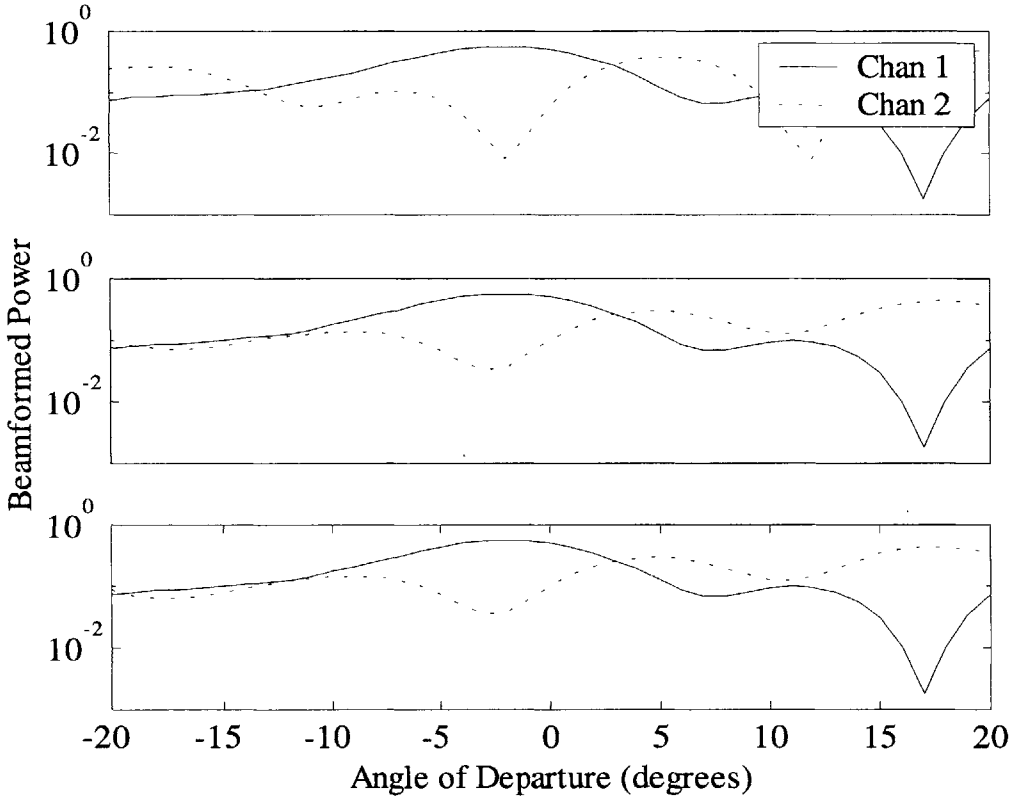

Figure 2.21. The steering vectors that result from an ensemble decomposition of the shallow ocean example are shown here transformed into angle space using a plane wave match filter. The realizations are different ranges between 950 m and 1050 m. The top panel uses measure 2, the middle panel uses measure 3, and the bottom panel uses measure 4 (see text for definition of measures). Note the peaks and nulls at –3, 12, and 17 degrees.

The beamformed steering vectors, shown in figure 2.21, indicate that the first parallel channel is formed by near axis eigenrays with the second parallel channel placing a null near axis. The second parallel channel excites a higher angle group of rays near 17° while the first channel has a null at those angles. The different performance measures yield little difference except for the null near 12° in the pattern of the second performance measure. To see the consequences of this, the beamformed response at the receiver array over the optimization range (figure 2.22) will be examined. The figure shows the response due to the first steering vector in the left panels and response due to the second steering vector in the right panels. As before, the top panel corresponds to

measure 2, the middle panel corresponds to measure 3, and the bottom panel to measure 4. In all cases, the first parallel channel seeks to excite the near axis rays. The second parallel channel excites a group of off-axis rays with a notable asymmetry in the measure 2 response. This is the consequence of the second null.

As noted before, the interference power that is represented in performance measures 3 and 4 would result from a match filter receiver. Another way to interpret the interference measure is that it seeks to maximize the orthogonality of the subspaces occupied by the received signal vectors due to each parallel channel excitation. Alternative receivers may offer substantially increased interference rejection. If the receiver is assumed to be capable of determining the optimal MSE filter for each source-receiver range, the performance of the various fixed steering vectors may be compared in terms of the MSE they achieve over the range of interest rather than $SINR_{avg}$. Figure 2.23 gives this information for measures 2, 3, and 4. Note the nearly 10 dB MSE increase for ranges over 1025 m that measures 3 and 4 suffer. The result of using a vector derived from the non-linear constrained optimization given by performance measure 5 is also shown. It was initialized as the vector derived from measure 3. The regions of poor performance are largely eliminated. The similar performance of measures 2 and 5 suggests that the straightforward method of generating mean parallel channels may yield near optimal performance in some cases. The final curve depicted gives the optimal MSE achievable if one used the first and second right singular vectors of the single channel realization at 1 km. The ensemble decompositions of measure 2 and 5 result in performance that is substantially more robust to range uncertainty than that of a single

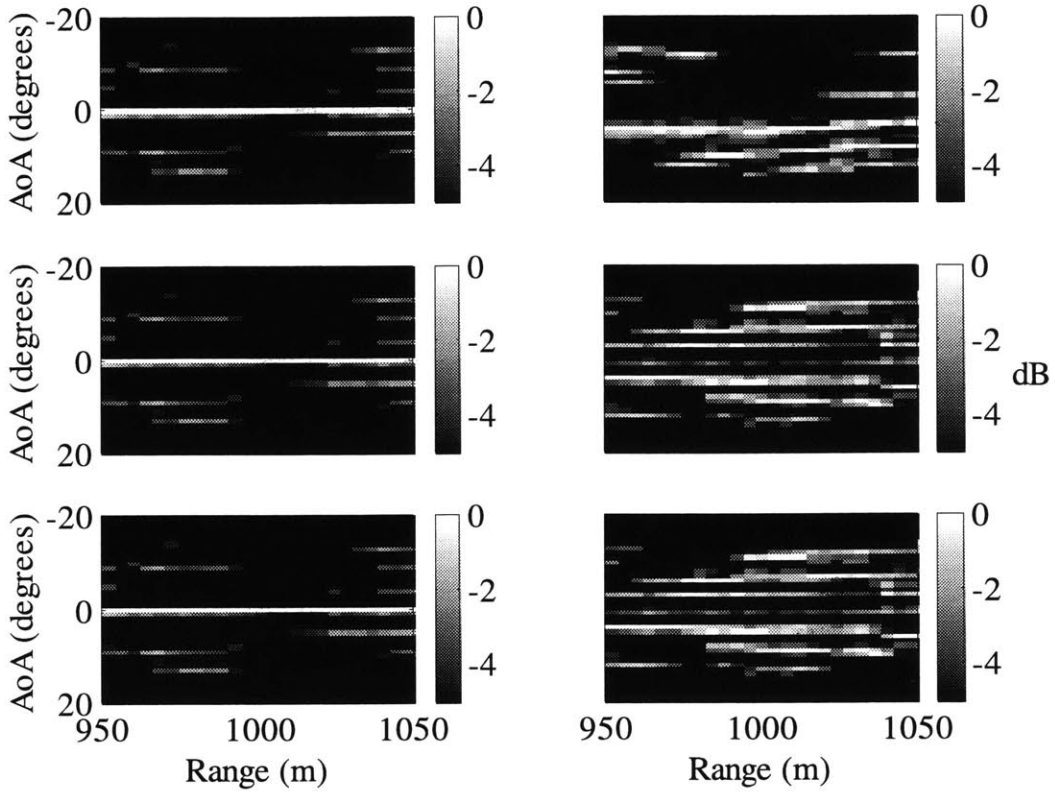

Figure 2.22. The receive array responses that result from an ensemble decomposition of the shallow ocean example are shown here transformed into angle space using a plane wave match filter. The left panels result from the first steering vector while the right panels result from the second. The top panels use measure 2, the middle panels use measure 3, and the bottom panels use measure 4.

realization particularly for the first channel. For reference, a MSE of –18 dB corresponds to the noise floor defined in the problem.

The chapter began with a discussion of the fundamental communication performance improvements one may achieve by properly exploiting parallel channels. Two derivations of how a given channel impulse response matrix may be transformed into a set of parallel channels giving several analytical examples were then presented in detail. Finally, the technique was extended to include methods for improving average performance over an ensemble of channels. For some methods, the performance may be uniquely described by the second and fourth order moments of the transfer function

matrix, **T**. Others required non-linear iterative solution techniques using all realizations of an ensemble. In the next chapter, these decomposition methods will be applied to both a particular probabilistic description of the channel as well as experimental data.

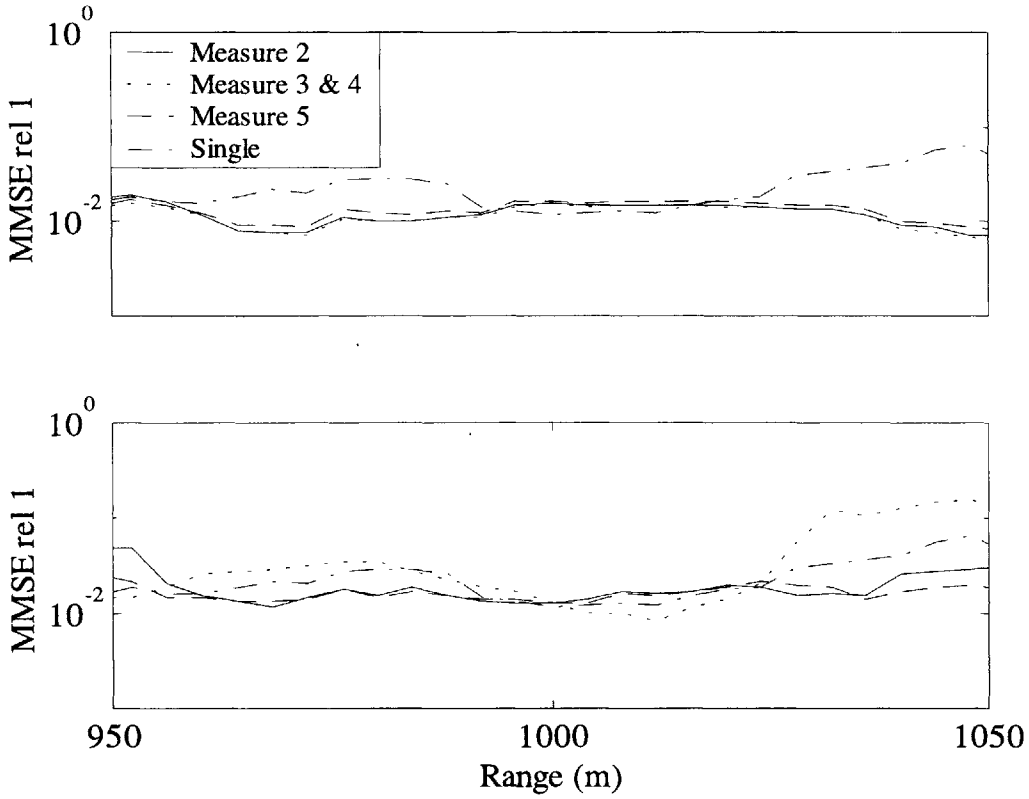

Figure 2.23. The mean square error (MSE) that results from using an ensemble decomposition of the shallow ocean example is shown for the various possible steering vectors. The MSE is relative to a signal power of 1. Measures 2, 3, 4, and 5 are as defined in the text. Measures 3 and 4 gave nearly identical results and are shown with a single curve. The curve labeled single refers to the use of steering vector derived from the single channel realization at 1000 m. The top panel is for the first parallel channel while the bottom panel is for the second

Chapter 3 An Experimental Investigation of Underwater Acoustic Channel Decomposition

The underwater acoustic channel has a long history of challenging, if not defeating, straightforward applications of communication theory. Analog techniques, which dominated prior to 1980, suffered significant distortion due to the reverberation in time restricting such systems to close range, line of sight configurations. Performance of incoherent, digital systems often deviates strongly from predicted performance based on simple, additive white Gaussian noise or Rayleigh fading models. In short, understanding of the time-variability and noise processes in the underwater acoustic channel is too limited to support high fidelity models at this time. Experimental validation is crucial. Having presented the theoretical tools for decomposing the underwater channel into multiple, useful parallel channels, it remains to apply these tools to a real, practical ocean channel before their true worth to the field of underwater acoustic telemetry may be measured. In this chapter, four aspects of parallel channel creation will be examined.

1. The distribution of both ensemble average and sampled, short time averaged singular values, λ_i, over time will be explored. The ratio of λ^2 to the noise power dictates, to first order, whether a parallel channel may be used for communication. The stability of this distribution is important to avoid stringent requirements on feedback of channel information.
2. While governed by the singular value distribution, the average power projected through the channel will be considered explicitly. The ability

of fixed transmitter filters, that are derived from the channel, to increase average power throughput will be compared to the conventional strategy which will be referred to as broadside beamforming.

3. The transmitter filters given by the singular value decomposition will be examined for stability in time. In particular, the stability of the subspace occupied by the right singular vectors will be identified by projecting the time evolving vectors against a fixed coordinate system. In addition, ray theory techniques will be used to associate singular vectors with physical propagation paths as a tool for understanding their time varying behavior.

4. The suitability of ascribing Gaussian distributions to the elements of the transfer function matrix, **T**, will be tested against measured values. Analytic representations of average power throughput for individual parallel channels and average SINR between parallel channels (per the metrics defined in section 2.3) will be developed in terms an assumed Gaussian distribution for **T**. This work will be placed in the context of the ongoing research into space-time coding with transmitter arrays that is taking place in the field of wireless communication.

The data for the experimental validation derives from channel impulse response estimates made during the SM99 and SM00 tests. These tests are described in detail in Chapter 4 but will be briefly summarized here.

3.1 SM99 and SM00 Channel Measurement Methodology

In both SM99 and SM00, signaling took place between a 6 element vertical line array of transducers and a 16 element vertical line array of hydrophones. Both sites took place in water with a nominal depth of 13 – 19 meters. The transducers were spaced approximately 1.5 meters apart with a total aperture of nearly 8 meters. The hydrophones were closely spaced with a separation of one wavelength at the carrier frequency of 9.6 kHz. Coherent, phase modulated symbols were transmitted at a rate of 4 symbols/second. As an aid to visualizing the experimental configurations, the eigenrays connecting the six transducers to the center of the receiver array are shown with the bathymetry of SM99 (figure 3.9) and SM00 (figure 3.12) later in the chapter.

Both tests probed the channel with maximal-length sequences using binary antipodal phase. In SM99, three repetitions of a 1023-point ML-sequence were made from each transducer in turn while the other transducers remained silent. Each cycle through the six transducers required approximately 2.7 seconds. This enabled an impulse response estimate between each array element pair with a 0.25 msec arrival structure resolution averaged over 250 msec and sampled every 2.7 seconds. In SM00, transmissions were simultaneously made from each transducer with a single 4095-point ML-sequence repetitively sent. This enabled an impulse response estimate between each array element pair with a 0.25 msec arrival structure resolution averaged over 1 second and sampled every second. The sequences emitted from each transducer were distinguishable due to a 200 symbol offset in the shift register used by each element to generate its sequence. As this delay exceeded the reverberation time of the channel, the output of a match filter applied to a receiver element yielded clearly distinguishable impulse response estimates from each transducer to that hydrophone. Typical impulse

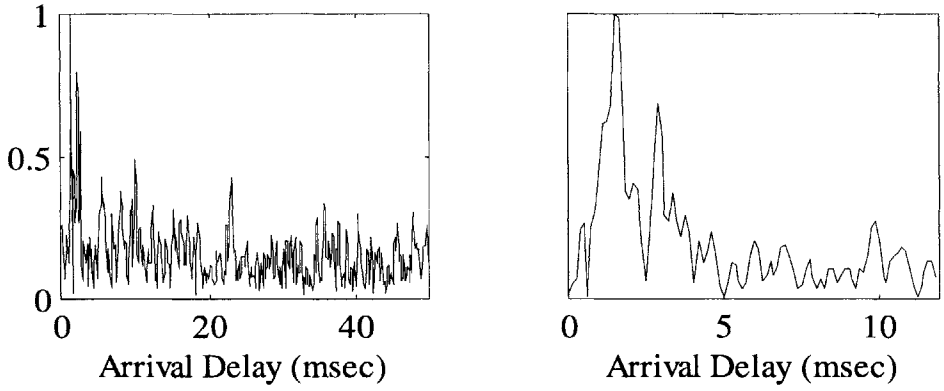

Figure 3.1. Typical impulse responses for the SM99 experiment (left panel) and the SM00 experiment (right panel) are shown here. The lower processing gain of the SM99 channel probe is evidenced by the pronounced noise. The shorter range of the SM00 experiment is likewise evidenced by the shorter total delay spreads.

responses for each experimental site are shown in figure 3.1. All experimental results presented in this chapter come from these two data sets (SM99 and SM00).

3.2 Singular Value Distributions

The fundamental requirement for generating multiple parallel channels within the single, physical channel is that they are spatially separable and convey enough energy relative to the relevant noise processes to be useful. As extensively discussed in Chapter 2, the singular value decomposition of the channel transfer function matrix provides this information. While the excitation filters need not be the right singular vectors themselves, the distribution of singular values dictates the maximum number and strength of parallel channels achievable. In this section, the distribution and stability of channel singular values will be investigated.

Using the estimated transfer function matrix, $\mathbf{T}(f)$, for each of 111 consecutive channel estimates for SM99, singular values at each frequency for each right singular vector (a potential parallel channel) were computed. If $\mathbf{T}^{(q)}(f)$ is the transfer function of a given realization, the sample singular values refer to a SVD of $\mathbf{T}^{(q)H}(f)\mathbf{T}^{(q)}(f)$. The

frequency sampling was discrete at approximately 16 Hz intervals (512 point FFT's at an 8 kHz sampling rate). The solutions were linked across frequency using a "smoothness" criterion. This rule took each singular vector at a given frequency and projected it onto each singular vector from an adjacent frequency increment. Singular vectors with the highest projections (most similar) were paired. This strategy results in time-domain filters with confined temporal support in the sense that the filters are as smooth as possible in the frequency domain. One could pursue other strategies for matching in frequency as was discussed in Chapter 2. The total power transferred by the resulting six filters was computed by summing the square of their singular values in frequency.

The result, shown in figure 3.2, indicates a relatively stable distribution in power between the sample parallel channels over the five minute sampling period. The standard deviation in sample λ^2 ranges from 1.3 dB for the strongest to 3.1 dB for the weakest. The efficiency of each sample channel falls off nearly linearly as 5 dB per parallel channel. Also shown in the figure are the channel gains resulting from exciting the sample channels with the appropriate right singular vector of the average ensemble transfer function variance matrix, $\frac{1}{Q}\sum_{q=1}^{Q}\mathbf{T}^{(q)H}(f)\mathbf{T}^{(q)}(f)$, shown as dotted curves. These will be referred to as ensemble average quantities. Two aspects of this data will now be discussed.

As the example in section 2.1 showed, a 5 dB difference in efficiency or, equivalently, noise power between channels would suggest little benefit for spatial modulation in a ideal AWGN channel. Two factors mitigate this conclusion. First, in the absence of a decomposition such as this one, the conventional signaling strategy would typically be to uniformly excite the transducers. Using the measured data, such a strategy

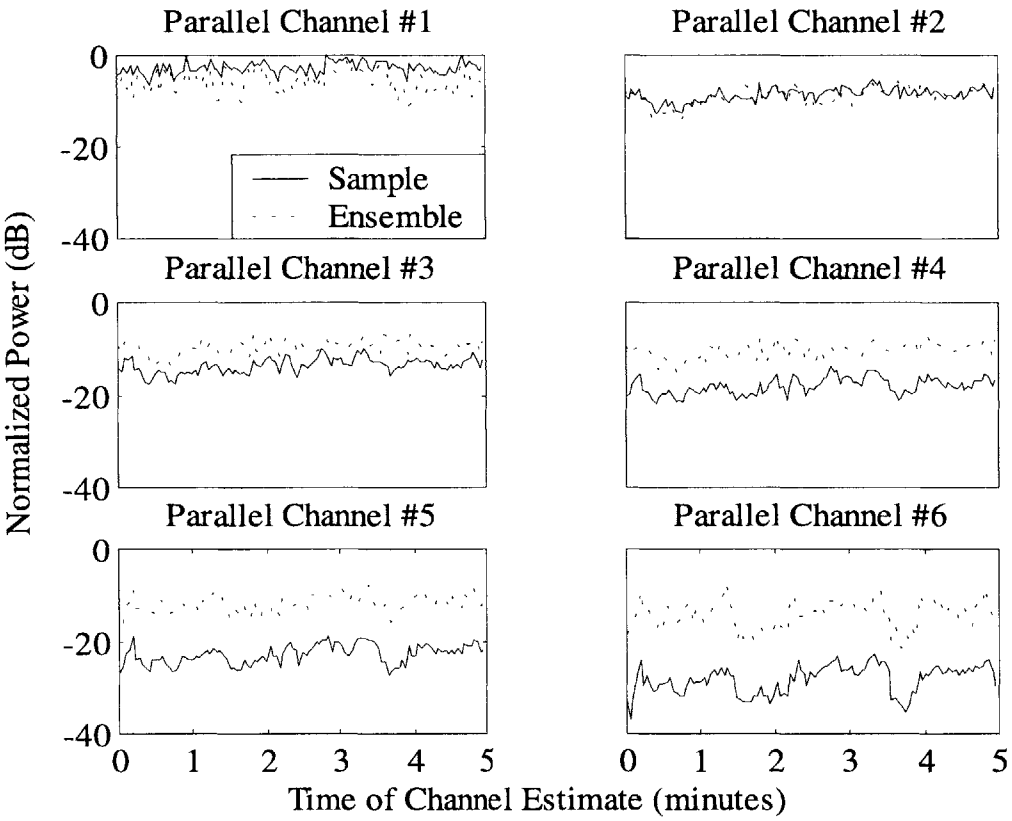

Figure 3.2. The normalized power transfer efficiency of the six parallel channels is shown here for each SM99 channel impulse response estimate (site 2) over a 5 minute observation interval at 2.7 second intervals. The curves labeled sample result from exciting the channel with the right singular vector of that sample's impulse response while the curves labeled ensemble result from using the fixed right singular vector of the channel ensemble, of $\mathbf{T}^H(f)\mathbf{T}(f)$. Each instantaneous sample channel's power falls off linearly by about 5 dB per channel.

would result in mean power transfer 6.5 dB lower than that achieved by the first right singular vector. If only the transducer with the most efficient power transfer were used, the mean power transfer would still be 5.0 dB less. Thus, even a single channel would benefit from the proposed channel formation methodology just by exciting the channel more effectively. Second, many underwater acoustic telemetry channels, including this one, are not power limited. The total noise power in each parallel channel is a function of residual ISI and largely independent of power efficiency as long as the signal power is sufficiently above the receiver ambient noise floor. As will be shown in Chapter 4,

spatial modulation of two parallel channels significantly improved performance in spite of a 5 dB difference in power transfer efficiency of the underlying parallel channels.

The difference between the ensemble average singular values and the "instantaneous" sample channel values points to a subtle but important issue. It is possible to have six, equal valued ensemble average singular values but only one usable parallel channel. If the channel has only a single propagation path yet that path fluctuates over the entire range of the signal space defined by the right singular vectors, the ensemble average matrix $\mathbf{T}^H(f)\mathbf{T}(f)$ would be full rank even though each member is only rank one. A frequency analog to this spatial problem would be that of a Doppler spread channel resulting from a single, slowly wandering Doppler shift. A useful approximate measure of the number of degrees of freedom in the channel is [32],

$$N_{dof} \approx \frac{\left(\sum \lambda\right)^2}{\sum \lambda^2} \qquad 3.1$$

The mean value of N_{dof} for this data set is 3.3 while N_{dof} for the ensemble average singular values is 5.3. One way to interpret this is that the channel would support 3 parallel channels at any point in time but these channels wander over a 5-dimensional subspace over time. As alluded to earlier, if the noise floor of the parallel channels is ISI limited, equation 3.1 may be a conservative estimate of the number of useful parallel channels as channel gain is not important.

Using the estimated transfer function matrix, $\mathbf{T}(f)$, for each of 300 consecutive channel estimates for SM00, the power transfer efficiency of the available parallel channels was computed as for SM99. The result, shown in figure 3.3, is qualitatively similar to SM99. The variance in power transfer efficiency ranges from 0.4 dB to 0.6 dB, however, which is substantially less than SM99. Array motion was substantially reduced

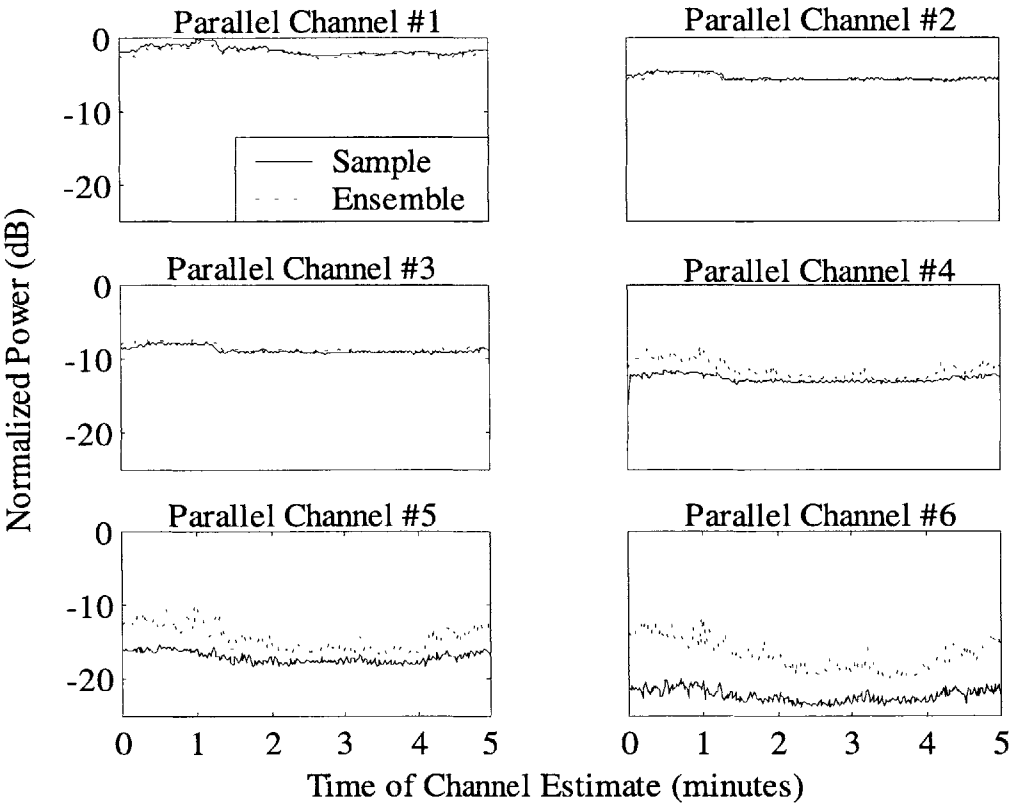

Figure 3.3. The normalized power transfer efficiency of the six parallel channels is shown here for each SM00 channel impulse response estimate (March 6) over a 5 minute observation interval at 1 second intervals. The curves labeled sample result from exciting the channel with the appropriate right singular vector of that sample's impulse response while the curves labeled ensemble result from using the fixed right singular vector of the channel ensemble, of $\mathbf{T}^H(f)\mathbf{T}(f)$. Each sample channel's power has a standard deviation ranging from 0.4 to 0.6 dB while the mean falls off linearly by about 4 dB per channel.

in this experiment. In addition, the data was taken in the early morning hours during slack tide when the surface was essentially flat. Interestingly, the fall off in from one parallel channel to the next is still linear at about 4 dB per channel. The average degrees of freedom number 4.0 while the ensemble average indicates 4.3 degrees of freedom. The similarity of these numbers is indicative of the stability of the channel. As before, there is *some* expansion of the subspace spanned by the parallel channels over the five minutes of channel estimation but it would appear that most of the variability is confined to the fourth parallel channel wandering a bit in the overall channel space exclusive of

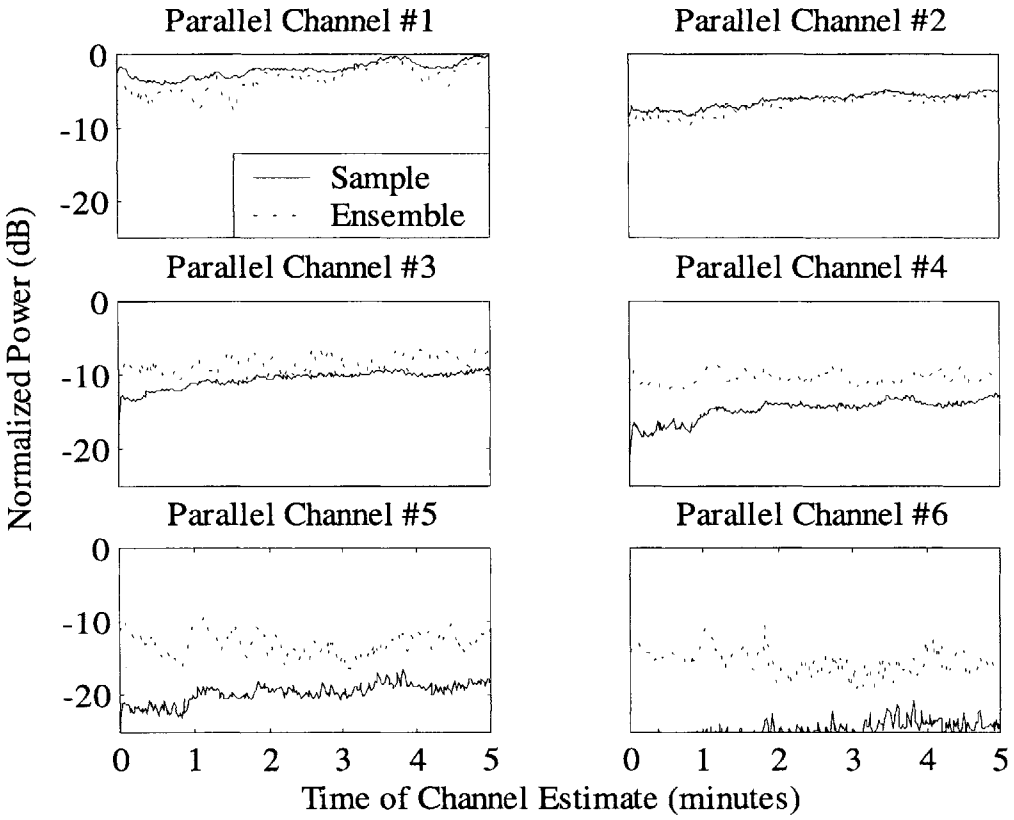

Figure 3.4. The normalized power transfer efficiency of the six parallel channels is shown here for each SM00 channel impulse response estimate (February 29) over a 5 minute observation interval at 1 second intervals. The curves labeled sample result from exciting the channel with the appropriate right singular vector of that sample's impulse response while the curves labeled ensemble result from using the fixed right singular vector of the channel ensemble, of $\mathbf{T}^H(f)\mathbf{T}(f)$.

channels 1 through 3 because these first three channels have equivalent sample and ensemble singular values.

An important concern for using the results of this decomposition is their stability over different time scales. Thus far, only the singular values and relatively short time intervals have been considered. In SM00, the same experiment was conducted on several different days allowing a look at singular value stability over longer time scales. The data presented in figure 3.3 was taken on March 6. In figure 3.4, the equivalent data taken 7 days earlier on February 29 is shown. The overall structure is quite similar with an approximately linear drop of 4 - 5 dB per channel between the efficiencies of the

parallel channels. Surface conditions were rougher as the wind produced waves of 6 – 8 inches height, introducing pronounced scattering losses for surface interacting propagation paths as this roughness is comparable to an acoustic wavelength in the test, as well as producing modest movement of the transmitter boat at anchor.

While the discussion thus far has not elaborated on the precise filters needed to generate and exploit parallel channels, the distribution of channel singular values has been shown to support multiple parallel channels consistently over time periods ranging from minutes to days. Furthermore, it has been shown that the singular values of an ensemble averaged $\mathbf{T}^H(f)\mathbf{T}(f)$ are representative of those of a single realization for these two channels implying the averaging time did not exceed the coherence time significantly. Extremely short time scale fluctuations (less than about a second) are not represented in this analysis as the processing of the ML-sequences averages the impulse response estimates over 250 msec (SM99) and 1 second (SM00).

3.3 Maximum Average Power Transfer through a Channel

As has been shown, the largest singular value of the ensemble average of $\mathbf{T}^H(f)\mathbf{T}(f)$ is, directly, the largest possible average power transfer efficiency in the channel. By comparing the largest gain of the sample singular vectors to the gain of the most effective ensemble singular vector, in figures 3.2 through 3.4, it is clear that the singular vector associated with the largest ensemble singular value is appropriate to use in constructing the transmitted signal if one desires to maximize power through the channel. As an additional argument for their practical use, the predictive reliability of using $\mathbf{T}^H(f)\mathbf{T}(f)$ to forecast average power transfer will be briefly explored for the channel in SM00.

As will be discussed in Chapter 4, several spatial modulation strategies were tested subsequent to the channel measurements under consideration here. Using the channel measurement data, the average power transfer of five such strategies will be predicted and then compared to experimental data taken subsequent to the channel probing (in this case, a half hour later). The first strategy, termed the conventional approach, is to equally apportion the available power between all six transducers and form a broadside beam. This quantity will be used as the reference in that the efficiency of other methods will be expressed relative to it. The second strategy, a simple spatial modulation approach, apportions power to a subarray, namely the top three transducers (Sub-Array 1). The third strategy will solely use the fourth transducer which was observed to have the best individual efficiency (Sub-Array 2). The fourth strategy will take the first singular vector of the ensemble average of $\mathbf{T}^H(f_c)\mathbf{T}(f_c)$ where f_c is the carrier frequency. This may be interpreted as narrowband beamforming. The fifth strategy will use the time domain version of the first singular vector of the ensemble average of $\mathbf{T}^H(f)\mathbf{T}(f)$. This may be interpreted as broadband beamforming. The predicted and measured power transfer efficiency of these strategies is given in Table 3.1. While the predictions are based on channel measurements made within an hour of the actual

Table 3.1. The predicted and measured power transfer efficiency of four spatial modulation strategies in the SM00 experiment on March 6 are given here in units of dB and are expressed relative to the efficiency of the conventional approach of broadside beamforming.

Strategy	Predicted Efficiency (dB)	Measured Efficiency (dB)
Sub-Array 1	-2.2	-1.5
Sub-Array 2	+2.9	+1.5
Singular Vector at f_c	+1.6	-0.7
Broadband Singular Vector	+5.4	+6.3

measurements, the specific transducer array excitations used in the last three strategies are based on channel measurements made *1 week* earlier. With this in mind, the agreement is even more remarkable.

The results documented in this section should be viewed as a principal accomplishment of this work. The decomposition tools described in Chapter 2 led to a signal design that improved power efficiency by over 6 dB and, perhaps more importantly, yielded a benefit that was stable and predictable over at least a one week time period. These results implicitly show the stability of the first singular vector for the channel. In the next section, the discussion will be expanded to explicitly examine the stability of all six singular vectors.

3.4 Interpretation and Evolution of the Channel Singular Vectors

The objective of this section is twofold. First, the stability of the singular vectors is to be characterized. This will be done by examining how the subspace spanned by singular vectors from successive channel realizations expands in time. Second, the singular vectors will be physically related to the channel and interpreted via beamforming and ray modeling techniques.

3.4.1 Temporal Variability of Channel Singular Vectors

In order for spatial modulation to offer a practical solution to improving communication reliability, the required time constants for tracking the channel and updating the transmitter steering vectors must be "acceptably" long. These requirements will derive from specific system capabilities and, therefore, will not be addressed here. Rather, the decomposition temporal variability in SM99 and SM00 will be investigated. Using the ensemble of channel impulse response measurements, $\mathbf{T}^{(q)}(f)$, singular value decompositions were performed for each realization yielding a set of right singular

vectors, $\mathbf{V}_i^{(q)}(f)$, where q denotes the realization and i denotes subspace number. They are ordered in descending singular values. $\mathbf{V}_i^{avg}(f)$ are the set of singular vectors resulting from the decomposition of the ensemble average of $\mathbf{T}^{(q)H}(f)\mathbf{T}^{(q)}(f)$. The set of $\mathbf{V}_i^{avg}(f)$ will form the fixed basis against which the $\mathbf{V}_i^{(q)}(f)$ are projected. The projections are squared and summed in frequency to finally arrive at what portion of the power carried by $\mathbf{V}_i^{(q)}$ is found in each of the six subspaces defined by $\mathbf{V}_i^{avg}$.

The projections of the SM99 data set, seen in figure 3.5, show a modest variability. The first and, surprisingly, the last right singular vectors of each realization remain well confined while intermediate vectors spread into the other subspaces. Array motion in this experiment was severe with tilts of 10 degrees and translations of 10 meters over 2 minute periods common. The data in this plot averages ten successive measurements of $\mathbf{T}^H\mathbf{T}$ and resulted in reduced spreading compared to projections based on single measurements.

The projections of the SM00 (March 6) data set, seen in figure 3.6, show an extremely high degree of subspace stability over the entire 5 minute duration of the data set. Even the higher singular vectors, associated with weak propagation paths, remain remarkably consistent. For the SM00 channel, the decomposition would support channel feedback delays greater than 5 minutes without any performance degradation.

Stability over a much greater time scale (1 week) can be assessed by projecting the SM00 (March 6) data set against the ensemble average basis vectors measured on February 29. Shown in figure 3.7, one may conclude that the first subspace is stable over that one week time period while the remaining subspaces undergo modest spreading. The

stability of the first subspace is consistent with the successful average power result of the previous section.

Surface conditions during the March 6 SM00 experiment were quiescent while 6 – 8 inch waves were present during the February 29 SM00 experiment. The greater environmental variability is reflected in a greater sub-space variability for this data set as seen in figure 3.8. The strongest sub-space remains stable while the remainder spread into adjacent subspaces over the five-minute observation interval. With the goal of explaining the observed variability in decomposition, classical ray theory will now be used in conjunction with measured sound velocity profiles to model the propagation paths in both SM99 and SM00.

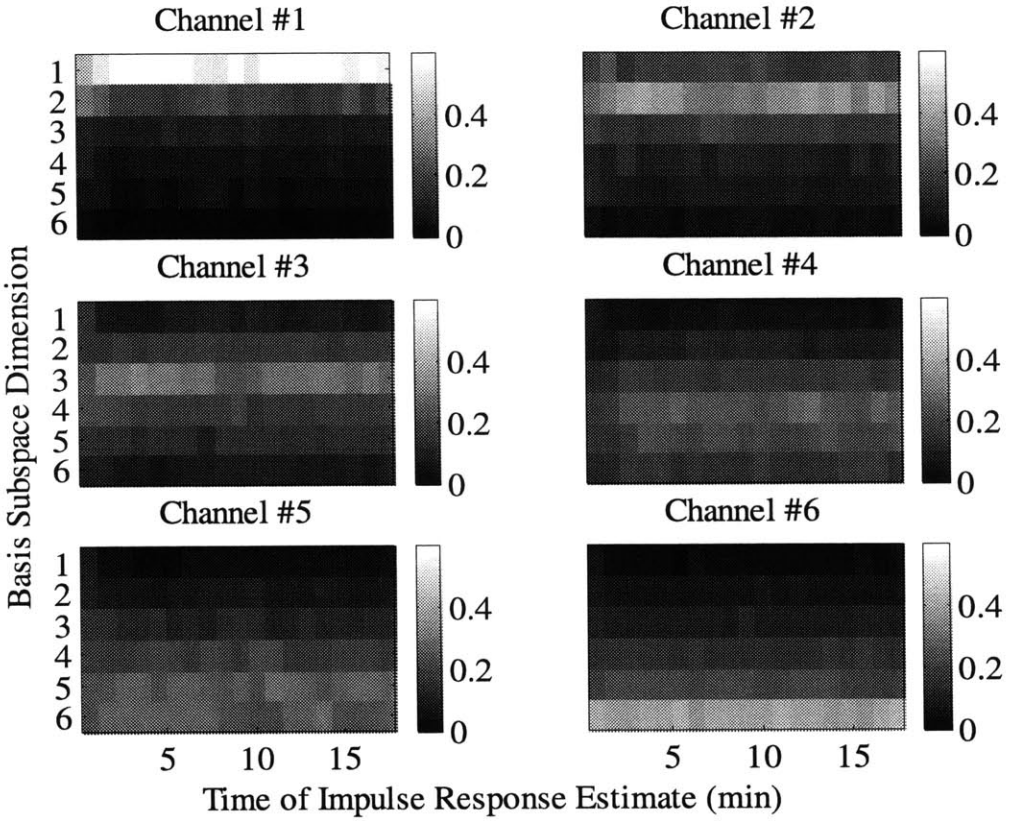

Figure 3.5. The six right singular vectors that result from an SVD of successive channel realizations from the SM99 site 2 experiment are projected into the fixed subspace defined by the right singular vectors of the ensemble average of $\mathbf{T}^H(f)\mathbf{T}(f)$. The fraction of the vector's power contained in each subspace is shown in the panels above in descending order of singular values from left to right and top to bottom.

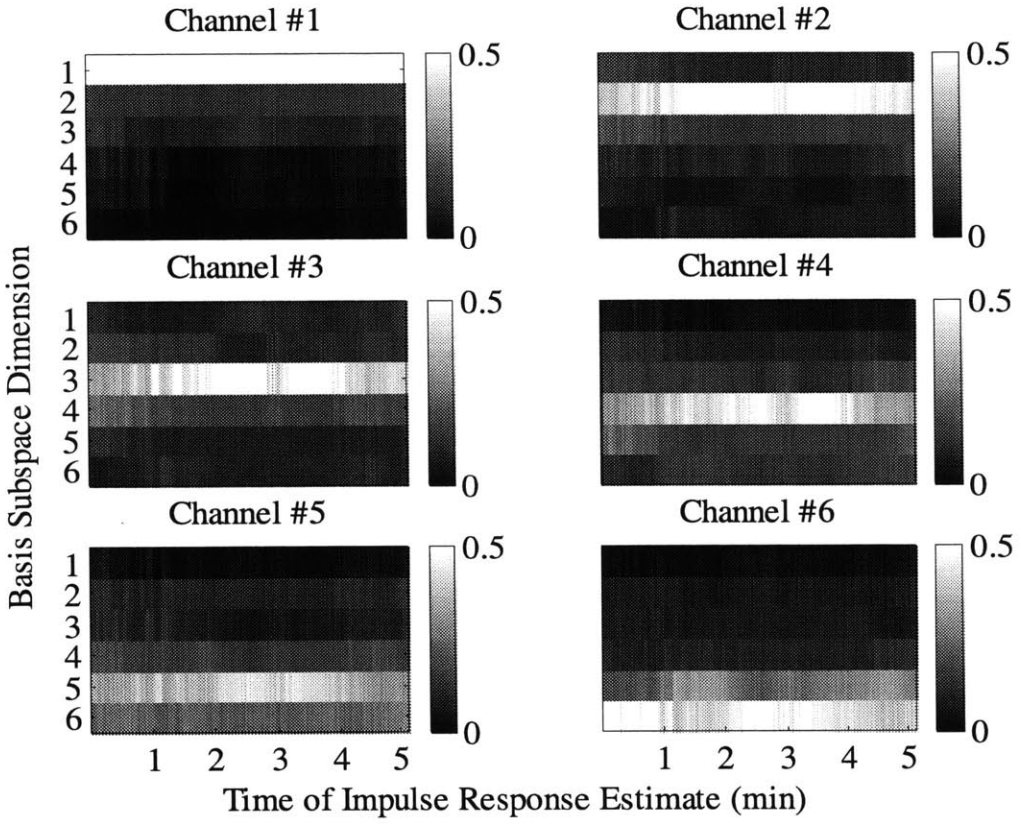

Figure 3.6. The six right singular vectors that result from an SVD of successive channel realizations from the March 6 SM00 experiment are projected into the fixed subspace defined by the right singular vectors of the ensemble average of $\mathbf{T}^H(f)\mathbf{T}(f)$ from that day. The fraction of the vector's power contained in each subspace is shown in the panels above in descending order of singular values from left to right and top to bottom.

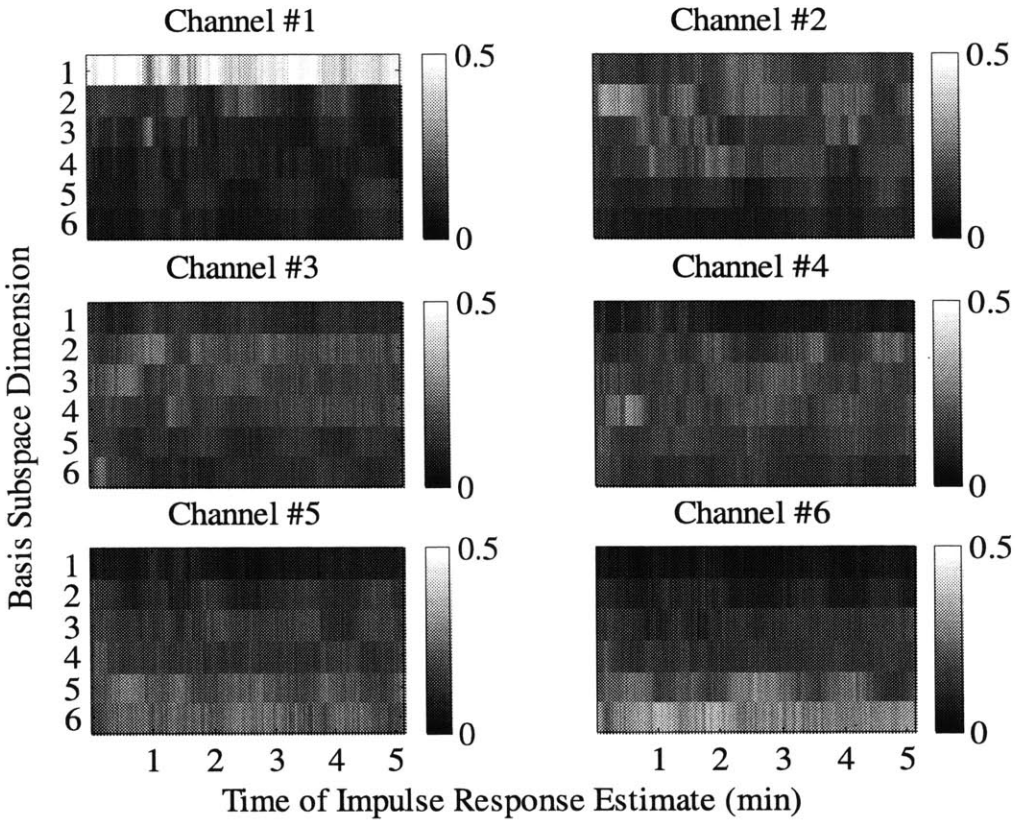

Figure 3.7. The six right singular vectors that result from an SVD of successive channel realizations from the March 6 SM00 experiment are projected into the fixed subspace defined by the right singular vectors of the ensemble average of $\mathbf{T}^H(f)\mathbf{T}(f)$ taken one week earlier. The fraction of the vector's power contained in each subspace is shown in the panels above in descending order of singular values from left to right and top to bottom.

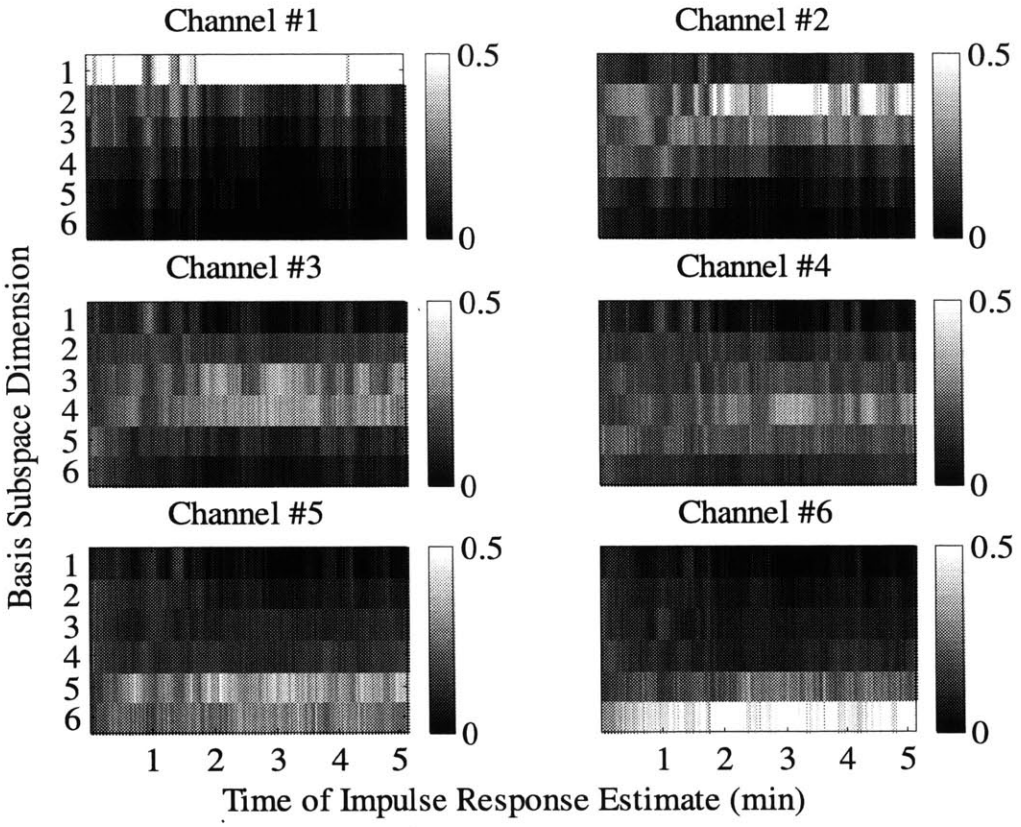

Figure 3.8. The six right singular vectors that result from an SVD of successive channel realizations from the February 29 SM00 experiment are projected into the fixed subspace defined by the right singular vectors of the ensemble average of $\mathbf{T}^H(f)\mathbf{T}(f)$. The fraction of the vector's power contained in each subspace is shown in the panels above in descending order of singular values from left to right and top to bottom.

3.4.2 Ray Theory Interpretation of Channel Singular Vectors

In both the SM99 and SM00 experiment, the transmitter array was quite sparse. As such, beamforming the right singular vectors yields results that are difficult to interpret. The receiver array, however, has a 15 wavelength aperture with 16 elements and is quite amenable to beamforming. The approach taken here will be to use ray theory to compute eigenrays from each transmitter to the receiver. The beamformed response to the ensemble average singular vectors will also be computed. Having associated ray arrival angles with paths through the water column, the behavior of the singular vector response will be explored in terms of the propagation paths they exploit.

For the SM99 experiment, the temperature profile was measured with a 16 element thermistor string collocated with the transmitter array. A range-invariant sound velocity profile was computed and used as input to a ray tracing program. The sound speed was approximately uniform to 8 meters depth with a value of 1529.5 m/sec with an approximately linear drop of 3 m/sec over the remaining 6 meters of depth. There was slight sound speed minimum at 5 meters amounting to a 0.2 m/sec deficit. The physical paths taken by the eigenrays from each transducer to the center of the receiver array are shown in figure 3.9. Surface conditions were rough during the experiment. As such, only eigenrays that interact with the surface no more than twice are considered. The arrivals can be grouped according to arrival angle. Transducer number 4 exploits the sound speed minimum and has a strong direct arrival component. The top three transducers primarily excite arrivals at +/- 2 degrees while the lower two transducers include a mix of these. Considering these responses with an eye towards spatial modulation, a scheme that uses transducer number 4 for one parallel channel and transducers 1-3 for another may be expected to work well as their spatial expression on

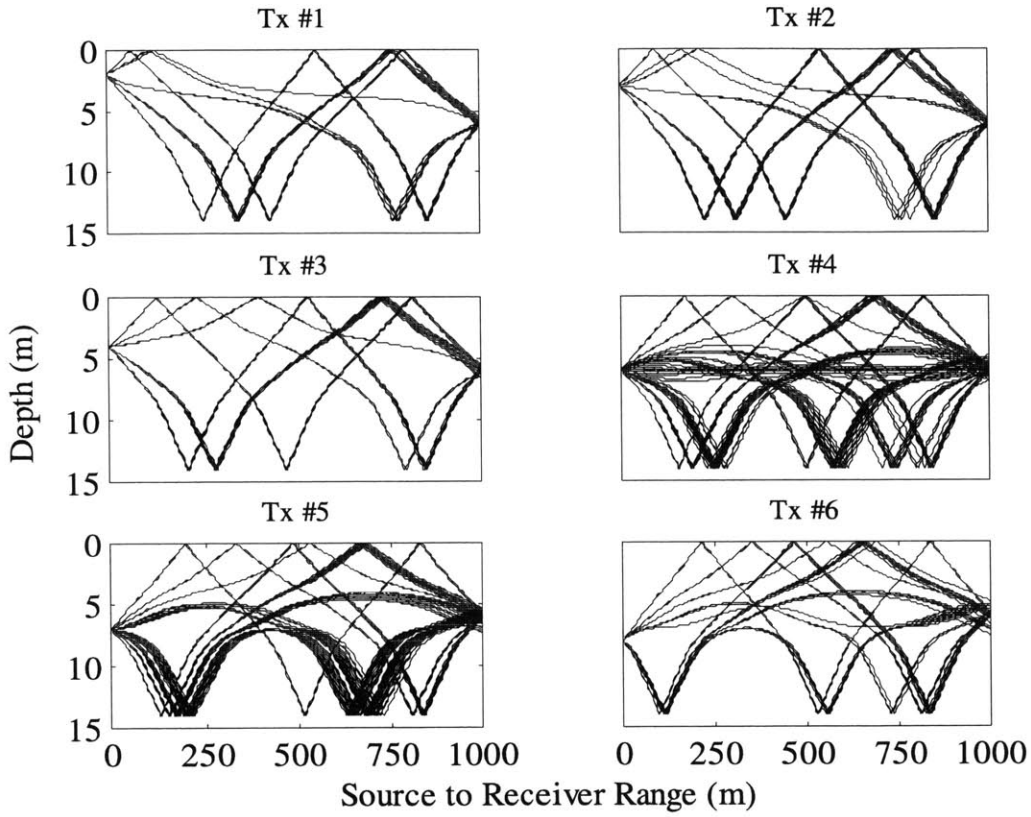

Figure 3.9. Using the measured sound velocity profile in the SM99 experiment, a ray model was used to discern the propagation paths from each transducer to the receiver array. Transducer 4 couples well into a weak sound channel giving a large direct arrival. The upper three transducers excite surface and bottom paths with angles of arrival 1 to 2 degrees off boresight.

the receiver array is distinct. As will be shown in Chapter 4, such a sub-arraying approach indeed works well.

Given these underlying propagation paths, it will be instructive to consider the beamformed response at the receiver array due to the use of the first two singular vectors that result from a SVD of the channel ensemble. The angle spread between eigenray arrivals is less than the conventional beamwidth of the 15 wavelength aperture receiver array. In order to resolve these arrivals, results will be given in a delay / angle of arrival space. As noted earlier, there was a great deal of array motion in the SM99 experiment making it difficult to show an average delay/angle response. Instead, measured impulse

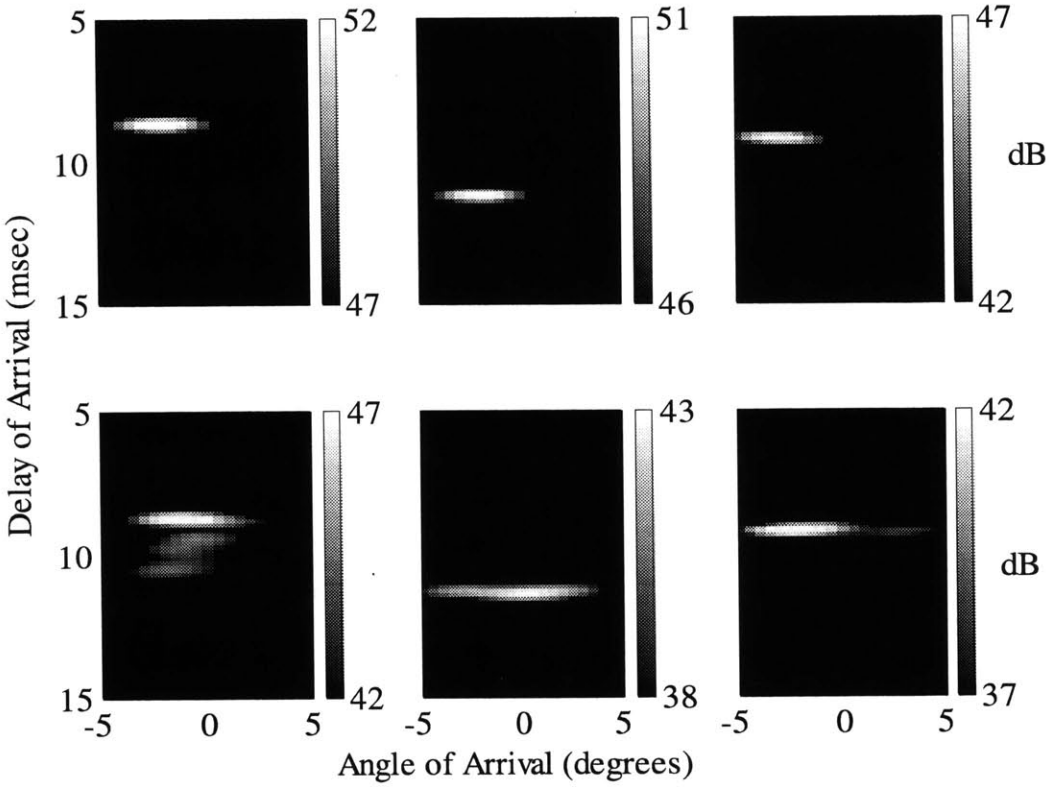

Figure 3.10. The scattering function in a delay-of-arrival versus angle-of-arrival space is shown for three channel realizations in the SM99 experiment. The top three panels show the response due to the first singular vector of an SVD for that realization while the bottom three panels show the response due to the second singular vector. From left to right, the panels give the responses using three different channel measurements. The angle separation between the response peaks due to the two vectors is approximately 1.5 degrees.

responses at the beginning, middle, and end of a several minute observation interval will be used to give snapshots of the response.

In figure 3.10, the responses due to the first two right singular vectors from an SVD of the three channel realizations are shown. The first singular vector, shown in the top three panels, exclusively excites the direct arrival. The reader is cautioned that the direct arrival wanders in angle with respect to the array perpendicular due to the tilting of the array in the currents. In addition, there is a mean movement of the array resulting in arrival delay wander. These wanders are consistent with the array motion. The second singular vector, shown in the bottom three panels, excites an arrival approximately 2

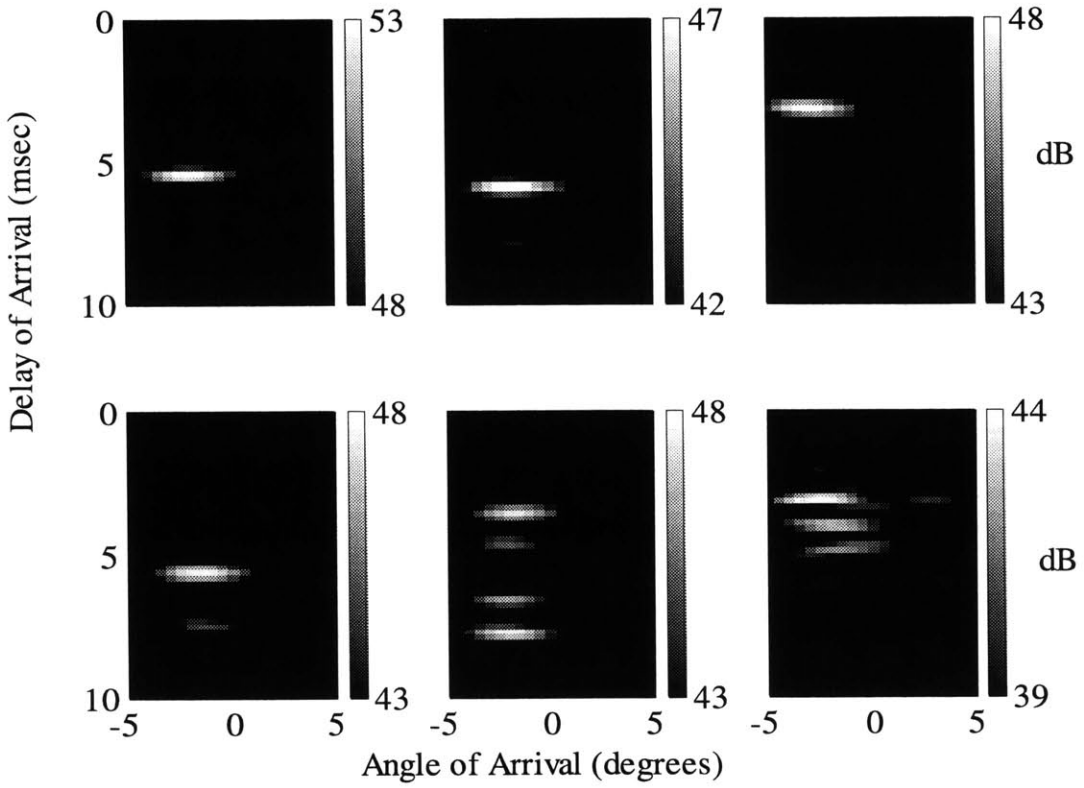

Figure 3.11. The scattering function in a delay-of-arrival versus angle-of-arrival space is shown for three channel realizations in the SM99 experiment. The top three panels show the response due to the first singular vector of an SVD for the channel ensemble while the bottom three panels show the response due to the second singular vector. From left to right, the panels give the responses using three different channel measurements. The spatial distinctiveness is substantially diminished compared to figure 3.10.

degrees off of the direct arrival. This result is consistent with the predictions made using the ray model. In light of the rough surface conditions during the test, surface interacting paths were expected to experience severe scattering loss. As such, the arrival associated with the second right singular vector is likely a bottom-only interacting path.

In figure 3.11, the same channels are excited with the singular vectors resulting from the ensemble SVD. The performance is substantially more variable in time with the first channel realization responding similarly while the other channel realizations give a less spatially distinct response to the two vectors while their temporal distinctiveness is large but highly variable. The high degree of array motion in SM99 imposed strict

constraints on decomposition stability as reflected in the differences between these two figures.

The SM00 data set may be similarly interpreted. Conditions in Woods Hole Harbor during the winter are well-mixed giving isothermal conditions. The bathymetry, however, was uneven. Water depth at each end of the channel was 20 meters while the bottom rose to a 13 meter depth in between. This range variability introduces an asymmetry in the arrival structure as rays that are initially downward going grow steeper upon interaction with the bottom. Figure 3.12 shows the propagation paths from each transducer to the receiver array computed using ray theory.

As with the SM99 data, a scattering function plot in a delay-of-arrival versus angle-of-arrival space for the channel response due to the use of the first and second singular vectors derived from a SVD of the particular channel realization allows a clear physical interpretation (figure 3.13). The first singular vector excites a powerful, boresight arrival while the second singular vector seeks to variably excite the initially downward going and initially upward going rays. The predicted asymmetry is evident with a larger downwardly arriving response angle compared to the upwardly arriving response angle. When the response due to the singular vectors of the channel ensemble decomposition is considered (figure 3.14), the result is strikingly different from SM99. Not only does the spatial distinctiveness remain but the variable emphasis on the downward and upward going off-angle rays disappears. The result is consistent with the overall stability of this channel. The reader is cautioned to remember that the stability is only in the dominant spatial structure. The challenges facing the equalizer in coping with

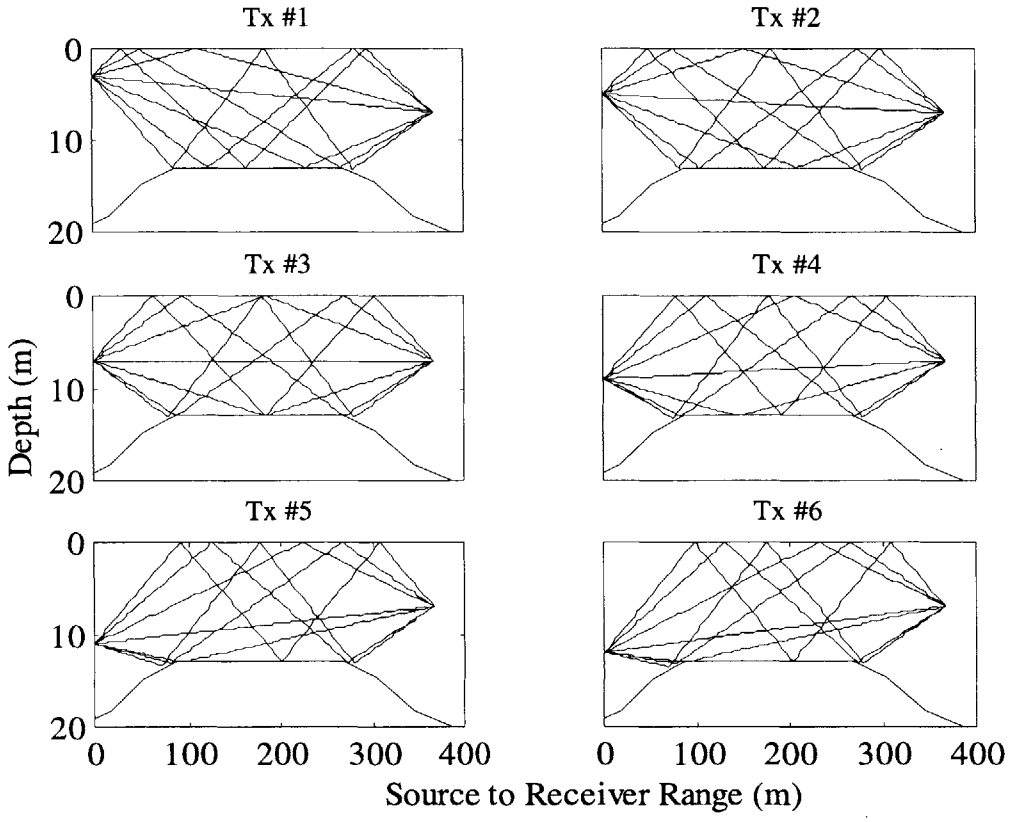

Figure 3.12. Using a uniform sound velocity profile in the SM00 experiment, a ray model was used to discern the propagation paths from each transducer to the receiver array. A direct arrival is evident for all transducers while off angle arrivals range from 1-4 degrees for upward arriving rays (positive angle) and 3-7 degrees for downward arriving rays (negative angle).

the phase variability and long, reverberation tails encountered in this channel are as, or more, difficult than many underwater channels.

This section sought to characterize the stability of the spatial sub-spaces described by the decomposition techniques of this thesis when applied to two data sets. The subspaces of SM99 were modestly variable with the dominant sub-space remaining confined while the remaining spaces intermingled over time. The stability of the SM00 subspaces is high over time scales of minutes while the dominant subspace persisted for over a week. The observed stability is an encouraging result for future spatial modulation work that seeks to implement real-time feedback. When the receive array response to the

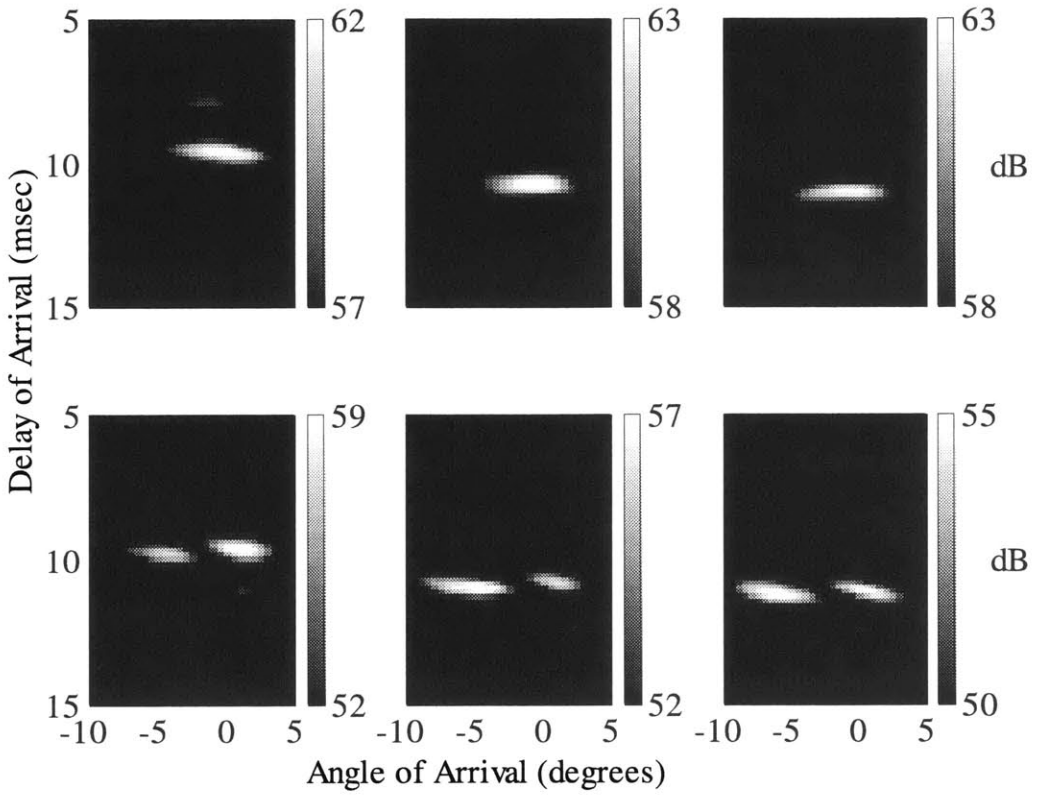

Figure 3.13. The scattering function in a delay-of-arrival versus angle-of-arrival space is shown for three channel realizations in the SM00 (March 6) experiment. The top three panels show the response due to the first singular vector of an SVD for that realization while the bottom three panels show the response due to the second singular vector. From left to right, the panels give the responses using three different channel measurements.

singular vectors was examined in light of a ray theory analysis, the association of singular vectors to particular propagation paths was clear. While other experiments will undoubtedly yield different interpretations, in both SM99 and SM00 the first right singular vector sought to excite the direct arrival while the second singular vector sought to excite the some combination of the next shallowest, resolvable ray group. This patern is to be expected as the first singular vector seeks the highest gain path which is typically the direct path while the next highest gains paths are the single surface interacting paths which are offset slightly in angle from the direct arrival. This correspondence is important for future work that seeks to use the decomposition tools to improve performance against a variety of metrics because it facilitates an intuitive understanding.

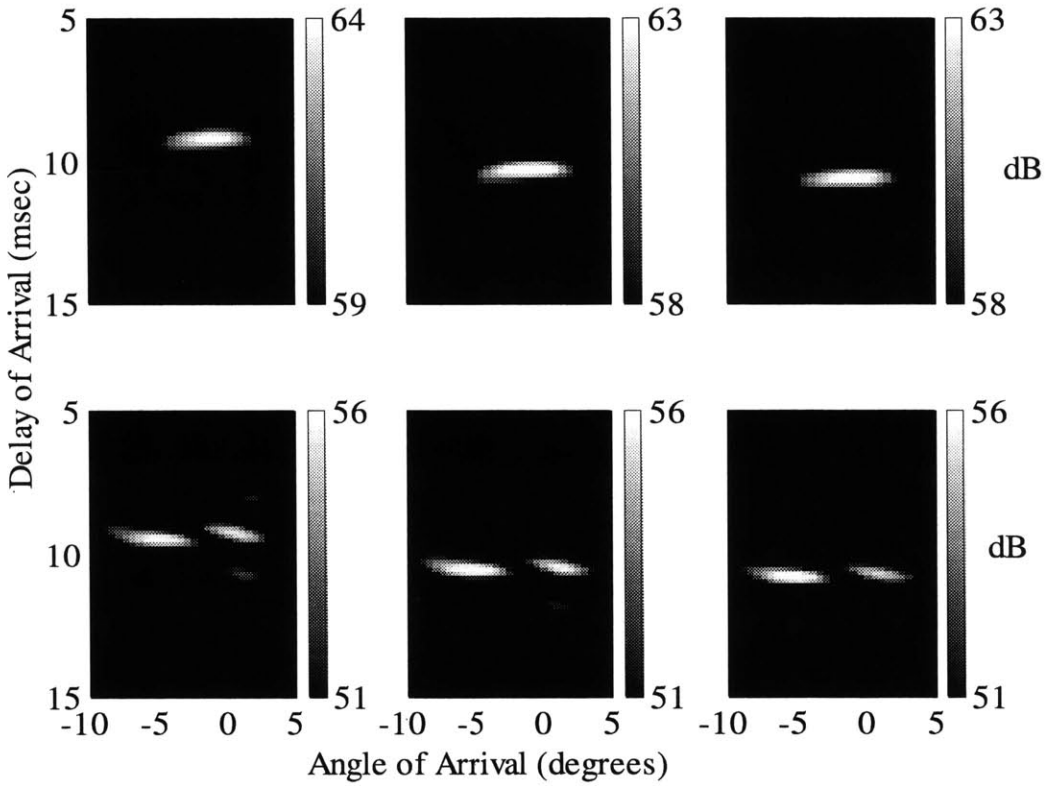

Figure 3.14. The scattering function in a delay-of-arrival versus angle-of-arrival space is shown for three channel realizations in the SM00 (March 6) experiment. The top three panels show the response due to the first singular vector of an SVD for the channel ensemble while the bottom three panels show the response due to the second singular vector. From left to right, the panels give the responses using three different channel measurements.

3.5 Experimental Performance of Average SINR Metrics

At the end of Chapter 2, several metrics were introduced that sought to govern selection of transmit steering vectors to variously maximize average power and minimize interference between spatial channels. In particular, the average crosstalk power between two channels, P_{kj}^{CT}, is defined in equation 2.50 and is minimized by solving a generalized eigenvalue problem. A second metric characterizes the average signal to interference plus noise ration ($SINR_{avg}$) and is defined in equation 2.56. In this section, the transmit steering vectors that minimize these two metrics will be computed and applied to the set of SM00 channel realizations. The resulting SINR will be compared to that of using the transmit vectors resulting from an SVD of the channel ensemble. The reader is reminded

that the interference, as defined in these metrics, presumes the receiver simply performs a match filter operation. More sophisticated processing algorithms may substantially reduce the interference. Nevertheless, this definition of interference may be used as a coarse measure of the orthogonality of the spatial channels. As in section 2.3, the analysis will be restricted to a single frequency for ease of analysis and interpretation.

This analysis will only consider creating two parallel channels from the measured SM00 channel impulse response estimates. The first spatial channel will be generated using the first singular vector from a SVD of the ensemble average of $\mathbf{T}^H(f)\mathbf{T}(f)$. The second spatial channel will be derived according to performance measures 2, 3, and 4 as described in section 2.3. As a reminder, performance measure 2 seeks to create channels whose average inner product of receive response vectors is zero and directly leads to the singular vectors of the ensemble average of $\mathbf{T}^H(f)\mathbf{T}(f)$. It does not explicitly address SINR and, as such, will serve as a basis to compare the benefits of using performance measures 3 and 4. Performance measure 3 seeks to minimize a weighted average of the interference power. Performance measure 4 seeks to minimize a weighted average of the SINR. The instantaneous SINR resulting from using each of these three vectors is shown in figure 3.15. An SNR per element of 30 dB for the first spatial channel was used. In addition, the data shown in the window has been processed with a sliding 5 second window to smooth the results. Measure 3 realized an average SINR improvement of 2.4 dB over that of measure 2. The improvement in $SINR_{avg}$ (the weighted average) was 5.2 dB. Measure 4 realized an average SINR improvement of 2.6 dB over that of measure 2 while the improvement in $SINR_{avg}$ was 5.4 dB. The loss in average power through the channel compared to that of measure 2 was 1.2 dB and 0.9 dB for measures 3 and 4,

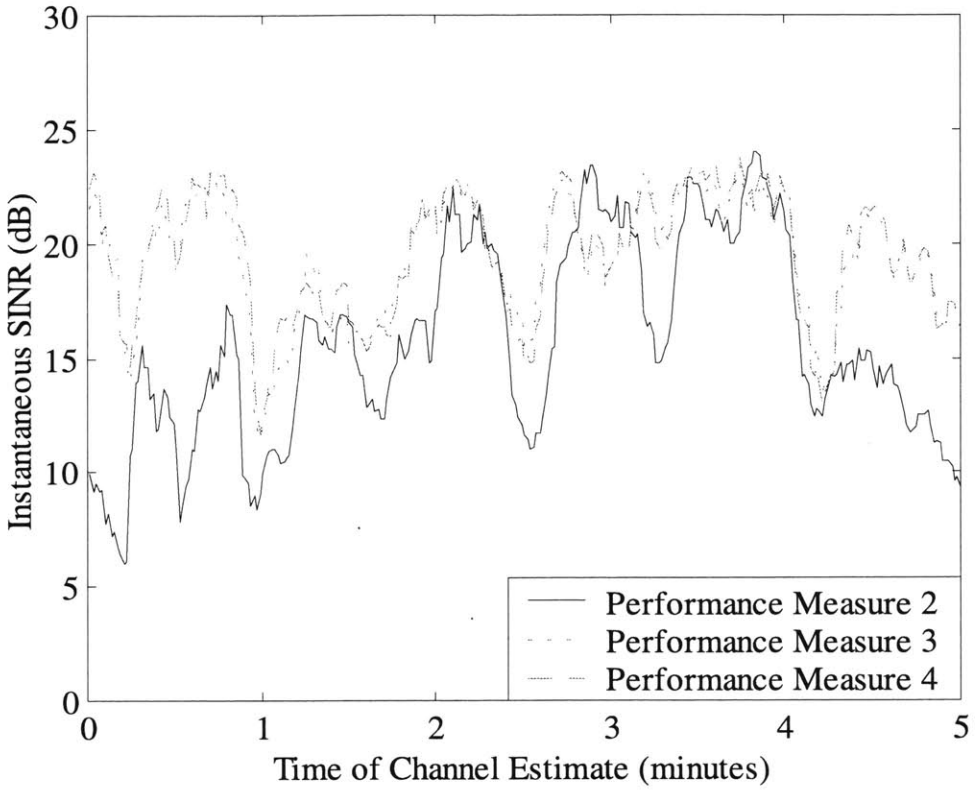

Figure 3.15. The instantaneous SINR achieved over the SM00 (Day 4) measured channel impulse response ensemble is given here assuming the first spatial channel is generated with the first singular vector of the ensemble SVD while the second spatial channel is generated via the criteria of performance measures 2, 3, and 4 as described in section 2.3. A 30 dB per receiver element noise floor is assumed with respect to the first spatial channel. The data has been smoothed with a sliding 5 second averaging window.

respectively. Of course, if co-channel interference or residual reverberation is limiting performance, this drop in average power is inconsequential. The average performance optimization tools of section 2.3 have thus been validated using experimental data.

There are several points that arise from this example. First, the increase in average SINR as compared to performance measure 2 over the entire record was modest. During the first and last minute of the measured sequence, however, the average SINR of method 2 is substantially less than in the middle of the record. The improvement due to the optimization procedures is dramatic over these intervals with average SINR increases ranging from 6 to 10 dB. Second, while the optimization was done with respect to

particular weighted averages of interference power and SINR, the instantaneous SINR nevertheless also benefited. The optimization procedures embodied in measures 3 and 4 are readily implemented and avoid the brute force non-linear optimization algorithm that maximization of the average instantaneous SINR would entail. Furthermore, the procedures readily accept second and fourth order moment characterizations of the channel in lieu of many realizations. The measures, while sub-optimal, are nevertheless valuable. The third, and final, point is that the performance advantage of measure 4 over measure 3 is slight while the additional computational complexity is substantial. If computational complexity is an issue for any future implementations, performance measure 3 may be considered adequate.

3.6 Extending the Decomposition to Complex Gaussian Channels

An active area of current research focuses on the benefits of multi-antenna systems communicating through complex Gaussian channels where each element of the transfer function matrix is a Gaussian random variable. Much of this research, which was briefly described in Chapter 1, does not exploit any knowledge of a given channel realization and, furthermore, presumes no coherence between the channels excited by each transmitter. Consequently, coherent excitation strategies are largely neglected and the performance benefits are characterized by increased diversity and achieved by particular coding strategies. Conversely, this thesis has concentrated on the coherent exploitation of multi-antenna systems over deterministic channels. By neglecting the consequences of stochastic phenomena such as Rayleigh fading, the performance benefits are largely capacity increases due to the additional spatial bandwidth and achieved by particular beamforming strategies.

The purpose of this final section is to lay a foundation for bridging the gap between these perspectives. The methodology will be to assume, as many others do, that the transfer function matrix is composed of Gaussian random variables. The average *SINR* (as described in section 2.3) will then be analyzed in terms of the second and fourth moments of these variables. The case where the random variables are independent and identically distributed will be considered and related to existing results. The consequences of coherence between the variables will also be discussed. To ease the analysis, only a single frequency will be considered.

3.6.1 Validity of the Complex Gaussian Assumption

The extensive channel measurements made in the SM00 experiment allow an experimental validation of the assumption that the transfer function matrix elements are Gaussian random variables. Specifically, the transfer function matrix, **T**, was measured each second over a five minute period. In figure 3.16, the estimated probability density function (pdf) of the real part of the complex attenuation coefficient at the carrier frequency for four selected transmitter / receiver pairings is shown. The data has been normalized by the estimated standard deviation. For comparison, a normal pdf with the same mean and unit variance has been overlayed. When a log-likelihood ratio test is performed to gauge the hypothesis that the underlying distribution is normal, the hypothesis is rejected with greater than a 99.9 % confidence for most matrix elements [34]. The assumption that **T** is a collection of Gaussian random variables would be an inappropriate one in this case for modeling channel behavior.

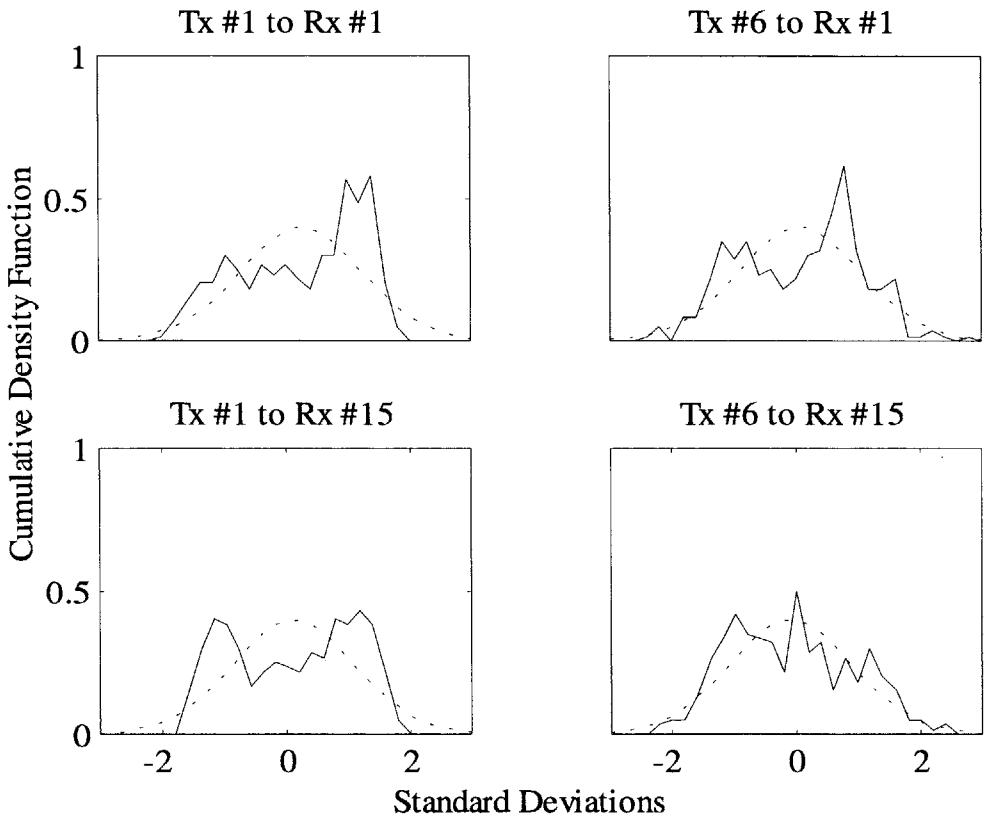

Figure 3.16. The estimated probability density function (pdf) of the real part of the complex attenuation coefficient relating 4 different transmitter / receiver pairs is shown here. The data, normalized by the estimated standard deviation, is from the SM00 March 6 experiment and is compared to a normal pdf (dotted line). The transfer function matrix at the carrier frequency (9.6 kHz) has been used.

The assumption that the Gaussian random variables are independent is also a poor one. Of course, the successful attempts to communicate coherently using coherent combining techniques implicitly demonstrate coherence, or dependence, over time scales of minutes. The coherence has important ramifications for arguments regarding diversity and capacity in this environment. Such issues are beyond the scope of this work. If the columns of **T** are "stacked" to create a single vector and the covariance of this "super-vector" is estimated, the correlation coefficient between all elements of **T** may be compactly depicted. As **T** is a 15 x 6 matrix, the "super-vector" will have 90 elements. Referring to figure 3.17, if the elements of **T** were independent, all off-diagonal terms would be zero. Note that there are 90 degrees of freedom and 300 snapshots used in this

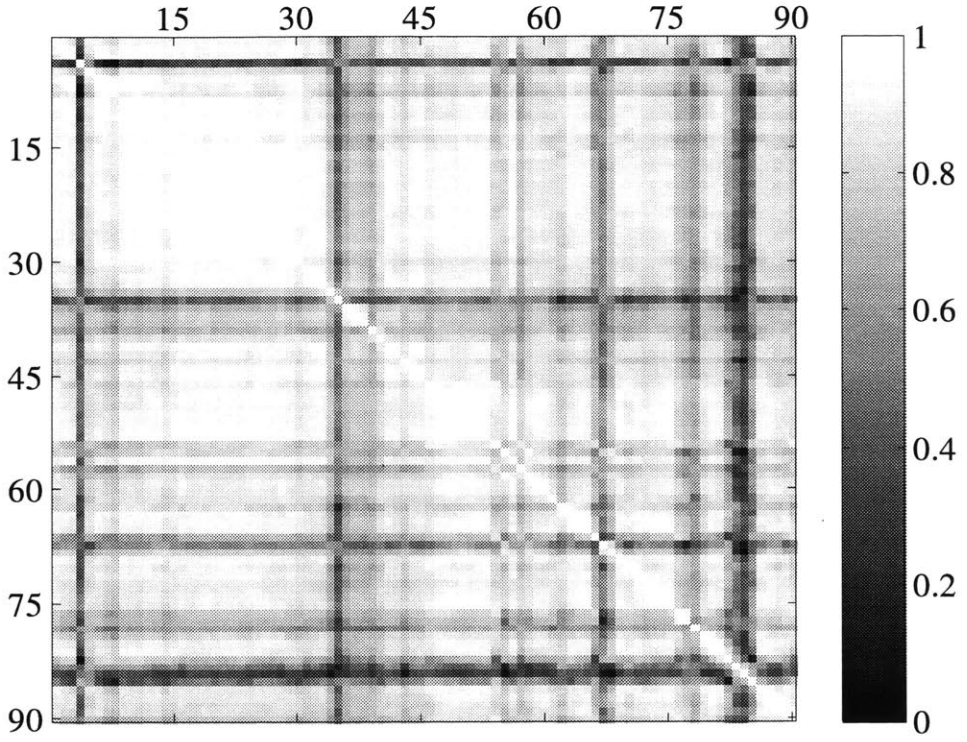

Figure 3.17. The correlation coefficient between all elements of the transfer function matrix, T, measured in the SM00 March 6 experiment is collectively shown. The columns of T were stacked to create a "super vector" whose covariance was then estimated using 300 channel samples over a 5 minute period. The indexing places the correlation coefficients between all 15 received signals due to source 1 at the top left and the coefficients between all 15 received signals due to source 6 at the bottom right. The remainder can be inferred from this description.

covariance analysis. Three snapshots per degree of freedom is usually considered adequate for covariance estimation but many caveats apply [35]. While one might expect coherence among receiver elements due to the signal from one source, the correlation between received signals due to separate sources is more striking. The dark stripes of low correlation correspond to elements of **T** with extremely low *SNR* and, as such, are only correlated with themselves.

To summarize, the assumption of independent, complex Gaussian behavior (Rayleigh fading) would seem inappropriate in this case. The assumption is made so prevalently, and without verification, in the communications literature, however, that the

behavior of the performance metrics for a truly Gaussian transfer function matrix will still be considered in spite of the lack of validity for this data set.

3.6.2 The Expected Value of Transfer Function Moments

Assuming that the elements of the transfer function matrix, **T**, are zero mean Gaussian random variables, the expected value of the matrices **A** (= $\mathbf{T}^{H}\mathbf{T}$) and **H** (= $\mathbf{T}^{H}\mathbf{T}\mathbf{X}\mathbf{X}^{H}\mathbf{T}^{H}\mathbf{T}$) may be computed from moments of the random variables. In addition, each random variable will be assumed Rayleigh in the sense that the real and imaginary parts are assumed independent. These quantities, **A** and **H** for an arbitrary given vector, **X**, appear in the performance measures described in section 2.3. In this final section, the expected values of **A** and **H** will be considered in light of varying types of coherence between the elements. Specifically, the consequences of complete independence, total correlation at the receiver, and total correlation at the transmitter will be elucidated. As a foundation for future work, a connection will be made between the classical Wishart distribution and estimates of **A** made with a finite number of channel realizations. Finally, the question of how many useful parallel channels are available in a given realization of T will be posed in terms of the ratio of fourth order products of Gaussian random variables.

The expected value of **A** is easily related to the covariance of the elements of **T**. In particular,

$$E[\mathbf{A}_{ij}] = E\left[\sum_{r=1}^{R} \mathbf{T}_{ri}^{H}\mathbf{T}_{rj}\right] \qquad 3.2$$

H may be interpreted as a linear combination of fourth order moments of the elements of **T**. While it was defined in equation 2.49, it is reproduced here in a somewhat different form..

$$E[\mathbf{H}_{kl}] = E\left[\sum_{m=1}^{S}\sum_{n=1}^{S}\sum_{r_1=1}^{R}\sum_{r_2=1}^{R}\mathbf{T}_{r_1k}^{H}\mathbf{T}_{r_1m}\mathbf{T}_{r_2n}^{H}\mathbf{T}_{r_2l}\mathbf{X}_m\mathbf{X}_n^{H}\right] = \tag{3.3}$$

$$\sum_{m=1}^{S}\sum_{n=1}^{S}\mathbf{X}_m\mathbf{X}_n^{H}\sum_{r_1=1}^{R}\sum_{r_2=1}^{R}\left(E[\mathbf{T}_{r_1k}^{H}\mathbf{T}_{r_1m}]E[\mathbf{T}_{r_2n}^{H}\mathbf{T}_{r_2l}]+E[\mathbf{T}_{r_1k}^{H}\mathbf{T}_{r_2l}]E[\mathbf{T}_{r_1m}\mathbf{T}_{r_2n}^{H}]\right)$$

The elements of the transmit steering vector for the interfering parallel channel appear as **X** in this equation. All transmit steering vectors are presumed to have unit norm. The second equality makes use of the following identity for any zero mean jointly Gaussian random variables [36]:

$$E[\mathbf{x}_1\mathbf{x}_2\mathbf{x}_3\mathbf{x}_4] = E[\mathbf{x}_1\mathbf{x}_2]E[\mathbf{x}_3\mathbf{x}_4]+E[\mathbf{x}_1\mathbf{x}_3]E[\mathbf{x}_2\mathbf{x}_4]+E[\mathbf{x}_1\mathbf{x}_4]E[\mathbf{x}_2\mathbf{x}_3] \tag{3.4}$$

As a first example, consider the case where all elements of **T** are independent, identically distributed Gaussian random variables. If R is the number of receivers and S is the number of transmitters, then $\mathbf{A} = R\sigma^2\mathbf{I}$ where σ^2 is the variance of the random variables and **I** is the S by S identity matrix. The principal eigenvector of **H** is **X** with an eigenvalue of $(R^2 + R)\sigma^4$. All other eigenvalues are equal to $R\sigma^4$. If the second channel steering vector is **Y** and **Y** = **X**, then the average SINR = $(\mathbf{Y}^H E[\mathbf{A}]\mathbf{Y})^2/(\mathbf{Y}^H E[\mathbf{H}]\mathbf{Y})$ is a constant that asymptotically approaches unity as R get large. One might expect the value to be 1 for all values of R but recall that this metric is essentially the ratio of the square of the second moment to the fourth moment which is not unity. All other eigenvectors of **H** have an equal eigenvalue of $R\sigma^4$. Therefore, as long as **X** is orthogonal to **Y**, the average SINR equals R. The optimal strategy is thus to pick *any* set of orthogonal steering vectors. This is quite similar to the strategy promulgated by researchers considering the capacity of radio frequency wireless multi-antenna systems [21].

As a second example, consider the case where the transmissions from a given source are perfectly coherent over the receiver elements but signals from other sources

are independent. This may occur, for instance, if there were a single, unique ray path connecting each source to the receiver array. If the ray paths were independently fading but coherent over the receiver array, the example considered here would result. Again, identically distributed Gaussian random variables are assumed for the elements of **T**. The expected value of **A** is unchanged as the expected value of the sum of random variables does not depend on their correlation. The interference matrix, **H**, however changes. The principal eigenvector of **H** will still be **X** but with an eigenvalue of $2R^2\sigma^4$. All other eigenvalues are equal to $R^2\sigma^4$. If **Y** is chosen to be **X**, then the average SINR = ½ and is independent of R. If **Y** is chosen to be anything else, the average SINR = ¼. Because the received signals are now completely correlated, $\mathbf{X}^H\mathbf{X}$ and $\mathbf{Y}^H\mathbf{X}$ grow similarly with increasing R and average *SINR* does not improve with increasing R. An essential point, however, is that only the match filtering approach to interference cancellation fails to benefit from an increased number of received signals. The residual interference power after processing the received signals assumes that a matched filter to the desired signal was used. Adaptive filters derived from a minimum mean square error criterion would be able to use the larger coherent aperture afforded by increased R to improve interference rejection. The metric considered here, however, does not reflected that residual interference power.

An important commonality between these examples is that the choice of **X** is unimportant. What matters is that the various transmit steering vectors are orthogonal. If one does not assume an identical distribution for the variables, clearly sources that convey more power would be preferred in the construction of **X**.

As a final example, the case of perfect correlation between transmitters is considered. The resulting performance is highly dependent on the particular form of the correlation. Specifically, the phase of the cross-correlation between source terms, its variability from receiver to receiver, and the choice of **X** all affect the eigenvalues and eigenvectors of **H**. In fact, full correlation between sources and how to exploit the coherence is the scenario that the bulk of this thesis addresses. With source correlation present, the choice of **X** *does* matter even when the Gaussian attenuation coefficients are identically distributed. This conclusion is an important discrimination between existing efforts to exploit multi-antenna systems and the work of this thesis.

Before concluding this discussion, two possible extensions are introduced. If every row vector of **T** is a zero mean, independent, and identically distributed Gaussian random vector, then an estimate of the expected value of **A** made with N channel realizations is the sum of R independent, identically distributed Wishart matrices of order N with covariance equal to the covariance of any row vector of **T** [37]. Using appropriate properties of Wishart distributions, one may investigate how many channel samples are required to obtain a reliable estimate of $E[\mathbf{A}]$. If correlation between receiver elements is considered, the problem grows in complexity to include the sum of correlated Wishart matrices. In addition, if one wishes to investigate the behavior of **H** estimates, products of correlated Wishart variables need be considered. In short, an analysis path is clear for investigations of the properties of **A** and **H** estimates.

A second, potentially fruitful extension would attempt to compute an average value of NDoF, (equation 3.1). To understand the importance of such a quantity, consider the following two scenarios. In the first, a single propagation path connects the

transmit and receiver arrays but its spatial expression varies dramatically over time. In the second, a spatially complex channel varies independently from one channel realization to the next but each realization maintains full rank. Both of these examples would lead to an $E[\mathbf{A}]$ that has as many degrees of freedom as source transmitters but performance on any one realization would be dramatically different. The expected value of NDoF would distinguish between these two variables. If $\mathbf{A}^{(q)}$ represents the matrix product $\mathbf{T}^H\mathbf{T}$ for a given realization and has eigenvalues, $\lambda^{(q)}$, then the expected value of NDoF is,

$$E[NDoF] = E\left[\frac{\left(\sum_{s=1}^{S}\lambda_s^{(q)}\right)^2}{\sum_{s=1}^{S}\left(\lambda_s^{(q)}\right)^2}\right] = E\left[\frac{Tr\left\{\mathbf{A}^{(q)}\right\}^2}{Tr\left\{\mathbf{A}^{(q)H}\mathbf{A}^{(q)}\right\}}\right] \qquad 3.5$$

For a transfer function matrix, $\mathbf{T}$, with Gaussian random variables as elements, *NDoF* is the ratio of the sum of squares of non-central Chi-square random variables. Thus the uncertainty expressed at the beginning of the paragraph may be resolved solely via consideration of the transfer function matrix distribution.

3.7 Channel Decomposition Conclusions

This chapter demonstrated several important aspects of the channel decomposition described in Chapter 2 for the two underwater channels utilized in SM99 and SM00.

1. The distribution of singular values is stable within 1 dB over timescales of five minutes. Furthermore, the singular values of the ensemble decomposition are well correlated with the singular values of the individual channel realizations.

2. Use of the principal singular vector of the ensemble channel decomposition can lead to increases of up to 6 dB in average power through the channel as compared to conventional broadside beamforming.

3. The subspace spanned by the principal singular vector of the ensemble decomposition consistently represented over half of the power contained in the principal singular vector of any realization. For SM00, this held true over a one week period and was also true for the other vectors.

4. The decomposition is readily related to physical propagation paths in the channel.

5. The performance metrics of section 2.3 were shown to be effective with experimental channel data.

Having demonstrated the effectiveness of the analysis machinery presented in Chapter 2, the focus in the next Chapter will be on the realized communication performance gains in SM99 and SM00.

Chapter 4. An Experimental Investigation of Spatial Modulation in the Underwater Acoustic Channel

The feasibility of spatial modulation in an underwater acoustic communication channel was investigated during the course of three experiments. The first experiment (BAH98) took place on the U. S. Navy test and evaluation range near the Grand Bahama Islands (AUTEC). In an attempt to simulate two simultaneous acoustic links spatially separated in a range-azimuthal plane, which would require three platforms, each link was independently established using two platforms with post-processing superposition serving to recreate this so-called horizontal slice configuration. Two parallel channels were demonstrated with a combined data rate that a single channel did not support. The second experiment (SM99) was conducted in shallow waters near Weepecket Island in Buzzards Bay, Massachusetts using two vertical line arrays. Once again, two parallel channels were demonstrated with superior performance to a single channel. The final test (SM00) took place in Woods Hole Harbor. In this test, channel measurements made the previous week were used to design the transmit steering vectors. In this case, two and three parallel channels were demonstrated. All three of these tests showed spatial modulation to increase communication performance.

This chapter is devoted to describing the acoustic communication performance of these three tests. It will begin with a description of the multi-channel, multi-user decision feedback receiver used to equalize and decode all signals. Each test will then be described in detail. A summary of what was demonstrated and accomplished will conclude the chapter.

4.1 The Multi-Channel, Multi-User Decision Feedback Receiver

Quadrature Amplitude Modulation (QAM), which encodes information in the amplitude and signal phase relative to a fixed phase reference, was the modulation method used in all tests. Symbol constellation sizes varied from 2 to 16. The advantage of coherent modulation is the higher bandwidth efficiencies; defined as the ratio of data rate to signal bandwidth, that is achievable as compared to incoherent methods. For a fixed bandwidth, higher data rates can be achieved by increasing the constellation size of the signaling alphabet at the expense of higher required energy per bit to maintain an equivalent error rate. The full range of alternatives was discussed in Chapter 1. Alternatively, one may strive to create parallel spatial channels to increase the data rate as proposed in this thesis. These approaches, larger constellations and spatial modulation, were compared in the tests to be described. The cost of coherent modulation for many channels, however, is the need to continuously track the phase and amplitude variability of the signal due to fluctuations in the channel impulse response. Fortunately, the same algorithms that accomplish this adaptation task are easily extended to decode multiple parallel channels with little added complexity.

The successful use of coherent modulation in the underwater channel is a relatively recent accomplishment [38] [6]. A multitude of equalizer and receiver implementations have been presented in the last decade. A comprehensive review of the approaches was prepared by Proakis [39] and offers a concise tutorial to the interested reader. This discussion will be restricted to the multi-channel, multi-user decision feedback equalizer (MU-DFE) presented by Stojanovic [40].

The essential elements of the MU-DFE are a set of conventional feedforward taps that sample the received pressure signal from each hydrophone channel, a set of feedback taps that provide previous symbol decisions for all users as well as introduce a non-linearity into the filtering, and a phase locked loop (PLL) that relieves the tap weight adaptive algorithm of the phase tracking task for the most dominate Doppler characteristics. The need for feedforward taps, which are direct samples of the received signal, is an obvious requirement. The feedforward sampling was done at an integer multiple of the symbol rate (e.g. twice) allowing the adaptive algorithm to perform fine scale synchronization. The use of feedback taps is important for avoiding the noise enhancement that a purely linear filter will incur when attempting to equalize a frequency response with nulls. The multitude of propagation paths in the underwater channel often leads to channel transfer functions with near zero gain at some frequencies. The inclusion of a PLL is an essential component of the algorithm. Under many circumstances, the most prominent time-varying feature of the signal is a mean variable Doppler shift. The PLL is capable of estimating and compensating for this phase offset in a rapid, stable manner leaving the equalizer to track the complex, relatively slowly varying channel response. The algorithm structure is shown in figure 4.1.

The stability of the coupling between these two adaptive processes, the equalizer which updates the feedforward and feedback tap weights and the PLL, is still an open research question [41]. Each adaptive process independently uses the same residual estimation error to modify parameters that influence inputs to both processes creating the potential for instabilities in their interaction. Nevertheless, successful methods for

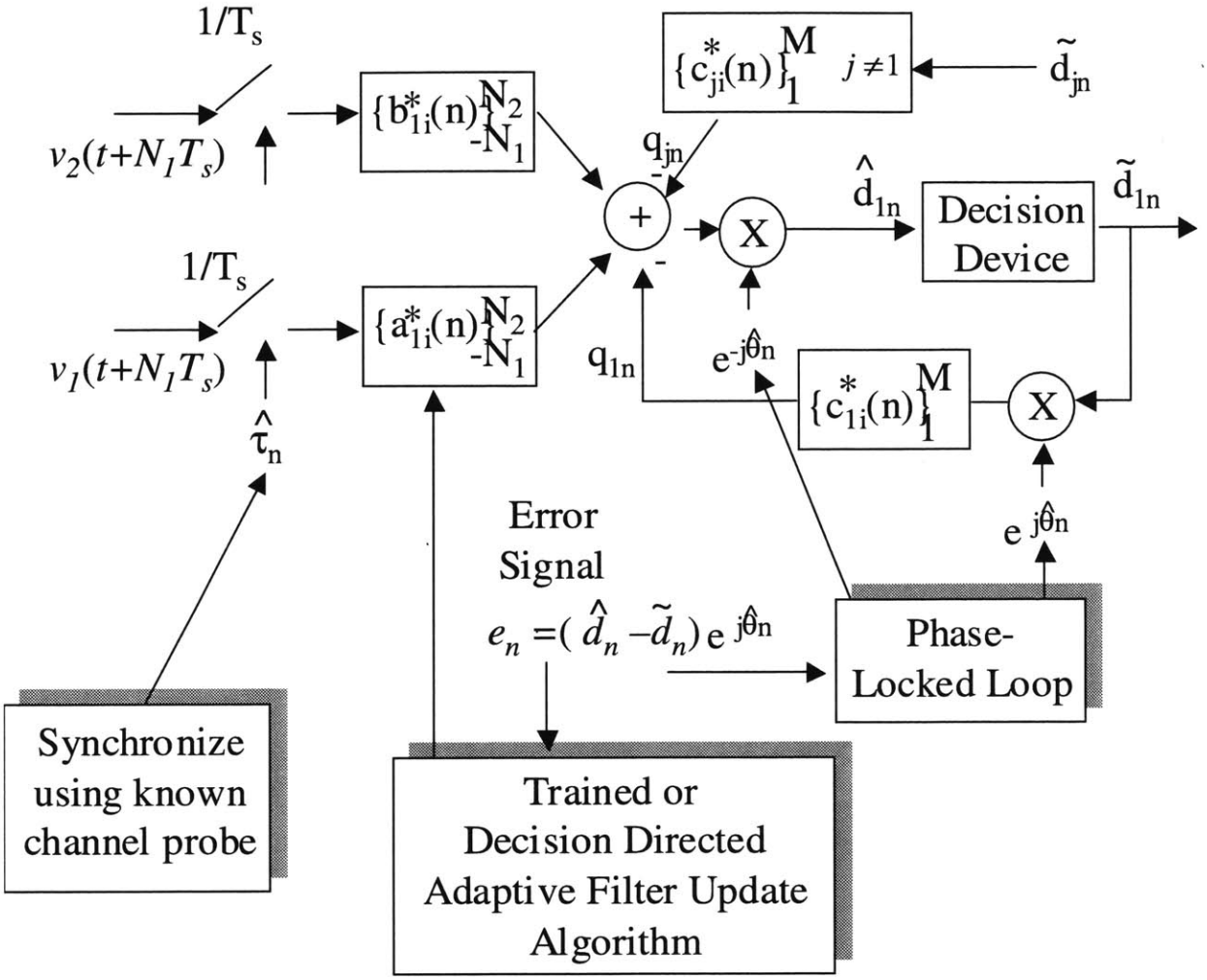

Figure 4.1. A schematic illustration of the multi-channel, multi-user decision feedback equalizer (MU-DFE) used to decode data from one parallel channel in all of the acoustic communication experiments described in this section is shown here. The feedforward tap weights, **a** and **b**, filter the incoming data, ν_1 and ν_2, while the feedback tap weights from parallel channel j, $\mathbf{c}_j$, compensate for residual intersymbol and multiple access interference. An estimate of the carrier phase, θ, is used to provide phase compensation while a coarse timing estimate, τ, synchronizes the process. Only two input channels are shown here but the extension to more channels is clear.

dealing with the mean Doppler shift have been described and were, in fact, implemented in the receiver for these tests [42].

Since the receiver structure was introduced into the community, a number of straightforward enhancements have been proposed to ease complexity [42]. The choice of adaptive weight update algorithm has also been addressed [43]. The focus of this

work, however, remains on the ability to create and exploit parallel channels. Therefore, it suffices to use one effective algorithm as the basis for comparison.

4.2 The BAH98 Horizontal Slice Experiment

The principal objective of the BAH98 Horizontal Slice Experiment was to demonstrate the communication performance improvements (higher data rates and increased reliability) possible with three or more platforms, a horizontal transmitting aperture, and an average power constraint. As the resources available in this experiment were limited to two surface vessels, the methodology is not entirely representative of a practical implementation but does serve to demonstrate feasibility. One such practical implementation would seek to increase the throughput of a data link from an autonomous underwater vehicle (AUV) to a tending surface vessel. An AUV transmitter array with a modest horizontal aperture would use elementary beamforming techniques in conjunction with onboard position and orientation estimates to form parallel spatial communication channels separated in azimuth. One beam would remain pointed towards the tending surface vessel while other beams would point towards signal relay buoys serving as simple repeaters. Another practical implementation would be in the context of an acoustic network. Any redundant paths afforded the signal by the network topology could serve as parallel spatial channels distinguished by the horizontal expression of their propagation paths. The severe spatial dispersion effects that are encountered in the vertical plane are usually absent in the horizontal plane. Dispersion is generated by sound velocity stratification (diffraction), medium inhomogeneities (scattering) and boundaries (reflection). The horizontal length scales associated with these qualities are often hundreds of times larger than the vertical length scales owing mostly to the slab-

like nature of the ocean. Consequently, parallel horizontal channels are much simpler to predict, track, and generate. While the ideal horizontal slice experiment would have an architecture similar to one of the practical configurations, the usual severe constraints on oceangoing resources forced some alterations as will be apparent in the following methodology and results description.

4.2.1 BAH98 Methodology

4-level phase shift keyed (QPSK) and 16-level quadrature amplitude modulation (16-QAM) communication signals were transmitted from the R/V *Skimmer*, a 30 foot boat operated by the Harbor Branch Oceanographic Institution (HBOI). The single transducer was mounted on an Endeco depressor fin, attached to a winch-driven cable, and towed behind the boat. Pre-recorded analog waveforms were used to drive a power amplifier which, in turn, energized the transducer. Due to cable damage incurred during the initial deployment, the radiated power was drastically reduced. As a consequence, the range was typically less than 1000 meters for the duration of the experiment. Reception occurred on a 16 element, 0.7 wavelength element spaced horizontally deployed hydrophone array tethered to the R/V *Sea Diver*, a 113 foot boat owned and operated by HBOI (figure 4.2). The element spacing was approximately 30 cm. The array was at a depth of approximately 3 meters directly below the R/V *Sea Diver* starboard side. Water depth was approximately 30 meters with an isothermal profile.

In addition to below normal radiated power levels, the noise levels were above normal. The standard practice in acoustic communication experiments is to suspend the receive elements from floats at a sufficient distance from the ship to minimize machinery noise levels. Constraints on available time precluded this for BAH98 resulting in substantial background noise levels. Single element signal to noise ratios (SNR) ranged

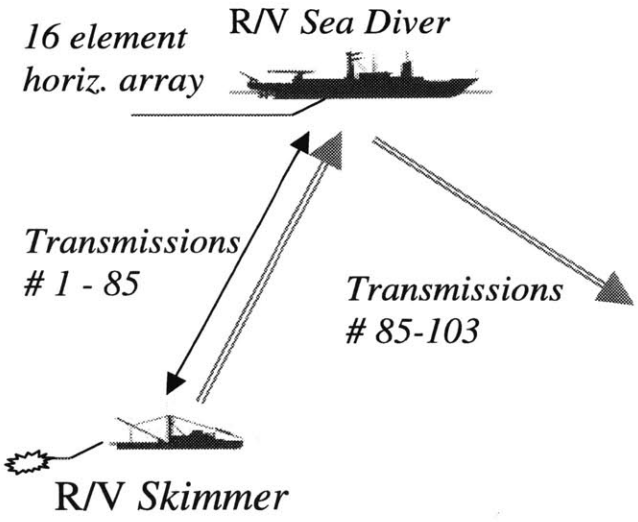

Figure 4.2. The ship positioning and range tracks are shown here for the BAH98 test. from 0 dB to 8 dB. Biological noise generated by the snapping shrimp endemic to the area resulted in burst noise events typically of one to several symbol durations. The top panel of figure 4.3 shows a typical received signal magnitude at short range while the bottom panel depicts a typical maximum range signal. The standard packet format used is evident with an initial frequency chirp, used for detection and impulse response estimation, a quiescent period to preclude interference of the data signal with the chirp reverberation, and, finally, the actual data transmission.

The R/V *Sea Diver* remained stationary during the experiment while the R/V *Skimmer* was closing on a 0 degree heading. At the point of closest approach, approximately 100 meters, the heading was altered to 140 degrees for a course leg with opening range. The complete transmitter course, as seen from above, would appear to make a "V" with the R/V *Sea Diver* located at the base. Data from these two legs was superimposed in a later pre-processing step in order to simulate the performance with two simultaneous transmissions, i.e. as if there were a transmitter on both legs of the "V" at the same time.

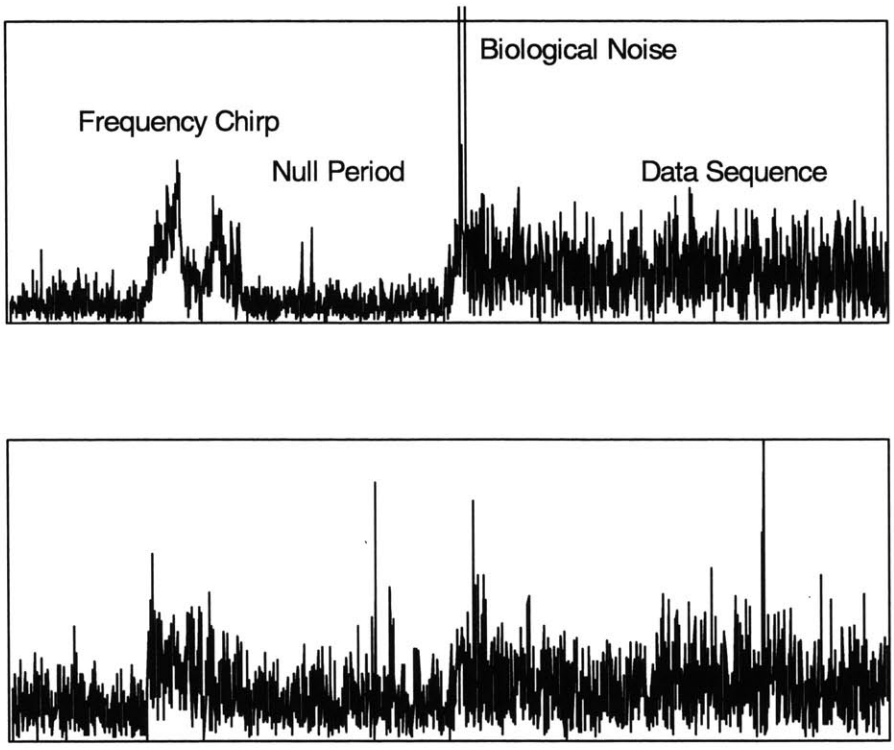

Figure 4.3. Examples of received signal magnitude over time at close range (upper panel) and maximum range (lower panel). The standard packet structure is clearly evident with a frequency chirp followed by a null period and the data. The impulsive character of the biological noise (shrimp clicks) is also clearly seen as the periodic noise spikes.

The signal waveform library consisted of quadrature phase shift keyed (QPSK) modulation, 8-ary phase shift keyed (8PSK) modulation, and 16-level quadrature amplitude modulation (16-QAM). The symbol rate was 1250 symbols/sec on a 3500 Hz carrier. During the closing leg, these three modulation were successively used for each packet with power levels controlled so that the energy per bit was constant. Thus, in dimensionless units, the 16-QAM waveform average power was 1.0, the 8-PSK waveform average power was 0.75, and the QPSK waveform average power was 0.5 for a constant energy per bit of 0.25. On the opening leg, a single QPSK waveform was likewise transmitted with an average power of 0.5. This was to be superimposed on the QPSK transmissions of the second leg to create the desired multi-platform configuration.

The receiver processing, described earlier and shown in figure 4.1, was the multi-channel decision feedback equalizer. In this case, only the previous decisions of the user being decoded were passed back to the equalizer. The signal was initially split with one copy of the digitized passband sequence stored on a bank of digital recording tapes for post-processing and analysis. Simultaneously, the Woods Hole Oceanographic Institution PC Modem card was used to continually correlate another copy of the received signal with the apriori known frequency chirp. When the correlation exceeded a preset energy threshold, a packet detection was declared. The baseband sequence, oversampled by a factor of two, was then passed to the onboard digital signal processor for real-time equalization. Each channel was assigned a tap-delay line. The outputs of these lines were summed and combined with the output from a symbol feedback filter to generate a symbol estimate. In an attempt to decouple the tracking behaviors of the adaptive algorithm used to update equalizer weights and the phase-locked loop (PLL) used for carrier recovery, the phase compensation was applied to the symbol estimate just prior to slicing. The difference between the decision and the symbol estimate was used to update the PLL while that same error without phase compensation was used to update the equalizer weights. This particular equalizer implementation is described by Freitag, et al.[43].

4.2.2 BAH98 Results

The data set contains 102 packets detected and demodulated over the course of both the opening and closing legs with the first 85 packets transmitted while closing and the remaining 17 packets transmitted while opening. All packets were contiguous with no missed detections between them. There are several ways in which the channel may be readily characterized for each of the packets including signal to noise ratio (SNR), mean

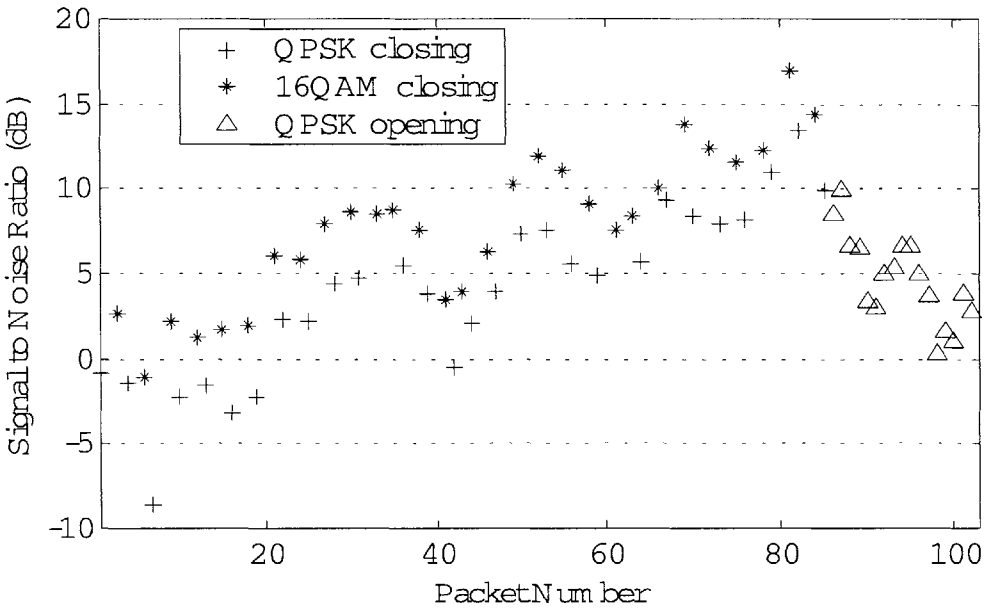

Figure 4.4. The estimated signal to noise ratio (SNR) per hydrophone element is shown here for all 102 packets. On the opening leg, transmissions alternated between QPSK and 16-QAM with constant energy per bit. As such, the QPSK SNR is systematically about 3 dB less than the 16-QAM SNR. On the opening leg, only QPSK packets were transmitted.

doppler shift, and impulse response estimates. As an aid to the forthcoming discussion of these results, we will describe the ensemble of packets using each of these metrics.

The SNR estimate was formed by averaging the power present in the middle of the packet for the signal plus noise estimate and the power present at the end of the packet after transmissions have ceased and reverberation died off for the noise estimate. This ratio (averaged over all channels) less one was taken as the SNR per hydrophone element and is shown in figure 4.4 as a function of packet number. By comparing adjacent 16QAM and QPSK transmissions, the intended systematic 3 dB average power reduction is qualitatively evident in addition to a substantial degree of variability presumably due to destructive multipath interference. The computed mean difference in SNR between these adjacent packets was 4.1 dB.

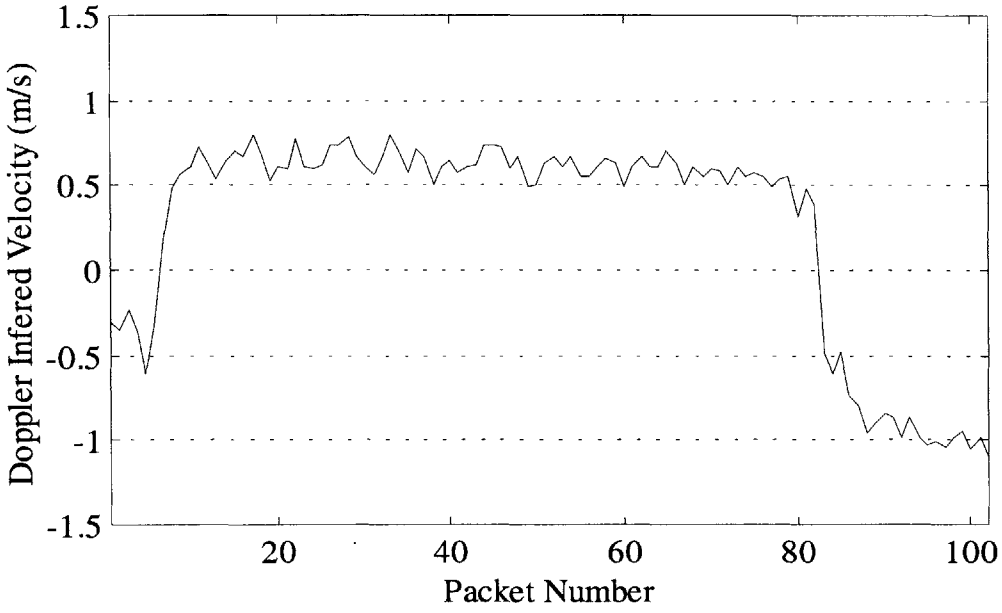

Figure 4.5.. Estimated line of sight velocity between transmitter and receiver based on frequency shift of the response peak in the ambiguity function for the training sequence of each packet. The shift from closing in range to opening in range is seen immediately after packet 80 in conjunction with a near doubling of speed. For reference, 1 knot is approximately 0.5 m/sec.

A mean Doppler shift estimate was generated for each packet using the peak of the ambiguity function based on the 512 symbol training sequence. While the Doppler compensation (phase shifting as well as resampling) is crucial for the equalization process, the mean Doppler also serves as a useful indicator of gross platform motion. As seen in figure 4.5, the R/V *Skimmer* approached at a relatively constant speed of 0.6 m/s and then opened at approximately 1 m/s. While a time-varying Doppler shift can pose substantial burdens for practical scenarios, we strove to keep this complication to a minimum for this experiment.

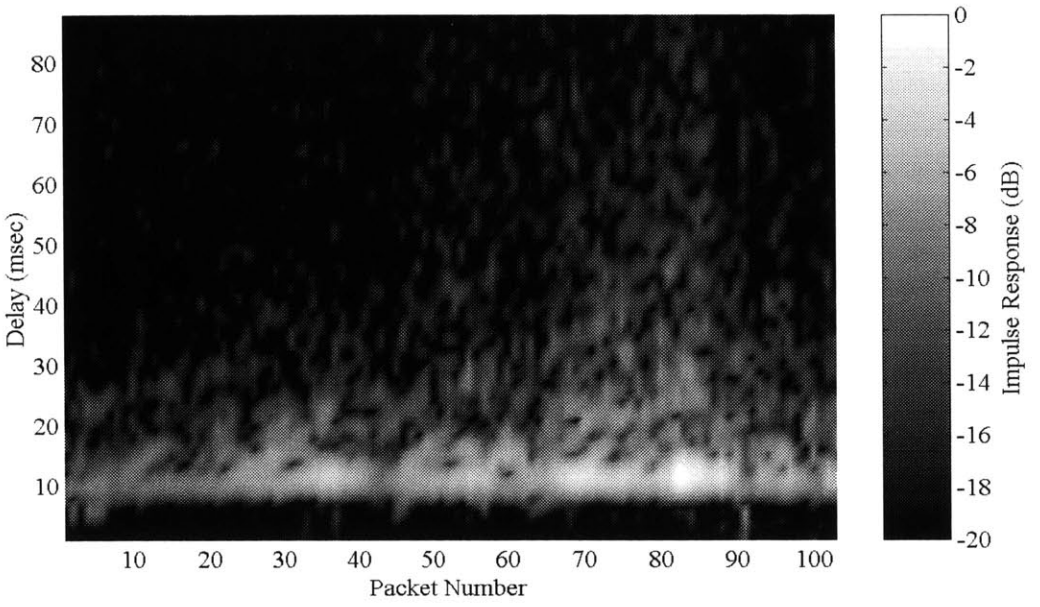

Figure 4.6. The impulse response evolution over the course of the experiment is shown here. Much of the energy is consistently within a delay spread of several symbols. The growing length of the reverberation tails is due to the decreased range and, therefore, decreased attenuation of the high angle rays that have multiple surface reflections. The range decreases linearly from 1 km initially to 100 m at packet 85 and opens to 500 m at packet 103.

A final view of the channel may be found in a waterfall representation of the impulse response estimates formed at the beginning of each packet by correlation with the frequency chirp (figure 4.6). The reverberation extent is only a modest number of symbols and retains a minimum phase characteristic. The responses shown are from a single element with fading presumably explaining the variability in peak response from packet to packet. The correlation between reverberation extent and decreasing range is explained by the extremely close range allowing high angle rays that would otherwise be attenuated by multiple surface reflections to retain significant power.

The true measure of any communication system performance must be the error rate. Each of the received packets was decoded using the equalizer structure previously described along with the appropriate training sequence of 512 symbols. For some packets, minor adjustments of equalizer parameters may yield slightly better decoding

results but we seek here to compare performance under similar, controlled conditions. As such, a single set of equalizer parameters is used for all packets. The most commonly adjusted parameters are the thresholds that determine tap delay locations and gain parameters controlling the adaptive behavior. Each packet consists of 6200 symbols. For reference purposes, error rates of 10^{-2} were empirically observed to ensure stable decision feedback equalizer behavior and are easily accommodated with modest error correction coding. As such, an error rate of $<10^{-2}$ is the criteria for successful packet in this test. Figure 4.7 shows symbol error rates for the four signal waveforms (depicted separately for clarity). In spite of the reduced relative power levels, only the signals with a single spatial channel of QPSK present successfully decode while the higher power, higher data rate rate 8PSand 16QAM signals do not.

To *simulate* the performance when 2 QPSK spatial channels are simultaneously received, the QPSK closing and QPSK opening packets were superimposed. This was done synchronously such that both signals are present during the training period. Implementation details arise if reception is asynchronous (e.g. second signal arrives after training period) but this issue is not relevant here. The simulation is quite conservative in that the background noise power is roughly double that of true simultaneous reception due to the superposition process imposing a 3 dB reduction in energy per bit. The upper panel of figure 4.8 shows symbol errors resulting from decoding the closing QPSK packets both with and without the opening QPSK packets superimposed. Likewise, the lower panel shows symbol errors resulting from decoding the opening QPSK packets both with and without the closing QPSK packets superimposed. Roughly speaking, the

superposition doubled the number of errors but two successful parallel spatial channels were nevertheless obtained.

A revealing indicator of what signal characteristics are actually limiting performance is the output mean square error (MSE) for packets with and without the superimposed signals. As an examination of figure 4.9 shows, the output SNR after superposition of the second signal falls roughly by 3 dB. If no additional co-channel interference were induced (both QPSK signals were completely separable in the receiver), one would expect the output SNR for each of the two QPSK signals to still fall by 3 dB simply due to the additional incoherent noise that cannot be filtered out. Thus, the observed drop of 3 dB suggests that the SNR only fell because of the superposition process and would not have been encountered with truly concurrent transmissions.

Some question remains as to whether the MSE is dominated by unmitigated intersymbol interference or background noise. To distinguish between these scenarios, the closing QPSK packets were decoded with an additional additive Gaussian noise component whose variance was set equal to the noise level of the opening QPSK that was previously superimposed. The MSE was seen to increase by 3 dB indicating that background noise was, in fact, dominating the MSE. The additional errors were thus the result of the artificially increased noise levels and not the inseparability of the horizontally expressed parallel channels.

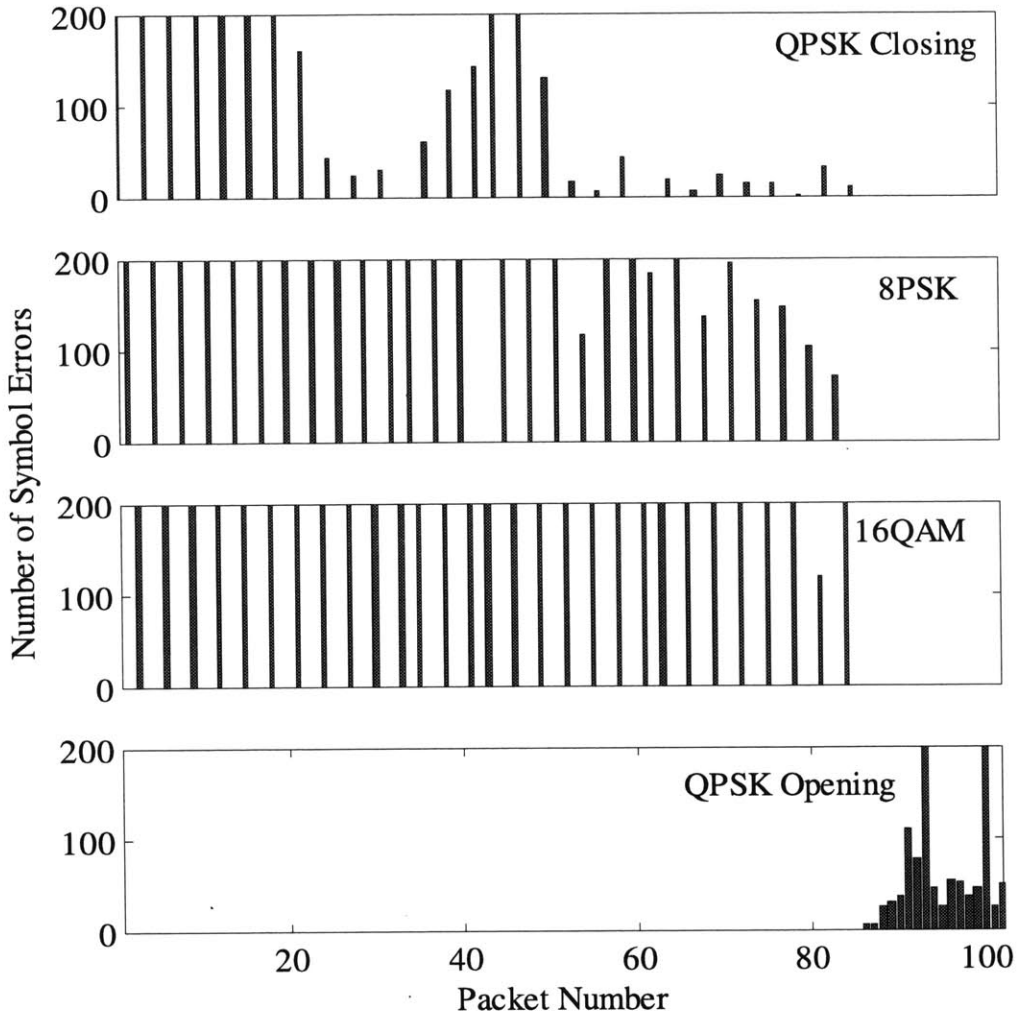

Figure 4.7. A histogram representation of symbol errors resulting from decoding the 102 packets received in the course of BAH98. The results for each signal waveform type have been segregated into unique plots. Errors in excess of 200 symbols are clipped for plotting purposes. Packets with less than 57 errors have error rates less than 10^{-2}.

The BAH98 experiment unfortunately suffered from numerous practical constraints. The transmitted power levels were severely cut due to equipment failure. The ambient noise levels were much higher than average due to the close proximity of the ship. The desired architecture of three platforms spread in a range-azimuth plane had to be simulated with two ships and superposition techniques. Finally, the superposition approach decreased the SNR 3 dB below what a truly simultaneous link would encounter.

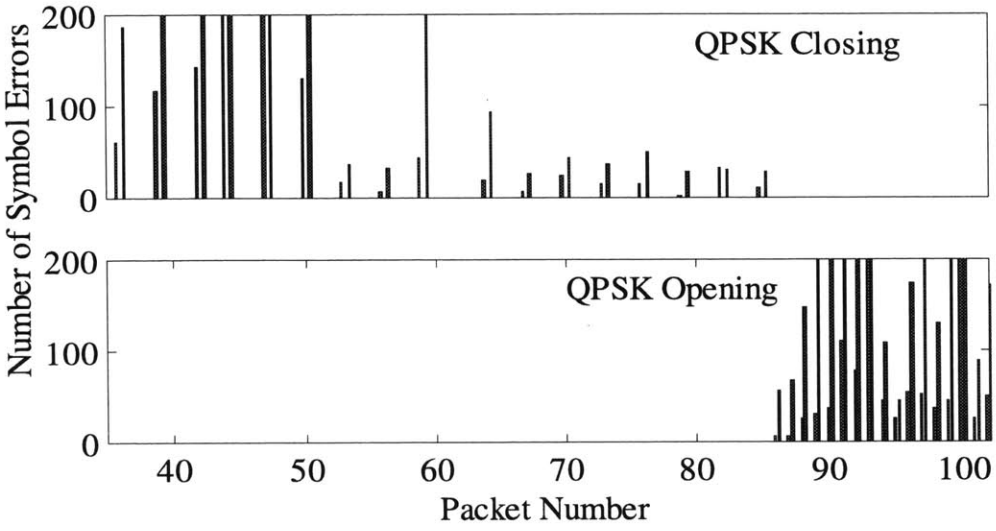

Figure 4.8. Symbol error rates for the closing and opening QPSK transmissions both with and without the superposition of the other QPSK signal. For each pair of bars, the left bar is the single signal case while the right bar is the two signal case. In most cases, the number of errors approximately doubles but decodable packets remain decodable thereby showing the successful use of two parallel channels. The performance degradation is almost entirely due to the 3 dB noise enhancement caused by the superposition of data sets.

In spite of these drawbacks, however, the data showed that 2 parallel channels carrying 2 bits of information each was supported while a single channel carrying 4 bits of information was not.

Spatial modulation offers substantial performance improvements to underwater acoustic networks and AUV scenarios where a third, horizontally distinguished platform is available. Recalling the earlier result from chapter 2, two parallel channels of QPSK can operate with the same error rate as 1 channel of 16 QAM but with 3.9 dB less total average power. This is a major benefit to an underwater network or an autonomous underwater vehicle.

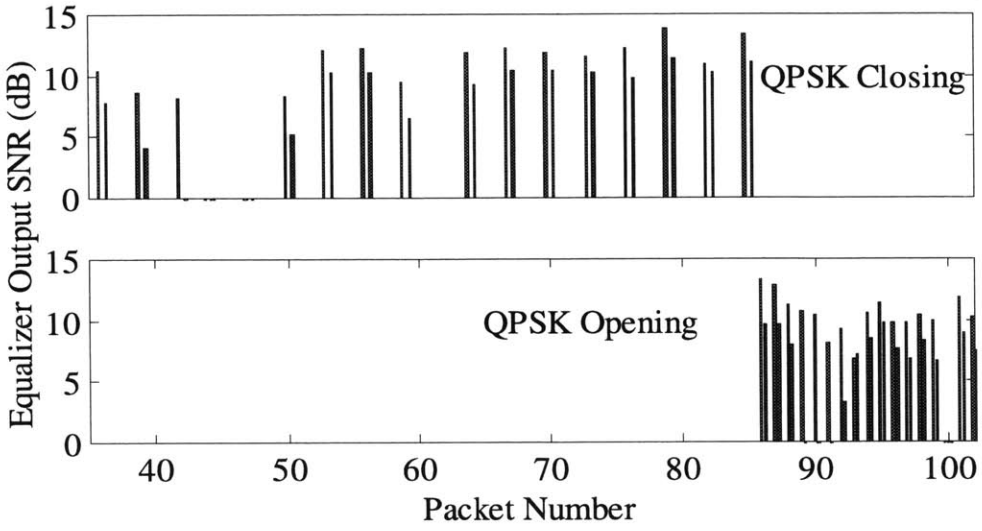

Figure 4.9. Synthesizing a three platform architecture by superposition of two data sets results in an artificial decrease of SNR by 3 dB. For each pair of bars, the left bar is the single signal case while the right bar is the two signal case. The above panels show the SNR of the symbol estimate from the equalizer for each leg when the other leg is superimposed. Note that the SNR decreases approximately 3 dB in all cases.

4.3 The SM99 Vertical Slice Experiment

While the BAH98 experiment showed the benefits of spatial modulation for an acoustic communication architecture with multiple horizontal apertures, a more prevalent system involves point to point communication with vertical apertures. The near total lack of horizontal dispersive effects led to the need for multiple platforms in BAH98. In SM99, we seek to show that the existing vertical dispersive effects are sufficient to create parallel channels for a single point to point system. This test was designed as an "open-loop" experiment in that no attempt was made to incorporate in-situ channel measurements into the signaling methodology.

There were two primary objectives. The first was to make channel measurements that would allow an analytic exploration of the possibilities for spatial modulation. The second was to demonstrate the creation and use of two parallel communication channels using a simple, albeit ad-hoc, filtering strategy at the transmitter; namely sub-arraying. Using equivalent bandwidth, power, and signal processing, two parallel channels were created with each having only a 4 dB reduction in output SNR compared to a single channel. As shown in section 2.1 (figure 2.4), this equates to a diversity gain of 2.9 dB. We will now describe the methodology and results in detail.

4.3.1 SM99 Methodology

The channel chosen for the test was near Woods Hole, MA in Buzzards Bay. Specifically, the test was conducted in 14 meters of water near the Weepecket Islands. As seen in figure 4.10, transmissions occurred between the R/V *Mytilus* (locations denoted by numbers 1 – 4) and the R/V *Asterias* (fixed location denoted by 'A'). The ranges from the hydrophone array on the R/V *Asterias* to the transducer array on the R/V *Mytilus* were 0.5, 1.0. 2.0, and 4.0 km, respectively, for sites 1, 2, 3, and 4. The tidal currents and wind conspired to create a great deal of array motion. Wind speed averaged 20 knots with 3 foot swells generally present.

The transmitter vertical line array consisted of 6 Datasonic AT-12E transducers tuned for operation between 7 and 13 kHz. Although calibration data was available on these units, the signals were not compensated for the inter-element variability. The peak source level difference was 3 dB and the peak phase difference was 40 degrees. This variability was entirely due to differences in the tuning circuits for the units. The element spacing was 1.5 meters giving an array that essentially spanned the water column. An

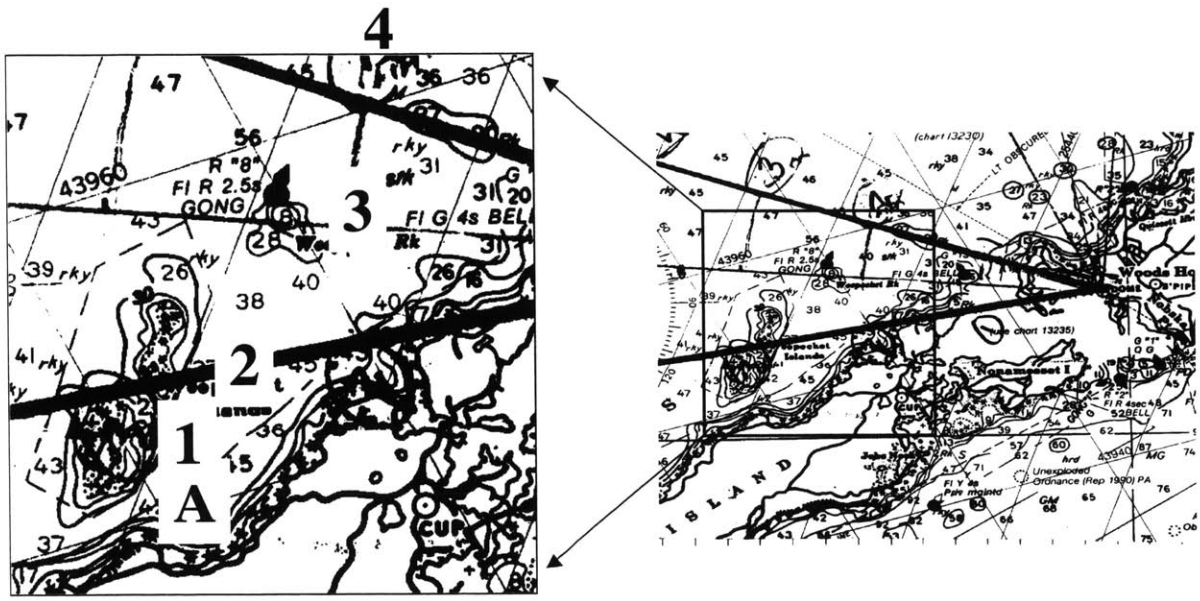

Figure 4.10. The SM99 experiment was conducted in 14 meters of water near the Weepecket Islands. The receiver array was located on the anchored R/V Asterias, denoted by the 'A' on the plot. The transmitter array on the R/V Mytillus was successively anchored at sites 1, 2, 3, and 4 at a range of 0.5, 1.0, 2.0 and 4.0 km respectively. The tidal currents were substantial at times.

environmental measurement package was co-located with the array and consisted of a 16 element thermistor string, a pressure sensor, and a two-axis tilt/compass sensor.

The receiver vertical line array was composed of 16 Hi-Tech hydrophones with a 6 inch spacing (approximately 1 wavelength at 10 kHz). The array was suspended from floats allowed to drift away from the R/V *Asterias* and positioned to hold the array at a depth of approximately 7 meters. Passband data was digitally recorded on tapes at a 48 kHz sampling rate. Prior to recording, the data was filtered with a 7 – 13 kHz bandpass analog filter.

The signal waveform library was designed to measure performance in a two-dimensional parameter space. In each of four cases, a conventional packet was transmitted where all 6 transducers were driven with the same waveform. Immediately following the conventional packet was a spatially modulated packet that sought to create

and exploit two parallel channels. All packets conformed to the standard format of a frequency chirp for detection, a null period to allow reverberations to fade, and then the data sequence. The first test parameter selected between BPSK modulation for both conventional and spatially modulated packets with a total average power constraint (fixed power, variable rate) and 16-QAM modulation for the conventional packet, QPSK for the two parallel channels, and equal power for all channels (fixed rate, variable power). The second test parameter selected between methods of spatial modulation. The first method created two sub-arrays with elements 1-3 being used for the first parallel channel and elements 4-6 being used for the second parallel channel. The second method employed time-delay beamforming to steer a beam up five degrees for the first parallel channel and down five degrees for the second. Thus, there were four packet configurations corresponding to the four combinations of these two parameter spaces. These choices are summarized in figure 4.11. The symbol rate was set at 4000 symbols/sec with a carrier frequency of 9600 Hz. As an aid to interpreting impulse responses, the duration of a single symbol was then 0.25 msec.

4.3.2 SM99 Results

In the discussion of BAH98 results, the performance metric was chosen as the number of symbol errors. As this experiment did not suffer from extremely poor SNR, most packets were decoded with no symbol errors. As such, we will use the output SNR from the equalizer as the performance measure. If one is willing to assume a probability distribution for the noise (such as additive, white Gaussian), then one may derive an anticipated error rate for an average over many packets.

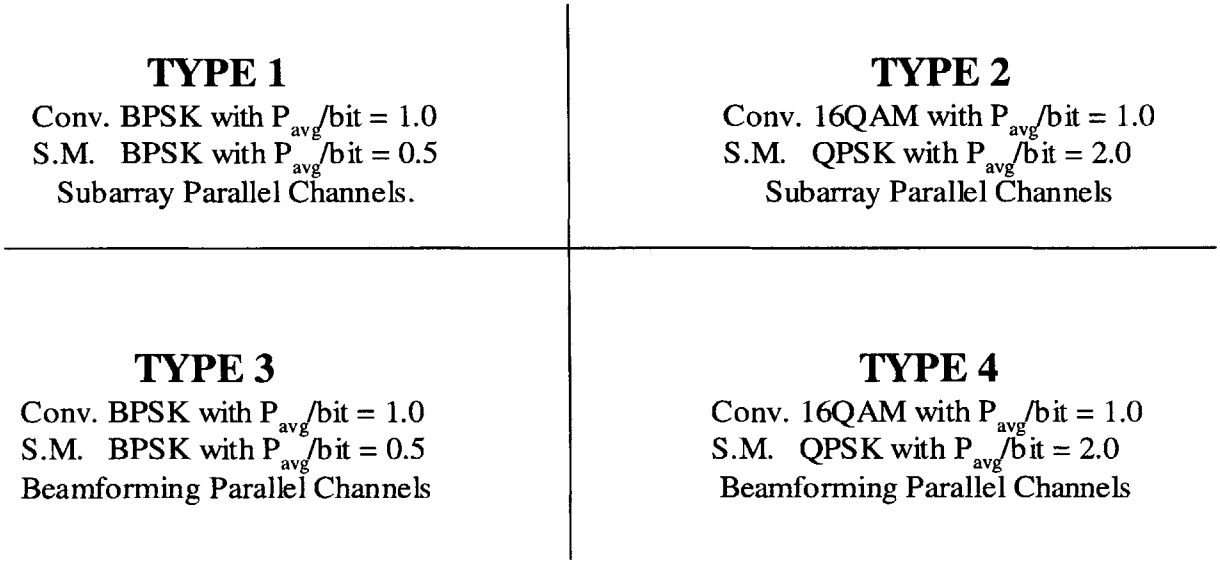

Figure 4.11. The four combinations of test parameters is graphically depicted here. Type 1 and 3 look at performance under a total average power constraint while Type 2 and 4 look at performance under a total data rate constraint.

While the previous chapter sought to directly relate performance to the measured channel characteristics, samples of the impulse responses will be presented here to simply provide a context for the difficulty of communication over this channel. To obtain accurate channel identification, 250 msec maximal length binary sequences were sent from each transmitter in a time-orthogonal manner at a 4000 Hz symbol rate. Specifically, three repetitions were transmitted from transducer 1, then transducer 2, and so forth. As seen in figure 4.12, the delay spread between any transducer / hydrophone pairing was approximately 4 –5 msec (~ 20 symbols). In addition, the arrival structure is substantially different between element pairs.

As alluded to earlier, the combination of wind and currents at the experimental site led to a great deal of array motion. Figure 4.13 shows the impulse responses between the top and bottom array elements (as before) over a period of 10 minutes. The large, periodic wander in arrivals is evident. A ray diagram was given in figure 3.9.

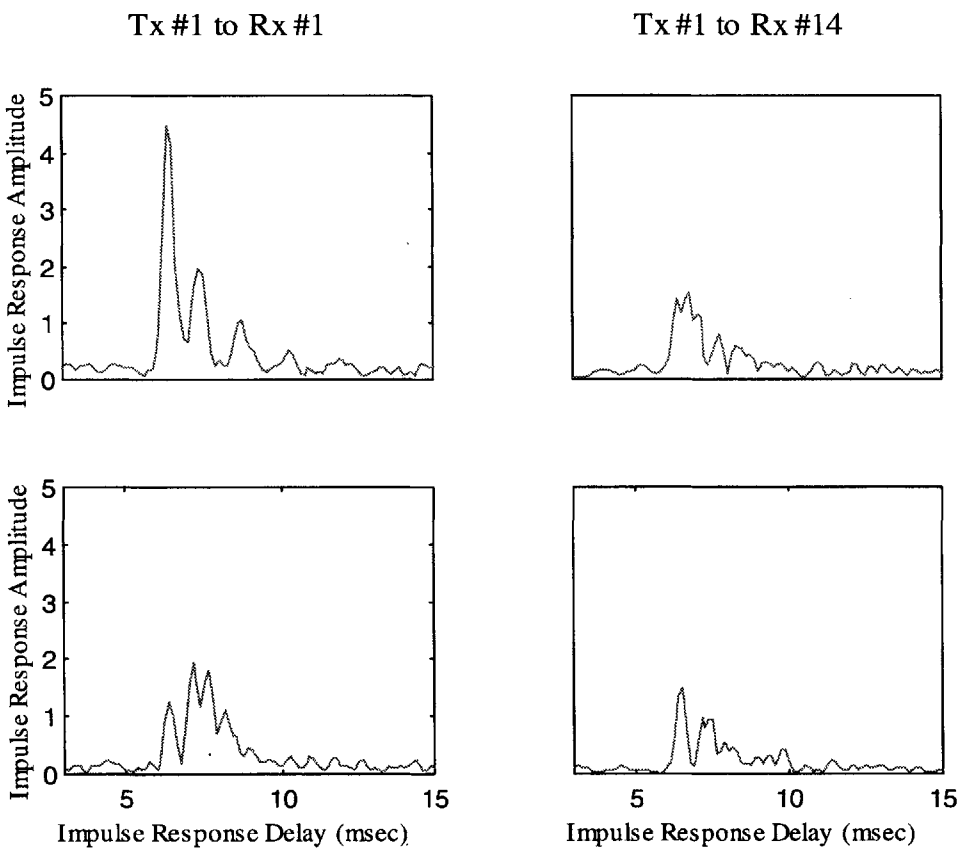

Figure 4.12. A sampling of the impulse responses between the top and bottom elements of each array is given here. Note that the delay spread is approximately 20 symbols in all cases with substantial energy in later arrivals. This data is for site 2.

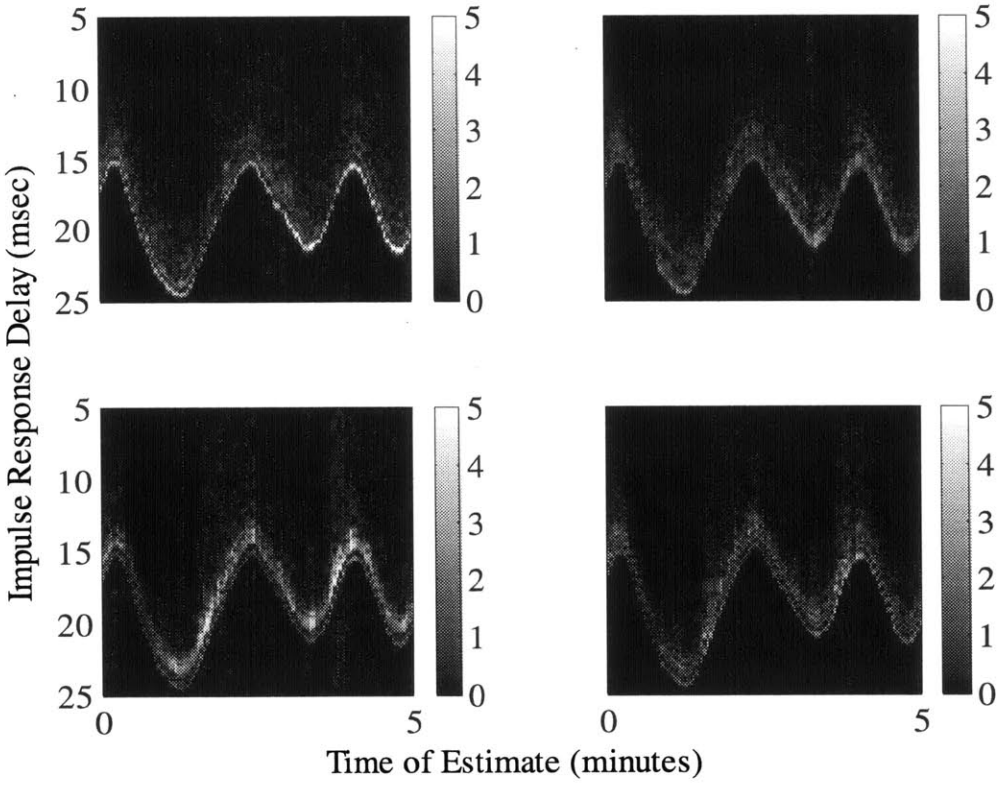

Figure 4.13. The combination of wind and current forcing on the R/V Mytilus conspired to generate a substantial, periodic oscillation at anchor that manifested itself in a wander of the arrival time. The dimensions are normalized amplitude. Clockwise from the top left panel, the impulse responses are for transmitter 1 to receiver 1, transmitter 1 to receiver 14, transmitter 6 to receiver 1, and transmitter 6 to receiver 14.

The signal to noise ratio per hydrophone element at the first three sites was in excess of 20 dB although the contribution of individual transducers to this total varied considerably. The fourth site had an intervening bathymetric feature that cut SNR per element to nearly 0 dB precluding any successful communication. As both ships were anchored, there were no appreciable Doppler effects.

Each type of packet was transmitted approximately 140 times. After processing with a MU-DFE, the average output SNR was computed for each packet. The result for all packets of type 1 transmitted at site 2 is shown in figure 4.14. The single channel (conventional packets) data achieved an average output SNR of 14 dB while the two

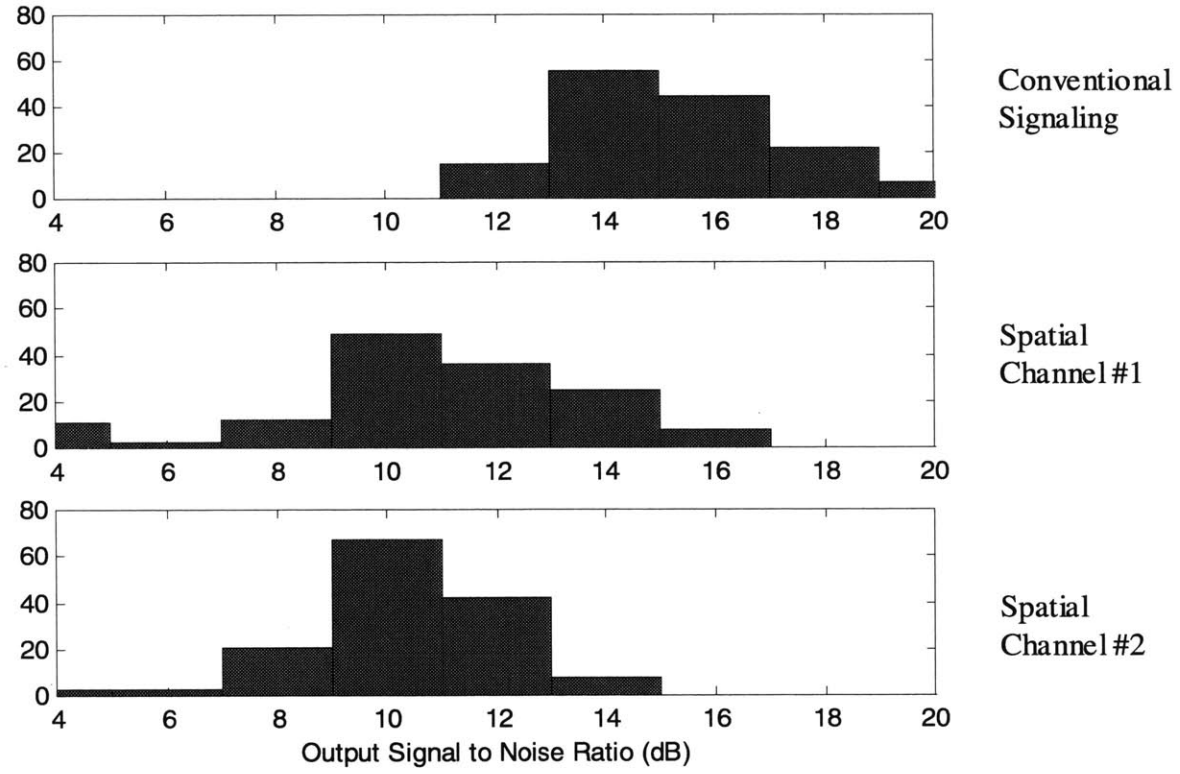

Figure 4.14. The output SNR for each of the 140 packets of Type 1 (a sub-arraying packet) transmitted during SM99 at site 2 is summarized here as a histogram. The single, spatial channel achieved an average SNR of 14 dB while each of the two spatially modulated channels achieved an average SNR of 10 dB

parallel channels (spatially modulated packets) achieved an average SNR of 10 dB.

A similar figure for type 2 packets is shown in figure 4.15. The two plots are quite similar which brings two points to light. First and, perhaps obviously, the size of the symbol constellation does not affect the output SNR. If 64-QAM had been sent with the conventional packet rather than 16-QAM, the output SNR would be unaffected as long as the decisions that were used by the equalizer were correct. Use of larger constellations would simply decrease the SNR per bit. The second point is that the output

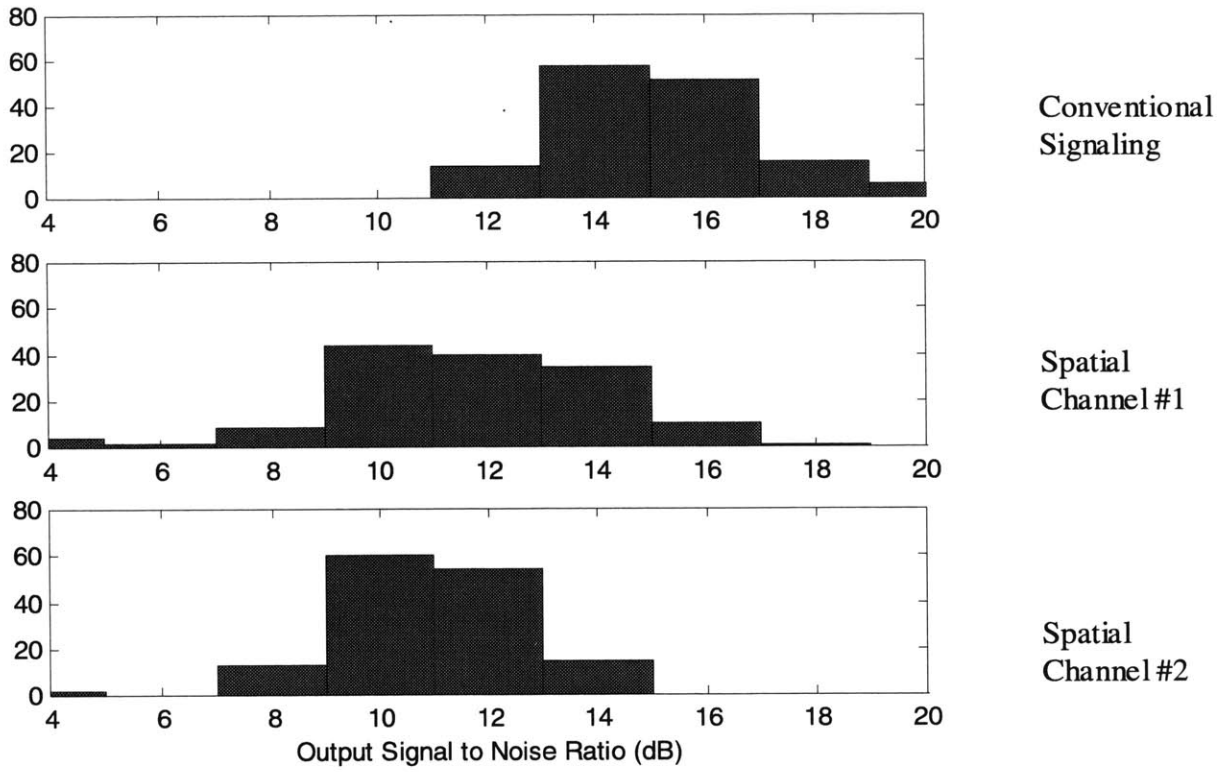

Figure 4.15. The output SNR for each of the 140 packets of Type 2 (a sub-arraying packet) transmitted during SM99 at site 2 is summarized here as a histogram. The single, spatial channel achieved an average SNR of 14 dB while each of the two spatially modulated channels achieved an average SNR of 10 dB. The performance is nearly identical to that of Type 1 highlighting the insensitivity to transmitted power or symbol constellation type.

SNR is not limited by transmitted power but interference power. In fact, the spatially modulated type 2 packets had twice the power as the spatially modulated type 1 packets but no increase in output SNR.

The output SNR of type 3 packets sent at site 2 is summarized in figure 4.16. The somewhat ad-hoc choice of time-delay beamsteering fared worse than sub-arraying as evidenced by the 2 – 3 dB reduction in output SNR for the first parallel channel. These results will be interpreted in light of a ray trace simulation in the discussion section. The output SNR was inadequate to support the higher data rate packets of type 4 and, therefore, results are not given here.

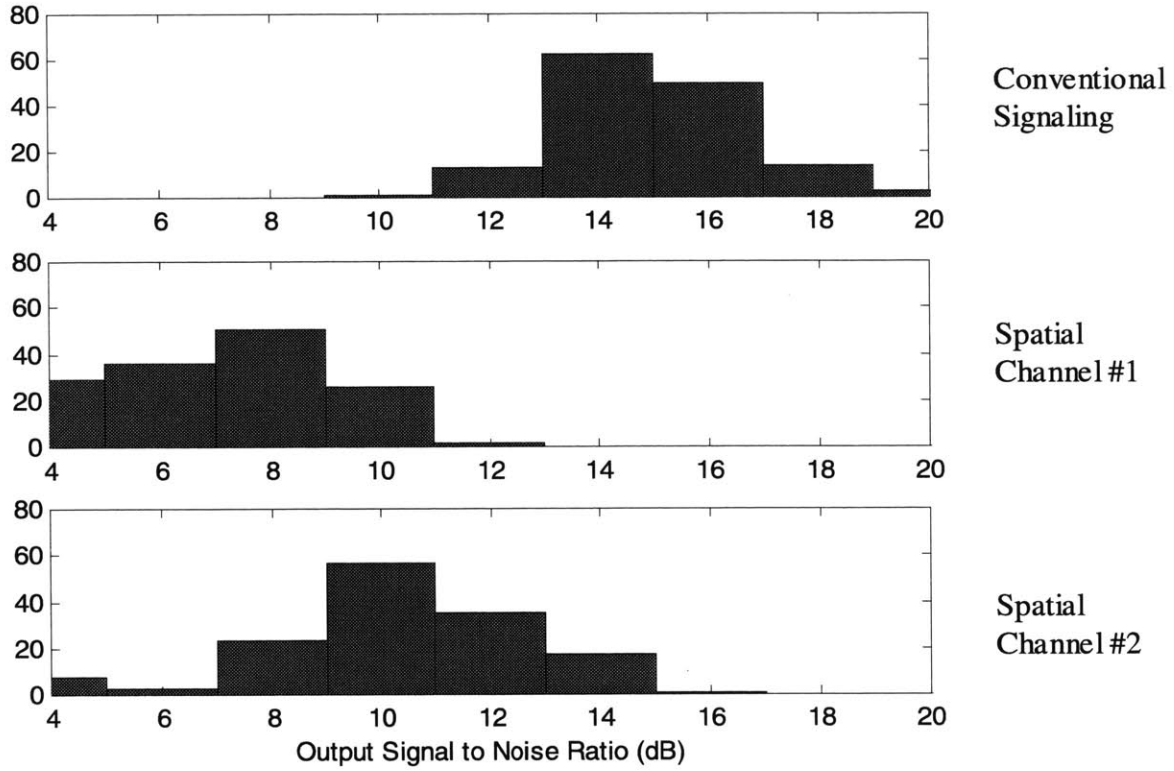

Figure 4.16. The output SNR for each of the 140 packets of Type 3 (a beamforming packet) transmitted during SM99 at site 2 is summarized here as a histogram. The single, spatial channel achieved an average SNR of 14 dB while the first spatially modulated channel only achieved 8 dB. The second spatially modulated channel maintained the 10 dB level seen for Types 1 and 2.

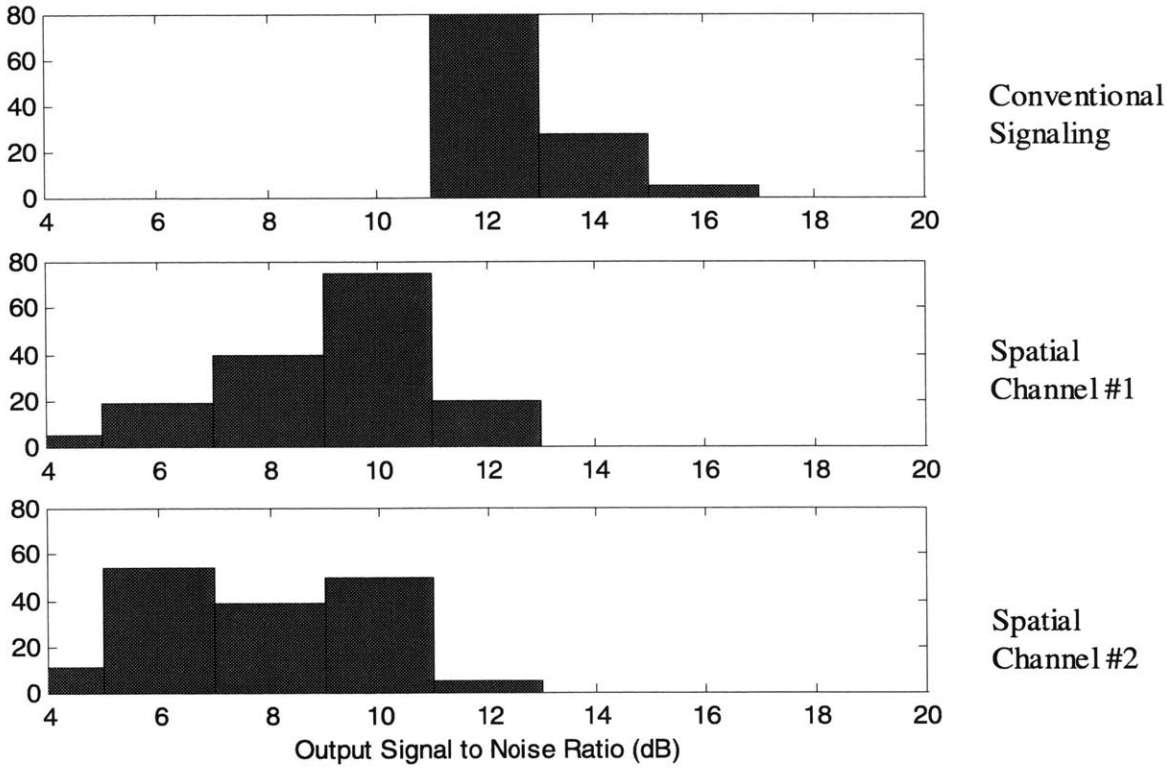

Figure 4.17. The output SNR for each of the 140 packets of Type 1 (a sub-arraying packet) transmitted during SM99 at site 1 is summarized here as a histogram. The single, spatial channel achieved an average SNR of 12 dB while each of the two spatially modulated channels achieved an average SNR of 8-9 dB

The results for site 1 are qualitatively similar to those of site 2. In figure 4.17, a histogram of output SNR for type 1 packets is shown. The results for type 1 packets at site 3 are shown in figure 4.18. In that case, the first spatial modulation channel fared poorly. Ironically, the poor performance of the first parallel channel results in reduced interference to the second parallel channel, thereby enhancing its performance.

4.3.3. SM99 Discussion

The most important conclusion from this data is that spatial modulation was shown to offer a *significant* performance advantage. The argument substantiating this

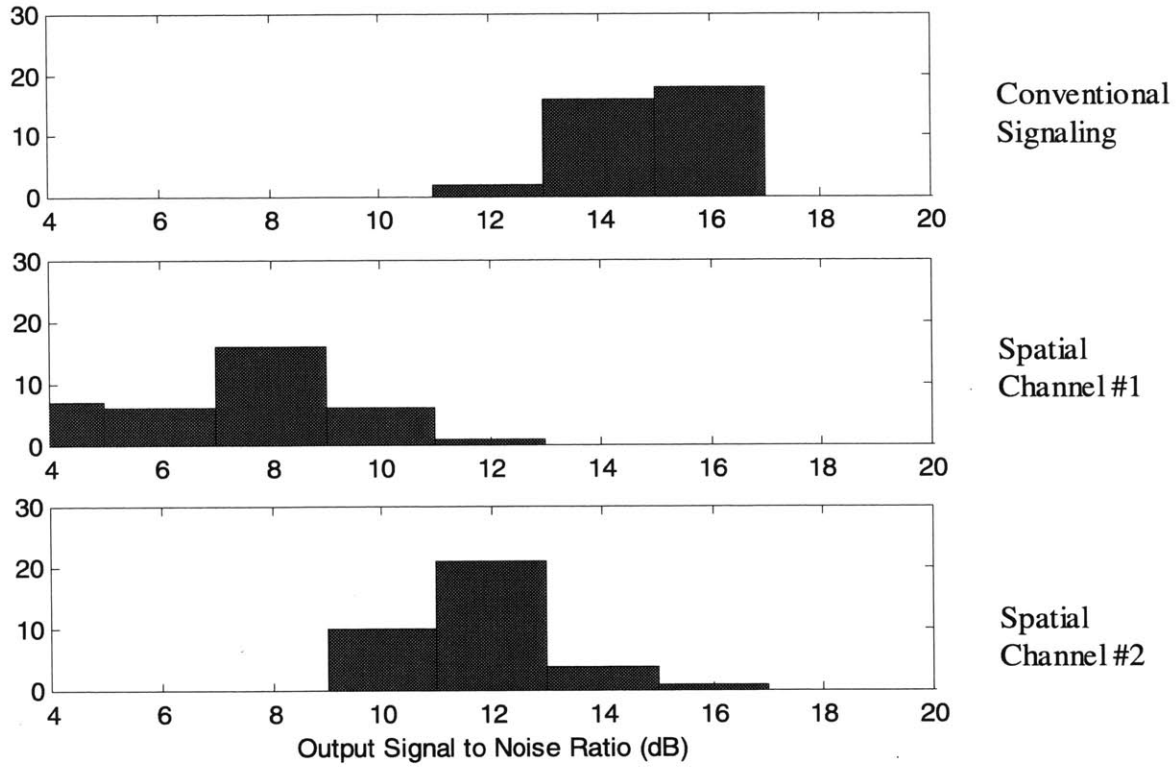

Figure 4.18. The output SNR for each of the 140 packets of Type 1 (a sub-arraying packet) transmitted during SM99 at site 3 is summarized here as a histogram. The single, spatial channel achieved an average SNR of 15-16 dB while the first spatially modulated channel only reached 8 dB. The second spatially modulated channel SNR increased to 12 dB in lieu of the reduced interference from the first channel.

claim will be made carefully as the claim will recur in the discussion of SM00 results. The symbol error probability for 16-QAM modulation with a regular, rectangular constellation and for two-channels of QPSK can be computed per equation 2.11. For modest SNR per bit (> 5 dB), two channels of QPSK achieve an equivalent symbol error rate to one channel of 16 QAM but with 3.9 dB less SNR per bit. To relate this advantage to the SM99 results, consider that the two parallel channels of QPSK had an SNR per bit of 7 dB on average while the single 16-QAM channel had an SNR per bit of 8 dB. Thus, the parallel channel combination enjoyed an error rate improvement

equivalent to a 2.9 dB diversity gain. This gain was achieved without an increase in power or a reduction in data rate. In fact, the advantages are quite similar to what trellis coded modulation offers a communications engineer [44]. This demonstrated improvement is the primary motivation for employing spatial modulation in the underwater channel.

The choice of spatial modulation techniques for this experiment was somewhat arbitrary. The success of the sub-arraying technique, in spite of this fact, speaks to the robustness of spatial modulation in the underwater channel. Understanding the performance in terms of the channel propagation characteristics is essential if the technique is to offer additional performance improvements. A detailed discussion of this underwater channel was undertaken in the previous chapter. A small subset of that analysis will be given here to aid in understanding the difference in performance between the sub-arraying technique and the time-delay beamsteering.

As noted earlier, one part of the signal waveform library was a set of time-orthogonal maximal length sequences that allowed identification of the impulse response between each transducer / hydrophone pair. Because the transmit aperture was extremely large and quite sparse, beamforming at the transmit array is not useful. The receiver array, however, is amenable to beamforming. Figure 4.19 shows a receiver array beamformer power output due to each of the transducers individually. The response is synthesized from the measured impulse responses. There are clearly two dominant arrivals separated by approximately ¾ msec in delay and about a degree in angle of arrival. A beamwidth at the receiver is about 5 degrees but the arrival separation in delay allows a more accurate bearing determination. Transducers 1 and 4 each deliver

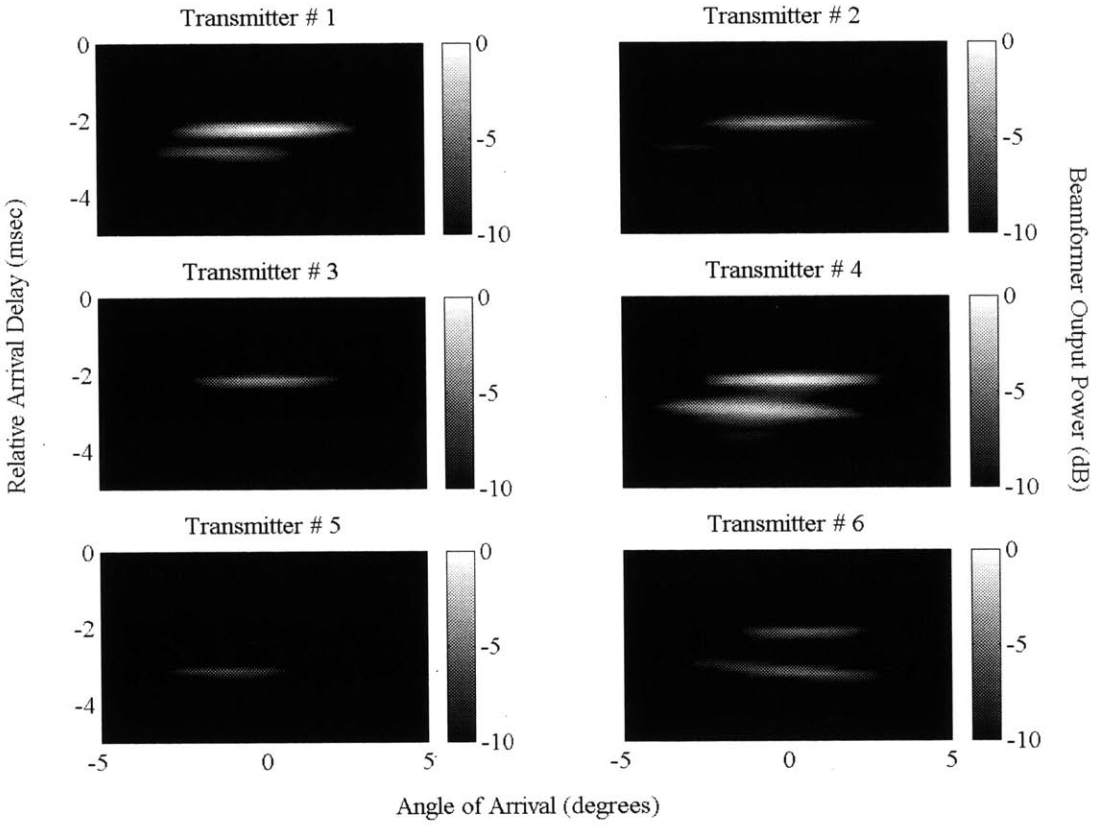

Figure 4.19 Using the measured impulse responses between transducer / hydrophone pairings, the relative power transferred by each transducer is shown in a delay of arrival versus angle of arrival space. Note the dominance of transducers 1 and 4 and their unique spatial structure.

significant power and affect the two arrivals differently. The sub-arraying technique employed these transducers in separate parallel channels. The time-delay beamsteering, however sought to point beams up and down approximately 6 degrees which is well in excess of the angle separation between eigenrays.

A ray theory calculation for the measured environment suggests the separation angle between the two dominant ray groups at the transmitter is only 2.5 degrees. This mismatch suggests that the two parallel channels formed by the time-delay modulation would not be equally energetic and orthogonal and, therefore, would have poor performance. Beamforming with a properly calibrated transmit array and some channel

knowledge taken into account may very well have performed as well as the sub-array technique. In fact, the next experiment to be discussed (SM00) showed narrowband beamforming and sub-arraying techniques to work equally well.

The data from SM99 demonstrated that spatial modulation over two parallel channels within a point to point underwater telemetry link with substantial vertical dispersion can achieve an error rate reduction corresponding to a 2 to 3 dB diversity gain. By taking the measured or estimated channel into account when designing the modulation, it *may have* been possible to further increase the spatial modulation advantage. The final experiment to be discussed (SM00), in fact, demonstrated diversity gains in excess of 4 dB in a shallow water, highly reverberant environment but, unfortunately, this gain could not be attributed to the use of channel measurement derived filters.

4.4 The SM00 Vertical Slice Experiment

The two objectives of this final experiment were to investigate the benefits of using in-situ channel measurements to design the spatial modulation filters and to extend the demonstrated success of spatial modulation to more than two parallel channels. The first objective was partially met while the second was clearly met. Equipment limitations dictated greater than a 24 hour delay between channel measurements and signaling using filters derived those measurements. Use of the derived filters variously degraded performance from simple sub-arraying techniques or left it unchanged. Use of the derived filters, did, however enable a 6 dB increase in power transfer efficiency through the channel. As an example, three parallel channels were created and exploited to yield the equivalent of a 4 dB diversity gain.

4.4.1 SM00 Methodology

The SM00 experiment took place in Woods Hole Harbor, MA. The arrays were the same as used in the SM99 experiment with a 16 element, 1 wavelength spaced hydrophone array and a 6 element transducer array. The hydrophone array was deployed from the dock with the array center at a 20 foot depth. Although the water depth at the receiver and transmitter was nominally 60 feet, intervening bathymetry rose to approximately 35 feet. A ray diagram with bathymetry shown was given in figure 3.12. The transducer array was deployed from the R/V *Mytilus* which was anchored in Great Harbor at a range of 0.5 km. Unlike in the SM99 experiment, calibration data was used to pre-code the signals and compensate for differing amplitude and phase response of the transducer tuning networks. The transmitter spacing was approximately 5 feet with the aperture extending from 25 feet to 50 feet. As before, the received signal was passed through an analog bandpass filter with band edges at 7 and 13 kHz and then digitally recorded.

All waveforms in the signal library were coherently modulated with a 4000 Hz bandwidth and a 9.6 kHz carrier frequency. Maximal length sequences with a 4095 symbol period (approximately 1 second duration) were used for channel probing. The same sequence was sent simultaneously and repetitively with 200 symbol offsets from the top transducer to each successive one. When the received signal from each hydrophone was match filtered by the maximal length sequence, the impulse responses from each transducer to each receiver was clearly separable. This allowed simultaneous measurements of the complete transfer function matrix between the arrays as long as the

channel delay spread did not exceed 200 symbols. The implicit averaging performed by the match filter operation suppressed any channel variability on scales faster than 1 Hz.

The communication signals were patterned on a typical packet structure. Detection was accomplished with a frequency chirp having a time-bandwidth product of 100. A 600 symbol null period followed to allow an impulse response estimate without interference from the information bits. Finally, 5000 symbols of data were sent. All signals used QPSK symbol constellations.

In order to generate spatial steering vectors from the channel data, channel measurements were made on February 29 using the ML-sequences described earlier. The set of impulse responses was transformed into a transfer function matrix, $\mathbf{T}(f)$, as described in Chapter 2. Three hundred channel realizations were formulated from 5 minutes of ML-sequence transmission. The average of $\mathbf{T}^H(f)\mathbf{T}(f)$ was computed from this ensemble and then subjected to a singular value decomposition. Each set of right singular vectors was paired with the set from adjacent frequencies using a "smoothness" criterion where the vectors with the largest projection on each other were "connected". As long as the frequency increment was small compared to (delay spread)$^{-1}$, the pairing was unambiguous. The outcome of this processing was a set of six right singular vectors, $\mathbf{V}_i(f)$. Three methods of using these singular vectors were demonstrated in the experiment that was conducted on March 6.

Five methods of spatial modulation were investigated. In each case, a conventional QPSK packet was transmitted where all 6 transducers received the same excitation. Immediately afterwards, a spatial modulation packet was sent with power controlled such that total average power and energy per bit was the same for all packets.

Specifically, if two parallel channels were created, each parallel channel was allotted one half of the total power and half the information while if three parallel channels were created, each channel was allotted a third of the total power and a third of the information. Each of these methods was used to generate either two parallel channels or three parallel channels. Roughly speaking, transmissions for each packet type required 10 minutes with 2 spatial channel versions using the first 5 minutes and 3 spatial channel versions using the next 5 minutes.

The five methods were:

1. Sub-array A: For two parallel channels, elements 1,2, and 3 carried one signal while elements 4, 5, and 6 carried the other. For three parallel channels, elements 1 and 2 carried one signal, elements 3 and 4 carried the second signal, and elements 5 and 6 carried the third signal
2. Sub-array B: For two parallel channels, element 4 carried one signal while element 2 carried the other. For three parallel channels, the third signal was carried by element 5. These were chosen in terms of the gain the afforded signals sent from them, i.e. which was most effective.
3. SVD A: Narrowband beamforming was implemented using either the first two or three right singular vectors evaluated at the carrier frequency of 9.6 kHz.
4. SVD B: A truncated broadband beamforming was implemented by transforming $\mathbf{V}_i(f)$ to the time domain, zeroing out all but the first arrival in the resulting filters, $\mathbf{v}_i(t)$, and convolving the signal for a given parallel channel with the corresponding spatial modulation filter.

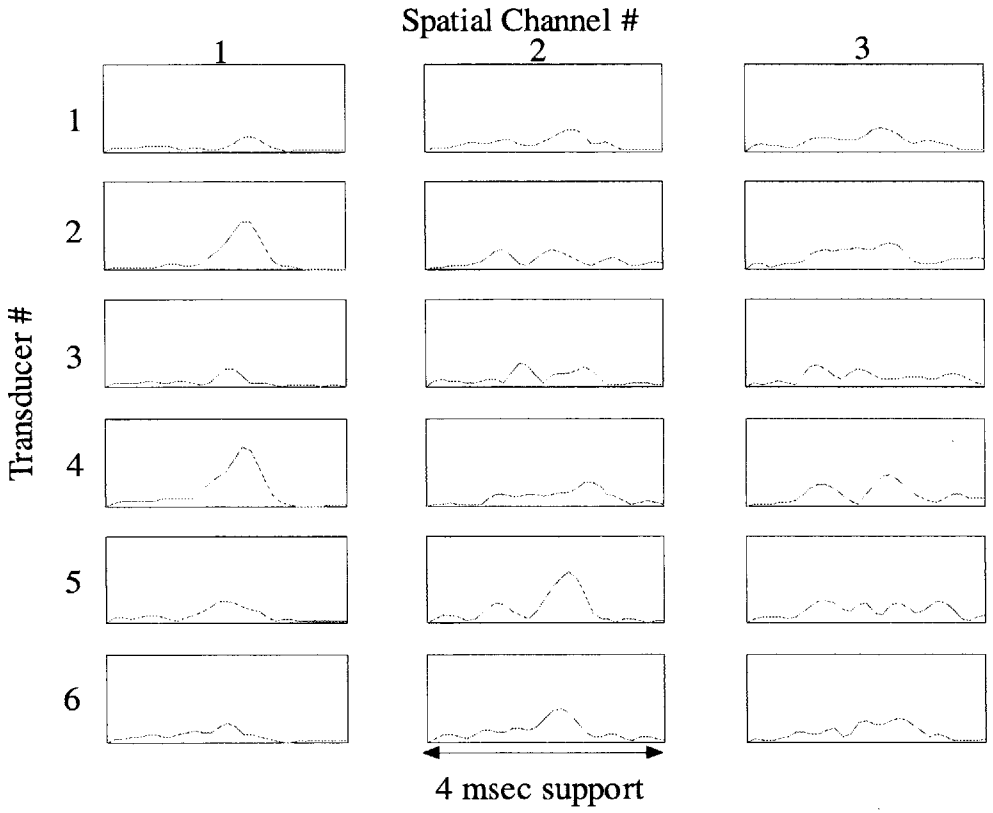

Figure 4.20. The magnitude of the broadband filters applied to each of the six transducers to create each of the three spatial channels is shown above. The magnitude is shown on a linear scale ranging from 0 to 0.5. The temporal support of the filters is approximately 4 msec (15 symbols). These filters were derived from measurements made on Day 3 of SM00 and used on Day 4.

5. SVD C: A full broadband beamforming was implemented by transforming $\mathbf{V}_i(f)$ to the time domain and convolving the signal for a given parallel channel with the corresponding spatial modulation filter. The magnitude of the broadband beamforming filters used to create the three spatial channels is shown in figure 4.20. Each column in the plot gives the filters applied to each of the six transducers for a spatial channel. The total temporal support of the filters is approximately 4

msec (15 symbols). The magnitude scale is linear and ranges from 0 to 0.5.

Thus, there were 10 variations of spatial modulation tested corresponding to either two-parallel channels or three-parallel channels and one of five different spatial modulation strategies. Each variation was allotted approximately 5 minutes of transmission yielding approximately 40 packets per type.

4.4.2 SM00 Results

As with the SM99 experiment, the output SNR for most packets was sufficient to preclude any errors in the limited data set. Histograms of the output SNR for the various packet transmissions are given in figures 4.21 – 4.25 for Sub-Array A, Sub-Array B, SVD-A, SVD-B, and SVD-C respectively. The panels are organized such that the conventional packet results are at the top while the lower panels present results for each successive parallel channel. The left-hand panels are for the two-parallel channel spatial modulation techniques while the right-hand panels are for the three-parallel channel spatial modulation techniques.

While results from other tests focused solely on error rates and output SNR, an additional metric will be examined in this case. As discussed in Chapter 2, the first right singular vector resulting from the ensemble channel decomposition should achieve the highest average power efficiency. To evaluate this claim, a power efficiency ratio for each of the five spatial modulation techniques has been computed. The ratio is defined as the power efficiency of the first parallel channel divided by the power efficiency of the conventional signaling method (all six transducers emitting the same signal). Thus, it represents the advantage in power through the channel (if any) that accrues due to the use

of spatial modulation. The power efficiency itself is defined as the ratio of total power received at the hydrophone array divided by the power transmitted. Only the first parallel channel of a particular packet conveyed the chirp used for detection. By computing the power in the match filter output to the chirp, the power transferred by the first parallel channel may thus be computed. The resulting efficiency ratios are:

Sub-Array A:	-1.5 dB
Sub-Array B:	+1.5 dB
SVD-A:	-0.7 dB
SVD-B:	+2.5 dB
SVD C:	+6.3 dB

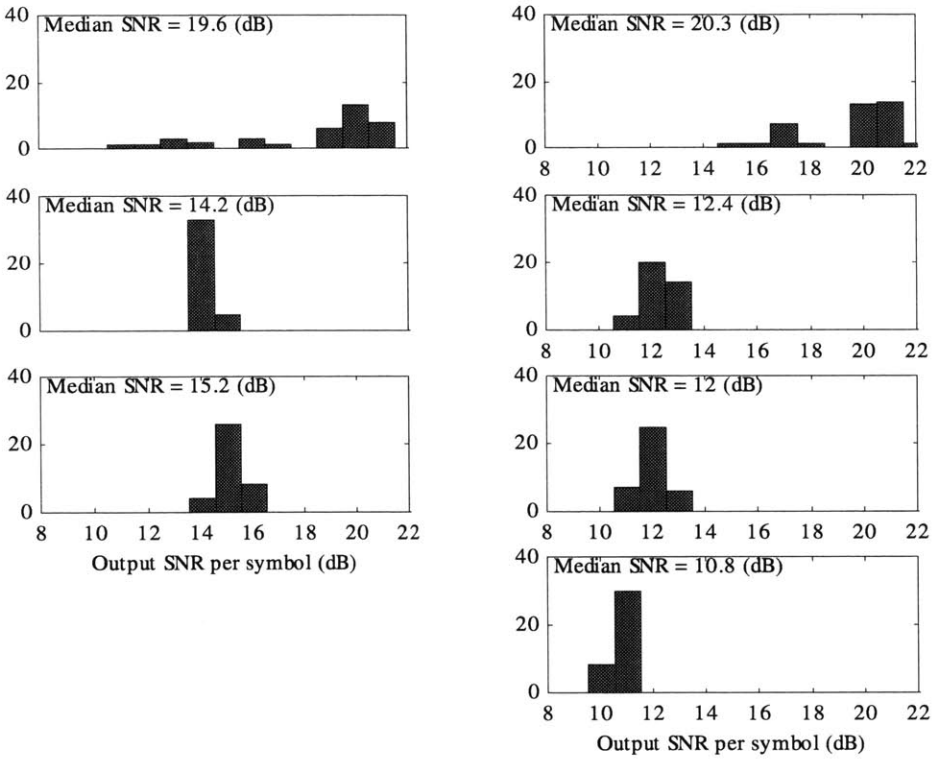

Figure 4.21. Each plot above presents a histogram of the output SNR from an ensemble of packets resulting from **sub-array A** modulation. The top panels are for the time-adjacent conventional packets while the lower ones are for the individual parallel channels in the presence of the others. The left hand panels are for the two-parallel channel packets while the right hand panels are for the three parallel channel packets. Median SNR is shown and will be used to characterize performance in the discussion.

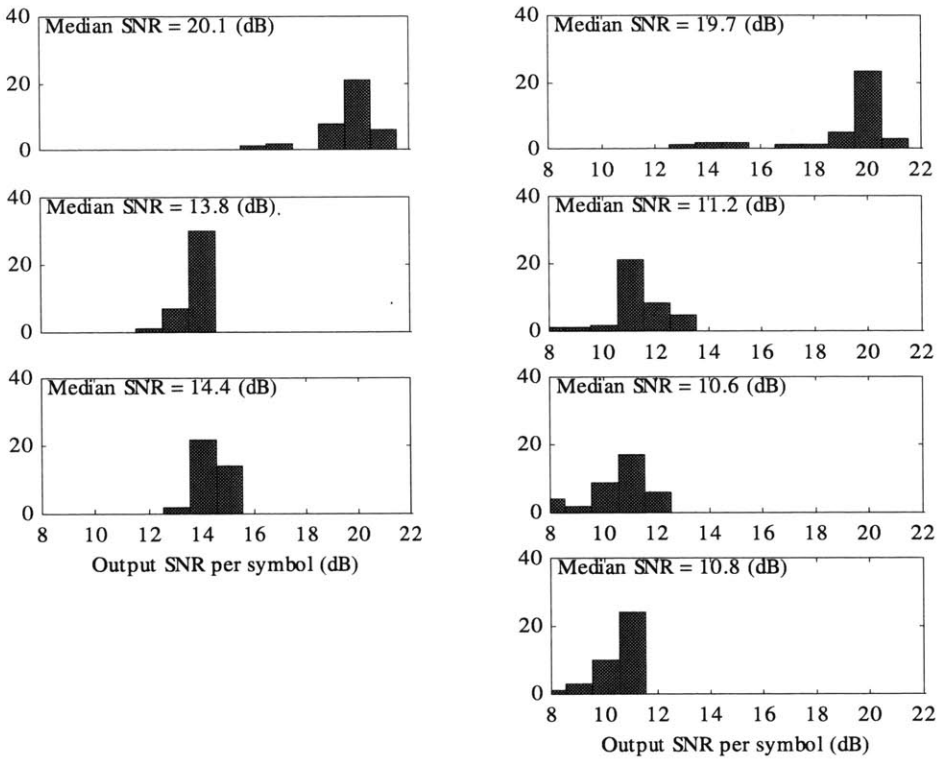

Figure 4.22. Each plot above presents a histogram of the output SNR from an ensemble of packets resulting from **sub-array B** modulation. The top panels are for the time-adjacent conventional packets while the lower ones are for the individual parallel channels in the presence of the others. The left hand panels are for the two-parallel channel packets while the right hand panels are for the three parallel channel packets. Median SNR is shown and will be used to characterize performance in the discussion.

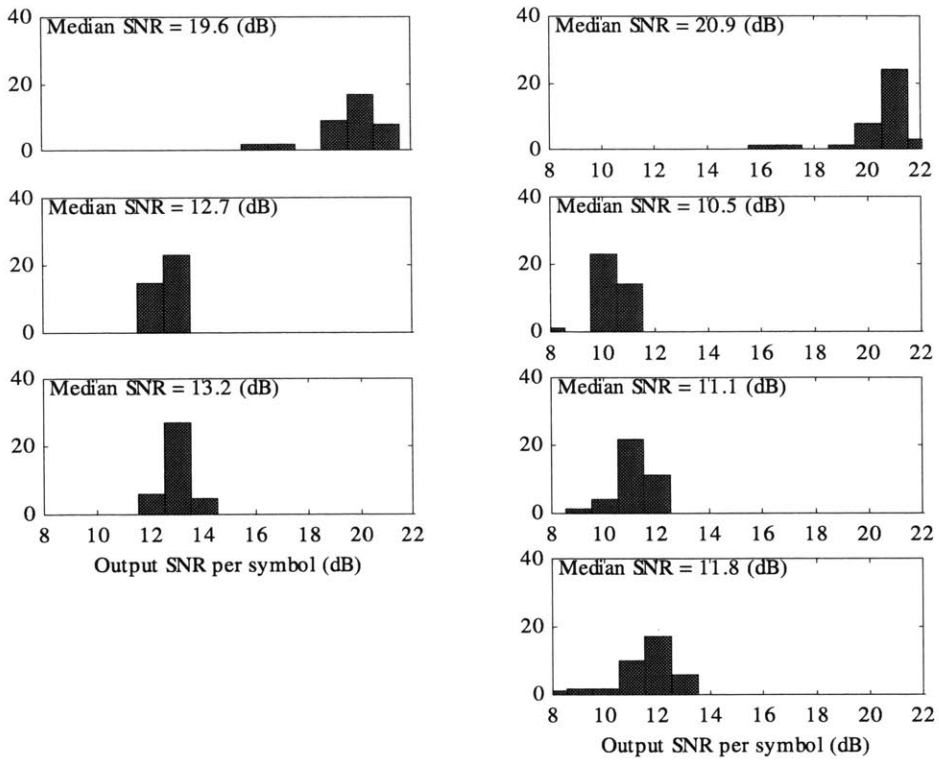

Figure 4.23. Each plot above presents a histogram of the output SNR from an ensemble of packets resulting from **SVD-A** modulation. The top panels are for the time-adjacent conventional packets while the lower ones are for the individual parallel channels in the presence of the others. The left hand panels are for the two-parallel channel packets while the right hand panels are for the three parallel channel packets. Median SNR is shown and will be used to characterize performance in the discussion.

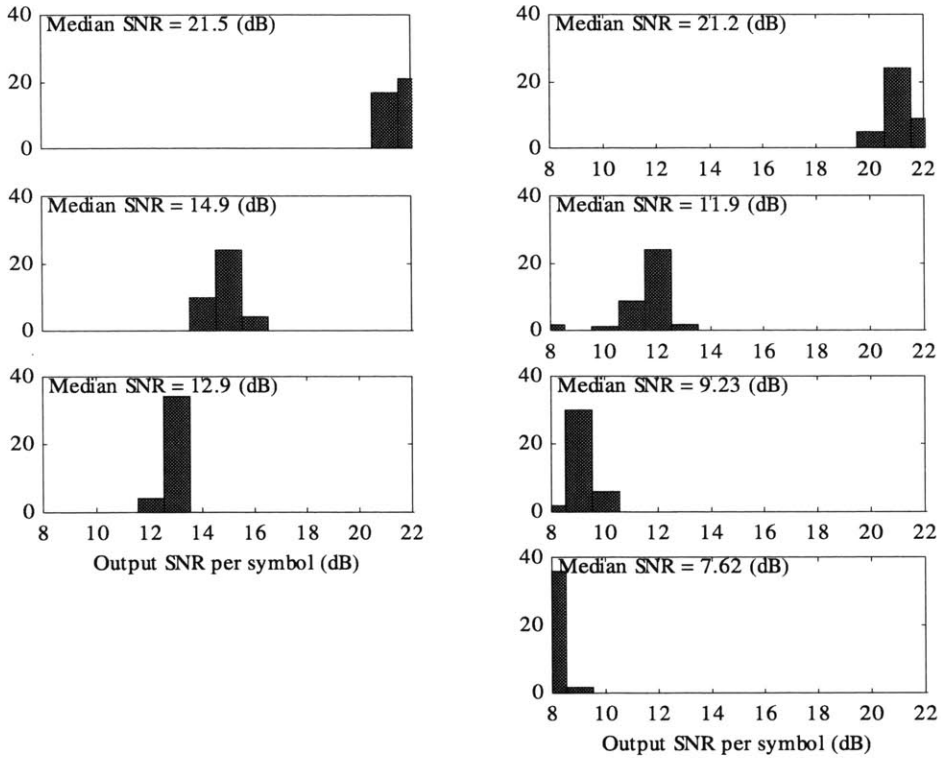

Figure 4.24. Each plot above presents a histogram of the output SNR from an ensemble of packets resulting from **SVD-B** modulation. The top panels are for the time-adjacent conventional packets while the lower ones are for the individual parallel channels in the presence of the others. The left hand panels are for the two-parallel channel packets while the right hand panels are for the three parallel channel packets. Median SNR is shown and will be used to characterize performance in the discussion.

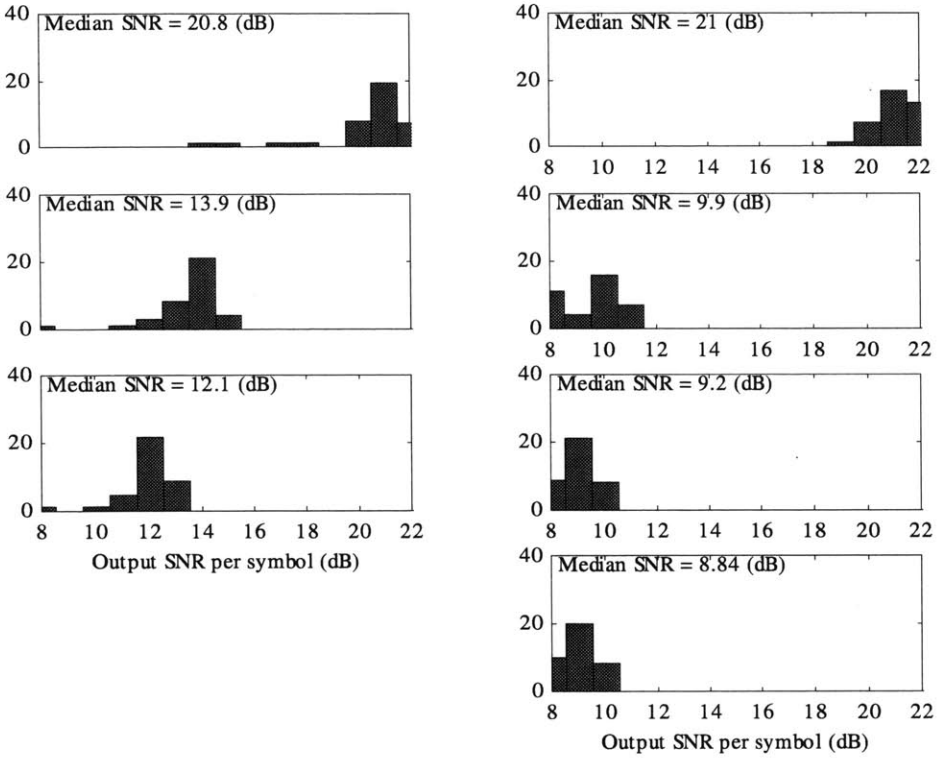

Figure 4.25. Each plot above presents a histogram of the output SNR from an ensemble of packets resulting from **SVD-C** modulation. The top panels are for the time-adjacent conventional packets while the lower ones are for the individual parallel channels in the presence of the others. The left hand panels are for the two-parallel channel packets while the right hand panels are for the three parallel channel packets. Median SNR is shown and will be used to characterize performance in the discussion.

4.4.3 SM00 Discussion

There are two important conclusions that may be drawn from the SM00 test. The first is that spatial modulation *improved* channel reliability. The second is that the channel decomposition described in Chapter 2 led to a spatial modulation strategy that improved achievable average power through the channel by as much as 6.3 dB.

As done earlier, the argument for improved channel reliability will be carefully constructed. An essential point in this discussion is that the output SNR was *not* power limited. The element level SNR was in excess of 20 dB. When additive, white Gaussian noise is superimposed on the data prior to processing, the output SNR remains unchanged. In this case, the residual inter-symbol interference due to the extremely long reverberation limits the performance. The impulse responses in this channel are qualitatively similar to those encountered in the SM99 test with a 20 – 30 symbol reverberation. Thus, additional power would not have improved performance. Another important, perhaps obvious, point is that the size of the symbol constellation for a particular parallel channel does not affect output SNR (neglecting the impact of decision feedback errors). SNR per bit may therefore be computed by taking the measured output SNR for each parallel channel and simply dividing by the number of bits one wishes to hypothesize sending over the channel. The constellation actually used is not important.

For the two parallel channel spatial modulation methods, 4 bits per symbol (16-QAM) will be assumed for the conventional channel while 2 bits per symbol (QPSK) will be assumed for each parallel channel. It has already been shown that two independent channels of QPSK achieve an equivalent error rate to one channel of 16-QAM with 3.9 dB less required SNR per bit. The experimentally demonstrated diversity gain may then

be computed by taking the output SNR of the conventional channel, dividing it by 4 to get SNR per bit and comparing it to the output SNR of the parallel channels when they are each divided by 2 to get SNR per bit. The two-parallel channel diversity gain thus obtained for each of the five methods is then (using the median output SNR for each packet ensemble),

Sub-Array A:	+1.8 dB
Sub-Array B:	+0.7 dB
SVD-A:	+0.4 dB
SVD-B:	-1.1 dB
SVD C:	-1.1 dB

The diversity gain here is defined as the change in output SNR of the conventional, single channel that would be required to achieve the probability of error that the parallel channel combination could achieve with its output SNR. One should recall that, in this case, output SNR can not be increased by increasing transmit power. The only recourse for reliable communication is coding. Of course, any benefits that would accrue to the conventional signal via coding could also accrue to the parallel channel combination.

The performance for the three-parallel channel spatial modulation packets may be interpreted in a similar manner. In this case, one compares QPSK over each of the three parallel channels to 64-QAM over a single channel. The asymptotic reduction in required SNR per bit for equivalent error is 8.2 dB. The experimentally demonstrated diversity gain may then be computed by taking the output SNR of the conventional channel, dividing it by 6 to get SNR per bit and comparing it to the output SNR of the parallel channels when they are each divided by 2 to get SNR per bit. The three-parallel channel

diversity gain thus obtained for each of the five methods is then (using the median output SNR for each packet ensemble),

Sub-Array A: 3.9 dB
Sub-Array B: 4.1 dB
SVD-A: 3.3 dB
SVD-B: 0.1 dB
SVD C: 0.7 dB

The average SNR per bit of the conventional channel (~14 dB) is *not sufficient* to sustain a 64-QAM signaling rate (error rates are worse than 10^{-2}). Thus, one cannot achieve a data rate of 24 kbit/sec over this channel with conventional signaling. Using three parallel channels generated via spatial modulation, however, 3 channels of QPSK may be sent at an SNR per bit of ~9 dB which *is sufficient* to sustain a total data rate of 24 kbit/sec. Thus, in this case, spatial modulation enabled a total data rate in excess of what conventional signaling could achieve. Of course, one may begin to employ coding to improve reliability of these higher data rates but presumably the same benefits would accrue to the three parallel channels and the advantage would remain.

The diversity gain resulting from the use of the channel-derived spatial modulation filters (SVD-A, SVD-B, and SVD-C) was, in general, equivalent or inferior to that achieved by simple sub-arraying. The reasons for this are unclear and would be a suitable area of future research. Such work would begin by determining what aspect of the propagation leads to the residual ISI and then determining how the decomposition procedure treats it. For instance, the 1 second averaging done by the ML-sequence processing or the averaging done in the formation of $\mathbf{T}^{H}(f)\mathbf{T}(f)$ may filter out those components of the impulse response. Any resulting decompositions would then be blind to the true performance limiting qualities of the channel. In some sense, impulse

response complexity is a factor in the residual errors. The SVD-B and SVD-C spatial modulation techniques introduced additional spreading in the channel and, perhaps, increased complexity in a manner that degraded performance. It should be noted that SVD-A (narrowband beamforming) performed equivalently to the sub-array techniques and did not introduce additional spreading.

A more robust indicator of the SVD filter performance is the total power transfer efficiency. As was shown in the previous section, filters derived from channel measurements three days prior to the test were sufficient to increase average power through the channel by as much as 6 dB. The increase was not due to simply using the most effective transducer. Sub-Array B modulation was designed so that the first parallel channel was sent using the transducer with the strongest response on the receiver (#4). That strategy increased power transfer by 1.5 dB over the conventional one of using all six transducers equally. SVD-B and SVD-C modulation principally used transducers 2 and 4 in a coherent manner and boosted power transfer by 2.5 dB and 6.3 dB respectively. While this communication experiment was insensitive to power efficiency, many underwater acoustic communication applications would benefit greatly from a 6 dB decrease in power requirements, particularly long-term autonomous monitoring missions. Even though the focus of this work has been on the use of several parallel channels, the value of using these tools to find and exploit the single, best parallel channel should not be overlooked. Channel-derived filters were therefore demonstrated to improve average power transfer but not to improve parallel channel separability.

The SM00 data set demonstrated that spatial modulation gives significant improvements in error rate characterized by diversity gains of 2 – 4 dB. In channels that

are limited by ISI and, therefore, will not benefit from more power, spatial modulation was shown to allow a higher data rate than would otherwise be obtainable. Channel derived spatial modulation filters did not improve the output SNR of the parallel channels but were nevertheless shown to increase average power transfer through the channel by more than 6 dB. This would be important in channels that were power-limited rather than ISI limited.

4.5 Summary of Spatial Modulation Experimental Performance

Each of the three experiments described in this section demonstrated the value of spatial modulation. BAH98 constructed two parallel channels in a horizontal plane enabling a bandwidth efficiency of 4 that was otherwise unsupportable with a single channel. SM99 constructed two parallel channels in a vertical plane and showed that a bandwidth efficiency of 4 was possible with a reliability improvement characterized by a 2.9 dB diversity gain as compared to the use of a single channel. Finally, SM00 constructed three parallel channels in a shallow, highly reverberant site achieving a bandwidth efficiency of 6 with a reliability improvement characterized by a 4 dB diversity gain. In fact, spatial modulation was able to reach a 24 kbit/sec data rate while conventional signaling could not. SM00 also demonstrated that the decomposition of $\mathbf{T}^H(f)\mathbf{T}^H(f)$, as described in Chapter 2, was able to increase average power transfer through the channel by over 6 dB. The presence of a one week delay between the channel measurement and the use of the channel-derived filters speaks to the robustness of the technique. This chapter has demonstrated the feasibility of spatial modulation in the ocean

Chapter 5. Conclusions

The primary objective of this thesis was to apply the concepts of spatial modulation to the underwater acoustic communication channel as a means to increase achievable data rates. To accomplish this, a set of analysis tools were required that would transform the multiple input, multiple output linear transfer function representation of the physical channel into a set of parallel channels. The tools, developed in Chapter 2, are not *required* to implement spatial modulation but, rather, serve as a convenient framework to investigate and understand the performance of a spatially modulated communication strategy. Based on the experimental results described in this thesis, the primary objective of this thesis has been met.

5.1 Unique Contributions of the Thesis

Rather than present a comprehensive summary of the last four chapters, an explicit list of the unique contributions of this thesis will instead be given.

1. While the notion of parallel channels has been considered for over 30 years and the mathematical technique of singular value decompositions has found widespread use in a variety of fields, the *synthesis* of the two and subsequent application to the problem of spatial modulation in the underwater acoustic communication channel is unique to this thesis.
2. The derivation of specific, coherent spatial modulation filters (i.e. the right singular vectors) for arbitrary physical channels is absent in previous and current work considering application of spatial modulation to wireless communication. The bulk of current research neglects the existence of any coherence between the

channels seen by transmitter elements and, therefore, gives no direction on how it may be exploited.

3. The derivation of average SNR and SINR performance metrics and the techniques for determining transmitter array excitation strategies that optimize them is unique to this thesis. Most existing design criteria for transmitter arrays focus on maximum directivity and null placement.
4. The field tests described in the thesis are the *first* experimental validation of wireless spatial modulation benefits for any medium outside of a laboratory.
5. The data obtained in the SM00 experiment conclusively showed that spatial modulation enabled a higher data for this particular channel than that achievable by conventional coherent signaling strategies under a power and bandwidth constraint.
6. The data obtained in the SM00 experiment demonstrated the robust ability of the average SNR optimization method to increase power transfer to the receive array. The technique has value for a wide variety of underwater acoustic applications.

5.2 Future Work

While many aspects of this work are amenable to continued development, two clear arenas for future work stand out from the rest. First, the value of channel information feedback from the receiver to the transmitter needs to be studied both theoretically with channel statistics and appropriate dynamics and experimentally with a range of ocean conditions. Performance of underwater communication systems increased dramatically when receivers were given the ability to coherently track and estimate the channel. One may hope for similar gains when the transmitter is also given such abilities.

Second, the average performance metrics consider, essentially, two factors governing performance; namely, the gain of a parallel channel and the orthogonality of the channel sub-spaces that the parallel channels energize, i.e. co-channel interference. While signal, noise, and interference power are crucial metrics, a large class of underwater acoustic channels is, in fact, limited by the residual reverberation energy that equalizers are unable to track. Two of the three field experiments described in this thesis (SM99 and SM00) fall into this category. The metrics presented, however, do not account for this constraint. Current understanding of this issue is largely empirical without a strong linkage to the physical channel. Of course, gross assessments such as non-surface interacting propagation paths are more readily tracked than surface interacting ones are possible but only offer crude guidance. A residual inter-symbol interference metric is needed.

Spatial modulation has much to offer underwater acoustic communication and should be aggressively pursued in the coming years.

BIBLIOGRAPHY

1. Coates, R., *Underwater Acoustic Systems.* 1989, New York: Wiley.
2. Urick, R.J., *Principles of Underwater Sound.* Third ed. 1983, Los Altos: Peninsula Publishing. 423.
3. Kilfoyle, D. and A. Baggeroer., *The State of the art in underwater acoustic telemetry.* IEEE Journal of Oceanic Engineering, 2000. **25**(1): p. 4-27.
4. Baggeroer, A., *Acoustic Telemetry -- An Overview.* IEEE Journal of Oceanic Engineering, 1984. **OE-9**(4): p. 229-235.
5. Catipovic, J., *Performance limitations in underwater acoustic telemetry.* IEEE Journal of Oceanic Engineering, 1990. **15**(3): p. 205-216.
6. Stojanovic, M., J.A. Catipovic, and J.G. Proakis, *Phase-coherent digital communications for underwater acoustic channels.* IEEE Journal of Oceanic Engineering, 1994. **19**(1): p. 100-111.
7. Voois, P.A., I. Lee, and J.M. Cioffi, *The effect of decision delay in finite-length decision feedback equalization.* IEEE Transactions on Information Theory, 1996. **42**(2): p. 618-621.
8. Salz, J., *Optimum mean-square decision feedback equalization.* Bell Systems Technical Journal, 1973. **42**(8): p. 1341-1373.
9. Gallager, R.G., *A simple derivation of the coding theorem and some applications.* IEEE Transactions on Information Theory, 1965. **IT-11**: p. 3-18.
10. Ebert, P.M., *Error Bounds for Parallel Communication Channels*, . 1966, Massachusetts Institute of Technology: Cambridge, MA.
11. Greenspan, R.L., *Error bounds for digital communication over spatially modulated channels*, . 1969, Massachusetts Institute of Technology: Cambridge, MA.
12. Shapiro, J.H., *Optimal spatial modulation for reciprocal channels*, . 1970, Massachussetts Institute of Technology: Cambridge.
13. Shapiro, J.H., *Reciprocity of the turbulent atmosphere.* Journal of the Optical Society of America, 1971. **61**(4): p. 492-495.
14. Shapiro, J.H., *Diffraction-limited atmospheric imaging of extended objects.* Journal of the Optical Society of America, 1976. **66**(5).
15. Anderson, B.L. *Spatial mode modulation of laser beams for optical communications.* in *IEEE International Caracas Conference On Devices, Circuits, and Systems.* 1995. Caracas, Venezuala: IEEE.
16. Killen, H.B. *Digital communications system design and analysis using simultaneous temporal and spatial modulation.* in *Canadian Communication and Power Conference.* 1976.
17. Brandenburg, L.H. and A.D. Wyner., *Capacity of the Gaussian Channel with Memory: The Multivariate Case.* The Bell System Technical Journal, 1974. **53**(5): p. 745 - 778.
18. Kennedy, R., *Fading Dispersive Channels.* 1969, New York: Wiley.
19. Proakis, J.G., *Digital Communications.* Third ed. 1995, Boston: McGraw-Hill. 928.
20. Narula, A., *Information Theoretic Analysis of Multiple-Antenna Transmission Diversity*, in *Department of Electrical Engineering and Computer Science.* 1997, Massachusetts Institute of Technology: Cambridge. p. 127.
21. Narula, A., M.D. Trott, and G.W. Wornell, *Performance Limits of Coded Diversity Methods for Transmitter Arrays.* IEEE Transactions on Information Theory, 1999. **45**(7): p. 2418 - 2433.
22. Foschini, G.J. and M.J. Gans, *On Limits of Wireless Communications in a Fading environment when Using Multiple Antennas.* Wireless Personal Communications, 1998. **6**: p. 311-335.
23. Foschini, G.J., *Layered space-time architecture for wireless communication in a fading environment when using multiple antennas.* Bell Laboratory Technical Journal, 1996. **1**(2): p. 41-59.
24. Golden, G.D., G.J. Foschini, R. A. Valenzuela, and P. W. Wolniansky, *Detection algorithm and initial laboratory results using V-BLAST space-time communication architecture.* Electronics Letters, 1999. **35**(1).
25. Bolcskei, H., David Gesbert, and Arogyaswami J. Paulraj, *On the Capacity of Wireless Systems Employing OFDM-based spatial multiplexing.* IEEE Transactions on Communications, 1999.

26. Tarokh, V., N. Seshadri, and A.R. Calderbank, *Space-time codes for high data rate wireless communication: Performance criterion and code construction.* IEEE Transactions on Information Theory, 1998. **44**(2): p. 744-765.
27. Cover, T.M. and J.A. Thomas., *Elements of Information Theory*. First ed. Wiley Series in Telecommunication, ed. D.L. Schilling. 1991, New York: John Wiley and Sons, Inc. 542.
28. Gallager, R.G., *Information Theory and Reliable Communications*. 1968, New York: John Wiley and Sons. 588.
29. Bello, P., *Characterization of randomly time-variant linear channels.* IEEE Transactions on Communication Systems, 1963. **CS-11**: p. 360-393.
30. VanTrees, H.L., *Detection, Estimation, and Modulation Theory, Pt. III*. 1971, New York: Wiley.
31. Collins, M.D., *FEPE user's guide*, . 1988, Naval Ocean Research and Development Activity: Stennis Space Center.
32. Brillinger, D.R., *Time Series: Data Analysis and Theory*. Expanded ed. Holden Day Series in Time Series Analysis. 1981, San Francisco: Holden-Day. 540.
33. Rice, J.A., *Acoustic signal dispersion and distortion by shallow undersea transmission channels.* in *High Frequency Acoustics in Shallow Water*. 1997. Lerici, Italy: NATO SACLANT Undersea Research Center.
34. Zar, J.H., *Biostatistical Analysis*. 2nd ed. 1984, Englewood Cliffs: Prentice-Hall. 718.
35. Reed, I.S., J. D. Mallett and L.E. Brennan, *Rapid Convergence Rate in Adaptive Arrays.* IEEE Transactions on Aerospace and Electronic Systems, 1974. **AES-10**(6): p. 853-863.
36. Helstrom, C.W., *Probability and stochastic processes for engineers*. 1984, New York : London: Collier Macmillan. 328.
37. Haykin, S. and A. Steinhardt, *Adaptive Radar Detection and Estimation*. Wiley Series in Remote Sensing. 1992, New York: J. Wiley. 473.
38. Stojanovic, M., J.A. Catipovic, and J.G. Proakis, *Adaptive multi-channel combining and equalization for underwater acoustic communications.* Journal of the Acoustical Society of America, 1993. **94**(3): p. 1621-1631.
39. Proakis, J.G., *Adaptive equalization techniques for acoustic telemetry channels.* IEEE Journal of Oceanic Engineering, 1991. **16**(1): p. 21-31.
40. Stojanovic, M., and Z. Zvonar, *Multichannel processing of broad-band multiuser communication signals in shallow water acoustic channels.* IEEE Journal of Oceanic Engineering, 1996. **21**(2): p. 156-166.
41. Eggen, T.H., *Underwater acoustic communication over doppler spread channels*, in *Joint Program in Oceanography / Applied Ocean Science and Engineering*. 1997, Massachusetts Institute of Technology / Woods Hole Oceanographic Institution: Cambridge / Woods Hole. p. 307.
42. Johnson, M., L. Freitag, and M. Stojanovic. *Improved doppler tracking and correction for underwater acoustic communication.* in *ICASSP 97*. 1997. Munich, Germany.
43. Freitag, L., M. Johnson, and M. Stojanovic. *Efficient equalizer update algorithms for acoustic communication channels of varying complexity.* in *Oceans '97*. 1997. Halifax, Nova Scotia, Canada: IEEE.
44. Ungerboeck, G., *Channel coding with multilevel/phase signals.* IEEE Transactions on Information Theory, 1982. **28**(1).